Mitigating the Effect of Propagation Impairments on Higher Layer Protocols and Algorithms in Wireless Sensor Networks

by

Pooyan Abouzar

B.Sc., University of Tehran, 2006
M.Sc., Chalmers University of Technology, 2008

A THESIS SUBMITTED IN PARTIAL FULFILLMENT OF
THE REQUIREMENTS FOR THE DEGREE OF

DOCTOR OF PHILOSOPHY

in

The Faculty of Graduate and Postdoctoral Studies

(Electrical and Computer Engineering)

THE UNIVERSITY OF BRITISH COLUMBIA

(Vancouver)

August 2016

© Pooyan Abouzar 2016

Abstract

Wireless sensor networks (WSNs) range from body area networks (BANs) that involve a relatively small number of nodes, short paths and frequent update rates to precision agriculture wireless sensor networks (PAWSNs) that involve a relatively large number of nodes, long paths and infrequent update rates. They are distinguished from wireless access networks by: 1) their mesh architecture and reliance on higher layer protocols and algorithms to perform routing, scheduling, localization, and node placement, 2) their need to operate for long periods of time with only limited access to battery or scavenged power.

Energy conservation has long been an important goal for developers of WSNs and the potential for reducing energy consumption in such networks by reducing the strength and/or frequency of transmission has long been recognized. Although the impact of propagation impairments on the physical and media access control layers of WSNs has long been considered, few previous studies have sought to assess their impact on higher layer protocols and algorithms and devise schemes for mitigating or accounting for such impacts. Here, we present four case studies that demonstrate how higher layer protocols and algorithms can be devised to achieve greater energy efficiency by accounting for the nature of the propagation impairments experienced.

In the first two case studies, we focus on BANs and: 1) propose a routing protocol that uses linear programming techniques to ensure that all nodes expend energy at a similar rate and thereby maximize network lifetime and 2) propose a scheduling algorithm that accounts for the periodic shadowing observed over many BAN links and thereby reduce the transmit power required to transfer information and thereby maximize network lifetime. In the second two case studies, we focus on PAWSNs and 3) propose an efficient localization algorithm based on the Bayesian model for information aggregation and 4) demonstrate that path loss directionality observed in sites such as high density apple orchards greatly affects WSN connectivity and, therefore, energy consumption and must be considered when designing node placement in agricultural fields.

Preface

Portions of Chapter 2 were presented at the IEEE VTC 2012-Spring [P. Abouzar, K. Shafiee, D. G. Michelson, and V. Leung, "Effects of relaying on network lifetime in 2.4 GHz IEEE802. 15.4 based body area networks," in *Proc. IEEE VTC 2012 Spring,* May 2012, pp. 1-5]. I was the lead investigator, responsible for all major areas of concept formation, data collection and analysis, as well as the majority of manuscript composition. V.C.M. Leung and K. Shafiee contributed to the organization of the work presented in Chapter 2. D. G. Michelson was the supervisory author on this project and was involved throughout the project in concept formation and manuscript edits. K. Shafiee served as the test subject during the measurement campaign.

Portions of Chapter 3 were presented at the IEEE PIMRC 2011 [P. Abouzar, K. Shafiee, D. G. Michelson, and V. Leung, "Action-based scheduling technique for 802.15. 4/ZigBee wireless body area networks," in *Proc. IEEE PIMRC 2011*, Sep. 2011, pp. 2188-2192]. I was the lead investigator, responsible for all major areas of concept formation, data collection and analysis, as well as the majority of manuscript composition. V.C.M. Leung and K. Shafiee were involved in the early stages of concept formation and contributed to manuscript edits. D. G. Michelson was the supervisory author on this project and was involved throughout the project in concept formation and manuscript edits. K. Shafiee served as the test subject during the measurement campaign.

A version of Chapter 4 has been accepted for publication by IEEE Transactions on Wireless Communications [P. Abouzar, D. G. Michelson, and M. Hamdi, "RSSI-based distributed self-localization for wireless sensor networks used in precision agriculture," accepted at *IEEE Trans. Wireless Commun.,* Jun. 2016]. Portions of the work were presented at the IEEE APS/URSI 2015 [P. Abouzar, D. G. Michelson, and M. Hamdi, "Localization of wireless devices in agricultural fields," in *Proc. USNC-URSI 2015*, Jul. 2015, pp. 218-218]. I was the lead investigator, responsible for all major areas of concept formation, data collection and analysis, as well as the majority of manuscript composition. M. Hamdi assisted with parts of the problem formulation and Bayesian inference analysis of the results. D.

G. Michelson was the supervisory author on this project and was involved throughout the project in concept formation and manuscript edits.

Portions of Chapter 5 were presented at the IEEE APS/URSI 2014 [P. Abouzar and D. G. Michelson, "Characterization of wireless mesh network performance in agricultural environments," in *Proc. USNC-URSI 2014*, Jul. 2014, pp. 125-125]. I was the lead investigator, responsible for all major areas of concept formation, data collection and analysis, as well as the majority of manuscript composition. D. G. Michelson was the supervisory author on this project and was involved throughout the project in concept formation and manuscript edits.

Table of Contents

List of Tables

List of Figures

List of Abbreviations

2DRMS	Twice distance root mean square
ADMM	Alternating direction method of multipliers
AOA	Angle of arrival
AODV	Ad hoc on-demand distance vector
BC	British Columbia
BI	Beacon interval
BP	Belief propagation
BS	Base station
CAP	Contention access period
CFP	Contention free period
CH	Cluster head
CI	Confidence interval
CICADA	Controlling access with distributed slot assignment
CIR	Channel impulse response
COTS	Commercial off-the-shelf
CSMA	Carrier sense multiple access
CTS	Clear to send
DIY	Do it yourself
DSDV	Destination-sequenced distance vector
DSR	Dynamic source routing
E-LEACH	Energy-LEACH
ECG	Electrocardiography
EEG	Electroencephalography
EMG	Electromyography
EWMA	Expected weighted moving average
GA	Genetic algorithm
GPS	Global positioning system

GTS	Guaranteed time slot
HCF	HART communications foundation
HDD	High directivity degree
HIT	Hybrid indirect transmission
HMM	Hidden Markov Model
HSA	Handheld spectrum analyzer
IG	Integrality gap
IMU	Inertial measurement unit
IP	Internet protocol
IoT	Internet of things
JJ	Jumping jacks
K-S	Kolmogorov-Smirnov
LDD	Low directivity degree
LEACH	Low energy adaptive clustering hierarchy
LLF	Link likelihood factor
LOS	Line of sight
LP	Linear programming
LPD	Lateral pulldowns
LS	Least square
M-LEACH	Multihop-LEACH
MAC	Media Access Control
MAP	Maximum a posteriori
MED	Modified exponential decay
MILP	Mixed integer linear programming
ML	Maximum likelihood
MMSE	Minimum mean square error
MRF	Markov random field
NBP	Nonparametric belief propagation
OLSR	Optimized link state routing
PAWSN	Precision agriculture wireless sensor network
PDA	Personal digital assistant
PDR	Packet delivery ratio
PEGASIS	Power efficient gathering in sensor information systems
PER	Packet error rate

PHY	Physical layer
PRPLC	Probabilistic routing with postural link costs
QoS	Quality of Service
RFID	Radio-frequency identification
RMSE	Root-mean-square error
RN	Running
RREP	Route reply
RREQ	Route request
RSSI	Received signal strength indication
RTS	Request to send
RW	Rowing
Rx	Receiver
SD	Superframe duration
SDP	Semidefinite programming
SGO	Sequential greedy optimization
SO	Superframe order
SOCP	Second-order cone programming
SPA	Sum product algorithm
TDMA	Time division multiple access
TICOSS	Timezone coordinated sleep scheduling
TOA	Time of arrival
TPA	Transmit power adaptation
Tx	Transmitter
UDG	Unit disc graph
UHF	Ultra-high frequency
UWB	Ultra wide band
VHF	Very high frequency
VSG	Vector signal generator
WASP	Wireless autonomous spanning tree protocol
WBAN	Wireless body area network
WLAN	Wireless local area network
WSN	Wireless sensor network
ZC	ZigBee coordinator
ZR	ZigBee router

Acknowledgements

There are so many individuals without whose help, I would definitely not have succeeded to complete the PhD program. First of all, I would like to thank my advisor, Prof. Michelson, for the productive meeting sessions we had throughout the entire program. His suggestions during write up and outlining of manuscripts were without doubt a blessing. Such was his influence, that at times I got the impression of grasping a concept when I myself was explaining the problem and state-of-the-art to him. I would also like to thank Prof. Victor Leung, my proposal committee member, for his productive suggestions particularly on the first part of thesis which is devoted to wireless body area networks. His hints greatly helped towards clarification and presentation of some major concepts in first and second chapters of the thesis. Besides Victor Leung, Prof. Shahriar Mirabbasi and Prof. Jane Wang were the other proposal committee members who made very useful suggestions for future direction of my program. Many thanks to them.

I would like to thank Maziyar Hamdi and Kaveh Shafiee for their invaluable contributions during different stages of my program. Further, Maziyar was always supportive with his math skills when it came down to mathematical formulations. The on and off-topic arguments we had kept my mind fresh. On the other hand, Kaveh helped with body area network measurement campaigns and thorough proofread of chapters 2 and 5 of the thesis. My collaborations with these two fellows played a key role towards enhanced readability and presentation of the thesis in many aspects.

Many thanks to Radio Science Lab 2012 and 2013 summer students who tolerated extremely harsh conditions in Similkameen, British Columbia to accelerate and facilitate our measurement campaigns and data analysis. I also appreciate SemiosBio, a startup company in Vancouver, who funded and supported our precision agriculture measurement campaigns and granted us access to apple orchards in Keremeos. Last but not least I would like to thank Pedram Ataee, Arghavan Emami, Sina Mashayekhi and Robert White for their support and kindness throughout the struggles and their presence during good times and laughters.

Dedication

To my beloved parents and brother who made a lot of sacrifices to help me pursue my dreams

Chapter 1

Introduction

Wireless sensor networks (WSNs), as illustrated in Figure 1.1, are generally defined as a set of sensors with wireless links between them which are scattered in an environment to cooperatively sense one or several features and forward them to a gateway or a computer so that a decision is made [1–4]. These networks are distinguished from wireless access networks by: 1) their mesh architecture and reliance on higher layer protocols and algorithms to perform routing, scheduling, localization, and node placement, 2) their need to operate for long periods of time with only limited access to battery or scavenged power. Moreover researchers have proposed higher layer techniques in order to meet various requirements in the network. Many different routing, scheduling and media access control (MAC) algorithms have been suggested to meet quality of service (QoS) requirements in terms of latency, connectivity, fairness and energy efficiency [5–7]. Deterministic and random node placement techniques are proposed to meet area coverage, network connectivity, network lifetime and data fidelity [8]. Various cooperative localization techniques have also been devised to address different scenarios in terms of number of nodes, mobility model, and presence or absence of landmarks in the network [9].

Energy conservation has long been an important goal for WSN developers because WSNs are battery operated and batteries are hard to access for recharging or battery replacement. Moreover, rise of WSNs over the past two decades and considering that almost 80% of the WSN energy is spent on communication [10], lots of higher layer algorithms and enabling technologies have emerged in order to facilitate communication between WSN components. The potential for reducing energy consumption in such networks by reducing the strength and/or frequency of transmission and increasing the duration of sleeping time has long been recognized. In other words, IEEE802.15.1, IEEE802.15.4 MAC and physical layer (PHY) specifications [11, 12] in addition to radio-frequency identification (RFID) were proposed and frequently modified to address short range communication in wireless personal area networks (WPANs). WSNs have revolutionized our lives in many aspects varying from healthcare and fitness to home automation, industrial and military applications [13, 14].

(a) A WSN is composed of a set of distributed sensors and a gateway

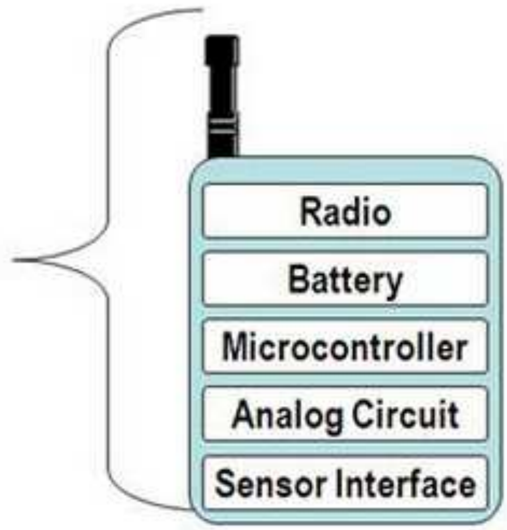

(b) Sensor nodes are composed of different entities and modules

Figure 1.1: A WSN is composed of a set of sensors for monitoring and a gateway which is responsible for data collection. A sensor node is composed of different components with radio being accountable for communication

The impact of WSNs on various industrial, military, and consumer applications has been increasingly growing over the past two decades. Particularly in body area networks, a wide range of applications varying from athlete performance monitoring in indoor and outdoor sports fields to elderly monitoring applications in clinics and homes have emerged [15, 16]. Also in precision agriculture, a wide variety of applications such as automated irrigation, fruit growth, soil health monitoring, and pest management has increased the profitability of agricultural fields [17].

A recent survey by IDTechEx [18] shows that the WSN market will grow from \$0.45 billion in 2012 to \$1.8 billion in 2024, whereas a different market study by Frost & Sullivan, anticipates the earned revenues to grow from \$1.2 billion in 2014 to \$3.26 billion in 2020 [19]. Particularly in healthcare industry, there will be 18.2 million health WSN systems worldwide, whereas wearable/implantable WSNs will increase by a 75% compound annual growth rate over the next five years [20]. Wireless healthcare solutions will increase by

1600% over the next 5 years [20] as the elderly population (people of age 60 years and over) in the world which was 759 million in 2010 will reach 1,198 million in 2025 and this group will occupy 15% of the world population [21]. As a different application, agriculture industry, increasingly growing world population which will reach 9 billion by the middle of the century [22], along with thinning land, water and resources raises the importance of WSNs deployment to help precision agriculture for resource and crop management. The precision agriculture market, as one of WSNs applications, will be worth $4.8 billion by 2020 [23].

1.1 Significance of Higher Layer Algorithms in Wireless Sensor Networks

The impact of propagation impairments on the PHY and to the lesser extent on the MAC layer of WSNs has long been considered. Further, adjustment of PHY layer parameters directly depends on channel propagation. In MAC layer studies, even though retransmissions are attributed to collisions, the effect of fading and path loss on packet drops and MAC layer performance in general has been taken into account. Moreover, impact of realistic channel assumptions on throughput and power consumption of MAC protocols, e.g., IEEE802.15.4, is proved to be significant [24]. In IEEE802.11 contention-based MAC protocol, features such as handshaking which work based on request to send (RTS)/clear to send (CTS) messages to address the hidden terminal problem are affected by directional path loss and asymmetric links. Furthermore, carrier sensing which is used to access the channel is affected by these phenomena [25].

On the other hand, few previous studies have sought to assess the impact of propagation impairments on higher layer protocols and algorithms or have devised schemes for mitigating such impacts. Even though impact of unrealistic channel propagation assumptions such as circular radio transmission area, i.e., unit disc graph (UDG), link symmetry and power-law attenuation model has been recognized [25, 26], little attention has been paid to effect of these impairments on the design of higher layer techniques, e.g., routing, scheduling, localization and node placement. Further, mitigation strategies that increase energy efficiency and network lifetime in the presence of such impairments have not been studied adequately. In the remainder of this chapter, we present recent developments in WSNs higher layer algorithms and proceed to present their limitations and the manner in which we might address them.

1.2 Review of Recent Developments in Wireless Sensor Network Technology

In this section, we first briefly define wireless body area networks (WBANs), precision agriculture wireless sensor networks (PAWSNs) and proceed with state-of-the-art enabling technologies, their limitations and our objectives in order to address them.

Wireless Body Area Networks: WBANs are defined as a set of invasive or non-invasive miniaturized sensors responsible to monitor functions of the human body or environment [16, 27, 28]. WBANs support a wide range of applications in different industries such as military, healthcare, gaming, entertainment and sports.

Precision Agriculture Wireless Sensor Networks: Several definitions are suggested for precision agriculture [29–31], however in general it is defined as management strategy that takes advantage of information technologies to enhance resource utilization and increase the benefits resulted from crop management in agricultural fields. The most critical requirement in precision agriculture is a reliable decision support system so that number of correct decisions per unit area of land linked with net benefits rises [30]. Some of the precision agriculture applications are irrigation, pest management, fruit growth and soil monitoring. PAWSNs serve as the technology to bring data from the agricultural field to the base station (BS) by means of sensors and wireless technology so that such benefit making decisions are made.

1.2.1 Key Advances and Enabling Technologies

With IEEE802.15.4 becoming more popular, different alliances and groups of companies were formed to propose network protocols running on IEEE802.15.4 and to address different types of applications [32]. ZigBee Alliance proposed ZigBee networking protocol for a wide range of applications varying from patient monitoring in healthcare to environment monitoring in precision agriculture. Z-Wave Alliance which, as of today, is composed of more than 350 companies, suggested Z-wave communication standard for home automation applications [33]. HART communications foundation (HCF), comprised of 37 companies, provided WirelessHART for automation in process industry [34]. With the rise of internet of things (IoT), interoperability between Internet Protocol (IP)-based networking and IEEE802.15.4 compatible devices gained significant importance [35]. This led to IPv6 over Low power

WPANs (6LoWPAN) being proposed by a working group in the internet area of Internet Engineering Task Force (IETF) so that nodes in the WSN are connected to the internet. The enabling underlying and networking technologies for WSNs along with their features are shown in Figures 1.2 and 1.3. These standards are important from the perspective that they are deployed on commercial off-the-shelf (COTS) chipsets that are available in the market and are shipped to relevant third party companies in large quantities.

	ZigBee	Z-Wave	6LoWPAN	DASH7	WirelessHART	Wireless M-Bus	Bluetooth BLE	DECT ULE	Wi-Fi (802.11n)
Operating Frequency	2.4 GHz, 915 MHz, 868 MHz	900 MHz	2.4 GHz	433 MHz	2.4 GHz	169 MHz, 433 MHz, 868 MHz	2.4 GHz	1.9 GHz	2.4 GHz, 5 GHz
Max. Outdoor Range	~ 500 m	~ 100 m	~ 200 m	~ 2000 m	~ 250 m	1000m	~ 50 m	~ 300 m	~ 100 m
Max. Data Rate	250 Kbps	40 Kbps	200 Kbps	27.8 / 200 Kbps	250 Kbps	100 Kbps	~ 1 Mbps	~ 1 Mbps	~ 600 Mbps
Max. Nodes	65,536	232	~ 100	Too many	~ 30,000	~ 250	N/A for BLE; 8 is default for Classic Bluetooth	~ 400	N/A
Average Current Consumption	Tx: 25-35 mA; Rx: 20-30 mA;	Tx: 30-40 mA; Rx: 20-30 mA;	Tx: 20-35 mA; Rx: 12-25 mA;	Tx: 14-25 mA; Rx: 3-7 mA;	Tx: 18-25 mA; Rx: 6-10 mA;	Tx: 35-45 mA; Rx: 17-25 mA;	Tx: 15-20 mA; Rx: 15-20 mA;	?	Tx: 220+ mA; Rx: 215+ mA;
Multi-hop Capabilities	Yes	Yes	Yes	2 hops only, extra hops can be added with RPL	Yes	Yes	No	Yes	No
Certification / Qualification Cost	Medium	Medium	Low	High	High	?	High	?	High
Development Community Adoption	High	High	Medium	Low	Low	Medium	Medium	Low	High
Interoperability	High	High	Low	Medium	High	High	Medium	Medium	High
Reliability	Low	Low	Low	High	High	High	Medium	Low	Medium
Suitable for Industrial / Military?	No	No	No	Yes	Yes	Yes	Yes	N/A	Yes

Figure 1.2: Commercial enabling networking technologies for WSNs; The table is extracted from [36].

In addition to these industrial and commercial technologies, a large number of underlying MAC and higher layer networking protocols are proposed by research groups and labs. Here, we will discuss state-of-the-art enabling technologies that appear in the literature and will proceed with the missing part which will be addressed in this dissertation. We will be more focused on two specific applications of WSNs which are the main focus of this work; WBANs and PAWSNs. Even though throughput, latency, reliability are WSN performance measures, power consumption is the main concern in the way of WSNs deployment. Therefore, network reliability, latency and other QoS metrics are often compromised in favour of energy efficiency. Methods adopted in order to mitigate energy consumption are divided into PHY, MAC and network layer techniques. In PHY, transmission bit rate, frequency band, modulation scheme and transmit power level are adjusted in order to meet the channel propagation characteristics. On the other hand MAC protocols aim to minimize idle listening, collisions, amount of control packets and overhearing which are major reasons of power consumption in MAC layer [7]. On the other hand, a suitable network layer technique is required to be energy efficient in terms of setup (route discovery), route maintenance and data communication phases.

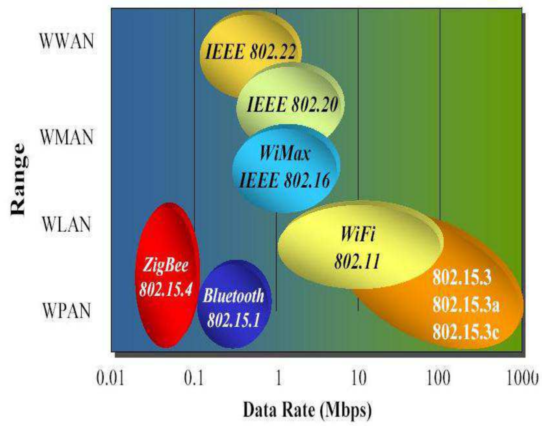

(a) Underlying PHY and MAC specifications proposed for different applications extracted from [37]

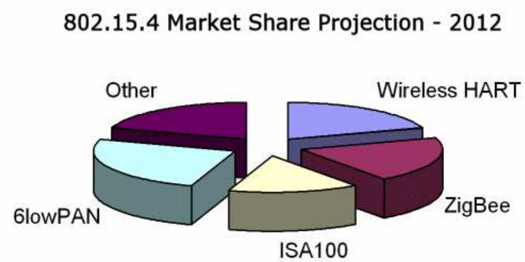

(b) Market share for IEEE802.15.4-based networking technologies extracted from [38]

Figure 1.3: The applicability space for different PHY and MAC specifications in addition to market share for networking protocols which are built upon IEEE802.15.4

Many MAC and routing protocols which specifically aim to address WBAN and PAWSN applications are proposed in the literature. The contribution of these in-house developed MAC algorithms mostly originates from the synchronization mechanism that reduces MAC overhead energy consumption. Further, time division multiple access (TDMA)-based MAC protocols, e.g., BodyMAC [39], MedMAC [40] and WiseMAC [41] are specifically proposed for deployment in WBANs. As far as routing is concerned and particularly for WBANs, literature is more extensive. Here, we summarize these routing protocols and proceed to present higher layer techniques in precision agriculture.

Routing and Scheduling in WBANs: Even though in the general WSN context, routing protocols are divided into three categories, including hierarchical, location-based and data-centric [5], in the WBAN literature they mostly fall into hierarchical [42–44], temperature-based [45], cross layer [46–48] and link-state [49–53] routing protocols each of which aiming to address a specific set of requirements. In link-state routing protocols, a cost function which incorporates link connectivity, remaining energy of the sensors or both is assigned to links so that the routing tables are updated in a way that energy depletion in sensors is balanced and reliable routes are formed. Hierarchical routing protocols are inspired by classic Low Energy Adaptive Clustering Hierarchy (LEACH) [54] and Power-Efficient Gathering in Sensor Information Systems (PEGASIS) [55] protocols, and mostly work based on forming clusters or chains of nodes and conducting data aggregation over them. After forming clusters or chains of sensors, one head is designated to collect packets from other sensors in the cluster or chain and forward them to the BS. In temperature-based routing protocols, traffic flow in the network is distributed so that temperature of body organs for intrusive WBANs and limbs for non-intrusive WBANs does not exceed a threshold. Cross layer studies in WBANs, mostly focus on integration of MAC, routing and application layer than taking channel propagation into account. Further, several scheduling techniques have been proposed for WBANs as well which can work in conjunction with MAC and routing protocols. Ruzelli et al. [46], have proposed timezone coordinated sleep scheduling (TICOSS) which is a scheduling algorithm built upon IEEE802.15.4 MAC layer. TICOSS is based on dividing network to different time zones where sensors belonging to the same time zone, simultaneously transmit their data to the nodes belonging to contiguous zone, while nodes in other zones are sleeping.

Latre et al. [47], have proposed wireless autonomous spanning tree protocol (WASP) and Cascading Information retrieval by Controlling Access with Distributed slot Assignment (CICADA) [48] where a spanning tree is set up in a distributed manner and data is forwarded to the sink based on a distributed scheduling. The focus of WASP and CICADA is to provide the desirable end-to-end delay in the network. Store and forward scheduling techniques [56, 57], increase likelihood of a packet reaching its destination by storing the packet at multiple hops, while opportunistic scheduling techniques [58–60] are designed to maximize resource utilization in the network while providing fairness among users by allocating the channel to the user with a more suitable channel state. In these studies, the transmission power is adjusted to the condition of the underlying fading channel for achieving a desirable data rate. However, the continuous link assessment make these techniques incompatible with WBANs where nodes ideally turn their radio off until it is their turn to transmit, as an energy-saving measure. Another class of WBAN scheduling techniques focus on adaptive or optimized guaranteed time slot (GTS) allocation in IEEE802.15.4 WBANs in order to meet latency and fairness requirements or to make best use of bandwidth [61, 62].

Higher Layer Techniques in PAWSNs: The literature for higher layer techniques in PAWSNs is less extensive compared to WBANs. Most routing protocols proposed for precision agriculture applications are cluster-based with one or multiple gateways placed at the corners of the agricultural field [63, 64]. Even though IEEE802.15.4 is the most common short range scheme used for monitoring applications [65], a few MAC protocols have also been specifically proposed for deployment in PAWSNs [66, 67]. Focus of these works is the same as in general WSN context where energy saving is achieved by keeping nodes in sleeping mode for longer durations. Further, in [66], a Genetic Algorithm (GA) based MAC protocol in which GA decides which nodes in the field should stay active or should be assigned cluster-heads is proposed. The proposed work in [67, 68], Ping-Drowsy MAC (PD-MAC) protocol, is more sophisticated and works based on having multiple transmit power levels and sensitivity levels for sensing. PD-MAC is inspired by more classic contention-based MAC protocols; S-MAC [69] and T-MAC [70]. In [71], a light-weight Carrier Sense Multiple Access (CSMA)-based MAC protocol is proposed, while Baggio et al. have deployed T-MAC as the underlying MAC protocol [72]. In terms of node placement techniques, square grid is the most common deployment technique used in literature [73–76], however effects of other deterministic node placement techniques, triangular and hexagonal patterns, in terms of connectivity and coverage have been discussed under isotropic power-law attenuation model in the field [76].

1.2.2 Key Limitations of Previous Work

As discussed in Section 1.1, significance of channel impairments and their impact on the performance of WSNs has been recognized for a long time [25, 26]. Even though Impact of channel propagation on MAC layer algorithms such as IEEE802.15.4 [24] and classic routing protocols such as ad hoc on-demand distance vector (AODV) and Dynamic source routing (DSR) [25] has been recognized to some extent [25], little attention has been paid to incorporation of channel propagation into design of routing and other higher layer techniques.

Most state-of-the-art WBAN higher layer protocols are either implemented on IEEE802.15.4 compliant COTS or have been simulated with network simulators such as OMNeT++. Even though WBAN performance has been studied in these simulated or implemented practices, either implications of channel propagation on design of these algorithms have been dismissed or integration of realistic models in the simulation environment has not been considered. On the other hand, most PAWSN implementations are field trials in vineyards and orchards. Moreover, channel characteristics that can degrade performance of these networks is not studied.

Most WSN routing protocols are composed of setup, data communication and route maintenance phases which are all affected by channel propagation assumptions. The setup phase in on-demand routing protocols relies on path-reversal technique which fails under link asymmetry, fast and shadow fading circumstances. Link asymmetry particularly disrupts setup phase in location-based and data-centric routing protocols. Further, setup and neighbour discovery phase in location-based routing protocols is based on sufficient node density in the network, accurate localization and high link reliability [77]. Seada et al. [77] have discussed the effect of realistic link packet error rate (PER) models on message overhead, and excessive power consumption in traditional location-based routing protocols that work based on greedy forwarding algorithm. In data-centric protocols [78], localized flooding occurs in order to create the routing table based on reverse route discovery techniques which rely on link symmetry assumption. Data communication phase works based on circular radio range where path loss is a simple function of distance, i.e., power-law attenuation model. Particularly, power efficiency of hierarchical routing protocols such as LEACH [54], PEGASIS [55] and other inspired protocols relies heavily on this path loss model. Route maintenance phase to recover from broken links which imposes message overhead and consequently excessive power consumption, is also hugely affected by fast fading channels. On the other hand, in cross layer techniques, a lot of attention has been paid to making use of the information from higher layers, i.e., network and application layer, to design MAC layer [79], however channel propagation has not been taken into account.

Opportunistic scheduling techniques use spatial and temporal diversity of channel to allocate bandwidth to the user that benefits from better channel state. Even though these techniques increase bandwidth utilization, they suffer from communication overhead associated with idle listening caused by sensing the channel. Only a few of the opportunistic scheduling studies consider the power constraints in the design of their algorithms [80, 81]. Transmit power control strategies [52] that work along with most of the scheduling techniques still result in high overhead due to frequent link assessments associated with transmit power adjustment. On the other hand, store and forward techniques achieve desired end-to-end connectivity with low transmit power levels at the expense of multi hop routing and exchange of control packets which result in excessive energy consumption. Moreover, most existing scheduling techniques aim to improve connectivity, fairness or dynamic allocation of bandwidth based on traffic. Therefore, they are not energy efficient due to high communication overhead or the fact that they follow different objectives than energy efficiency.

In terms of cooperative localization techniques, a lot of work has been done on Bayesian and non-Bayesian techniques [82, 83]. The state-of-the-art Bayesian and non-Bayesian techniques are not suitable for deployment on IEEE802.15.4 COTS due to the slow or lack of convergence, in addition to the the high number of messages that must be exchanged and also the computation burden that is imposed on COTS with low memory and processing power. Moreover, existing Bayesian distributed techniques suffer from the communication overhead required for setup phase in order to form loop-free graphs. Whereas non-Bayesian techniques are burdened with excessive communication overhead and computational complexity to solve optimization problems at each iteration, and therefore suffer from slow convergence. In these works, features of channel propagation observed in real world environments and their effect on the performance of these protocols in terms of energy consumption and convergence is dismissed. Further, connectivity among nodes and their cooperation outcome strongly depends on underlying channel propagation models, therefore incorporation of these features into design of energy efficient cooperative techniques is of great merit.

The literature on node placement techniques is extensive as well, however path loss model is not the centre of attention and most efforts are centred around meeting criteria such as connectivity, coverage, network lifetime and data fidelity [8], while isotropic power-law attenuation model forms the underlying channel propagation and path loss model. Particularly in precision agriculture, more focus has been put on the effects of application on node placement. Furthermore placing the nodes so that better variogram, i.e., independence of data points, is achieved has been of more interest while little attention is paid to realistic underlying path loss model in the agricultural field.

1.3 Objectives of This Work

Even though different techniques for node placement, PHY, MAC, and network layers have been proposed to make communications in WSNs more energy efficient, channel propagation characteristics must be taken into account in order to achieve more energy efficiency. Further, a lot of work has been done to integrate higher layers such as transport and application layers into the network layer and routing techniques, however the impact of channel propagation on design and performance of higher layer protocols is not much explored. Here, we focus on proposing higher layer methods which take channel propagation into account in order to reduce energy consumption in two radically different WSNs in terms of channel propagation; WBANs and PAWSNs. Further, we propose higher layer techniques such as routing, scheduling, localization and node placement that work based on channel propagation implications in specific environments so that energy efficiency and network lifetime are improved.

Deep fades cause WBAN on-demand routing protocols [51, 84] to fail because routing tables will not be valid short after they are established. Scheduling and transmit power control techniques also require excessive amount of beacon exchanges in order to conduct link assessments. These necessitate design of cross layer scheduling and routing protocols that work based on appropriate channel propagation assumptions so that energy efficiency is achieved. On the other hand, large network dimensions in PAWSNs along with different propagation mechanisms, e.g., ground and canopy reflection, result in directional radio range which affects higher layer techniques. For example, cluster formation in cluster-based routing protocols is significantly influenced by directional path loss and on-demand routing protocols are affected by link asymmetry in farm environment since long links suffer from link asymmetry more than shorter links [85]. It is well known that propagation model affects connectivity of the links and routes which consequently has impact on performance of reactive routing protocols such as AODV, DSR, optimized link state routing protocol (OLSR) and Destination-Sequenced Distance-Vector (DSDV) [86–89]. However, effects of directional path loss observed in realistic environments on such algorithms is dismissed. Particularly, AODV-based protocols are fundamental since they form basis for multi-hop networking deployed on IEEE802.15.4 COTS in WSNs. Therefore, node placement techniques that consider directional path loss and take distance dependence of path loss in the 2.45 GHz industrial, scientific and medical (ISM) band into account are critical. This is particularly important since path loss in orchard environment at 2.45 GHz is dramatically different from high frequency (HF)/ very high frequency (VHF) bands [90]. It is worth mentioning that most of the proposed path loss models in ultra-high frequency (UHF) band or higher only target excessive path loss through foliage propagation and are very site specific [91, 92]. Therefore, these models do not take different propagation mechanisms and directions, for example along or across the tree rows into account.

Here, we present four case studies that demonstrate how higher layer protocols and algorithms can be devised in order to achieve greater energy efficiency by accounting for the nature of the propagation impairments involved. WBANs and PAWSNs are extreme in terms of channel propagation behaviour and design considerations for higher layer algorithms. The way channel propagation impairments disrupt the performance of higher layer techniques, particularly routing protocols, is different in these two WSNs [86–89]. In on-body WBANs, severe shadowing is the dominant propagation mechanism and imposes deep fast fades over on-body links while distance is not an important feature. Whereas in PAWSNs, distance and direction are decisive factors while temporal variations are very small. In addition to propagation environment, these two networks are different in terms of number of sensors, node placement, application, and network lifetime definition. Further, in WBANs, a small number of sensors with heterogeneous applications are scattered on body, constrained to specific locations and decision making in terms of higher layer algorithms is centralized. On the other hand, in PAWSNs, deterministic node placement is the most common approach, while distributed higher layer algorithms are recommended due to high number of nodes in the field. Network lifetime definition is also different in these two types of networks. Moreover, in WBANs each node is responsible for observing a different feature therefore failure of each of these nodes disrupts performance of the network while in PAWSNs, a large number of sensors monitor a single parameter therefore failure of large number of these nodes is still tolerable. In this work we propose routing, scheduling, localization and node placement techniques that work based on channel propagation implications in specific environments so that energy efficiency and network lifetime are improved. To this end, the thesis is broken down to two parts each of which devoted to a different environment.

1.4 Contributions

In the first WBAN case study, we propose a routing protocol that uses linear programming (LP) techniques to ensure that network lifetime is maximized and all nodes in a WBAN expend energy at a similar rate during stationary human actions. Even though single-hop star networks are the most frequently implemented practice, they may not be efficient in terms of achieving connectivity or network lifetime. Further, whether multi hop or single hop communication needs to be used depends on many criteria [93]. On the other hand, the main limitation of the existing state-of-the-art routing protocols proposed for WBANs is the amount of control message overhead nodes use to estimate reliability of the links in addition to remaining energy in the sensors so that balanced energy depletion and high connectivity are achieved. In order to address this limitation, we propose a link-state probabilistic routing protocol based on IEEE802.15.4 MAC and PHY which enhances WBAN lifetime for stationary actions by: 1) conducting link assessment and transmit power level adjustment only when action variations are tracked, 2) using LP techniques to assign link likelihoods in order to ensure that balanced energy depletion is achieved, therefore lifetime is maximized.

In the second WBAN case study, we propose a scheduling algorithm that accounts for the periodic shadowing which may be observed over many WBAN links and thereby reduce the transmit power required to transfer information and thereby maximize energy efficiency at the expense of latency. A scheduling technique that achieves the desired end-to-end connectivity with low transmit power level and hop count at the expense of latency helps save energy for delay-tolerant WBAN applications such as ambient assisted living in which, latency can be tolerated since data analysis would be carried out in an offline manner.

We use measurements to show that periodic prolonged actions, e.g., fitness activities, cause on-body links, particularly extremity-torso links, to undergo periodic predictable connectivity sessions that can be exploited for low transmit power single-hop communications. The proposed technique could work in conjunction with routing protocols, e.g., the probabilistic routing protocol suggested in the first WBAN case study, to lower transmit power over periodic links over which, delay tolerant WBAN applications are running. Beside periodicity that is used for energy efficient communication, diversity of received signal strength indication (RSSI) samples over such links provide us with features, e.g., mean and standard deviation which makes simple real-time action recognition based on naive Bayes classification possible.

In the second pair of case studies, we focus on PAWSNs; In the first case, we propose an energy efficient localization algorithm based on the Bayesian model for information aggregation which is well-suited to run seamlessly on IEEE802.15.4 COTS. Further, in the route discovery phase of AODV, which forms the basis for routing in IEEE802.15.4 compliant modules, the node that is set to send its data to the gateway, originates a route request (RREQ) packet that will be multicast by every receiving node so that ID of the nodes that form the shortest path from the originating node to the gateway is logged. Consequently, gateway sends a route reply (RREP) packet over the shortest path to make the nodes aware of their next hop. Therefore, a cooperative localization algorithm in which, outgoing message by each node fits inside a IEEE802.15.4 packet, has a low computational burden that can be solved in COTS with low processing power and runs in parallel is significantly important. The algorithm is very beneficial since the cost associated with global positioning system (GPS) or time and labour associated with manual localization will grow significantly for large WSNs deployed in large fields.

The proposed algorithm, uses a Bayesian model for information aggregation and independence of shadowing over long links in agricultural fields to achieve energy efficiency and scalability. Scalable communication and computational complexity with respect to the number of nodes are achieved at the expense of accuracy while requirements for precision agriculture applications such as pest management are still met. The scalable RSSI-based algorithm proposed in this work, overcomes these limitations by: 1) using only local distance estimates with respect to neighbouring nodes, and 2) using a message passing schedule which benefits from a fixed size outgoing message that does not grow with number of neighbouring nodes, and 3) low computational complexity where computations only grow with field size and only involves summations and multiplications as opposed to non-Bayesian techniques where optimization problems need to be solved.

In the second case, we address the limitations of previous work in terms of characterizing anisotropic path loss in realistic environments and discuss implications of this phenomenon on node placement, and performance of routing protocols. Moreover, first we use measurements in a high density apple orchard to demonstrate that directional path loss is a real phenomenon in real world man-made and row-like environments such as agricultural fields, warehouse and libraries. We proceed to show that its impacts on performance metrics, i.e., network lifetime and latency of routing protocols such as AODV is measurable. Consequently, as a mitigation strategy, we suggest elongated grid deployment, i.e., decreasing internode distances along impaired directions in order to make node connectivity along various directions more uniform, therefore improving network lifetime and latency. This technique in fact mimics behaviour of isotropic, i.e., non-directional, path loss by distributing neighbouring nodes in a more uniform way along different directions which helps network achieve higher lifetime as a result of higher time it takes network graph to become disconnected.

1.5 Outline

This dissertation is divided into two parts that focus on WBANs and PAWSNs respectively. Chapter 2 proposes a link-state probabilistic routing protocol for maximizing lifetime in WBANs, while in Chapter 3, we propose a scheduling technique for periodic actions which is in complementary with the routing technique proposed in Chapter 2.

In Chapter 4, we propose a novel localization algorithm based on Bayesian model for information aggregation which is well suited to pest management application in agricultural fields. In Chapter 5, we demonstrate that directional path loss exists in the apple orchards and propose node placement strategies to mitigate the effects of this phenomenon on the performance of AODV-based routing protocols in similar environments. In Chapter 6, we conclude the thesis with conclusions regarding the effectiveness of our proposed schemes, the limitations of our algorithm and the implications for current research practice in addition to recommendations for the future research.

Chapter 2

A Routing Protocol for Maximizing the Lifetime of Body Area Networks

2.1 Introduction

The use of link-state routing techniques to improve lifetime and connectivity of WBANs has been proposed in the past. The aim is to assign cost metrics or link likelihood factors that cause nodes with lower remaining energy, unreliable links or both to be avoided. Here, we utilize a novel transmit power control algorithm to meet connectivity requirements with minimum communication overhead and LP techniques to assign link likelihoods, i.e., the assignment probabilities of next hops, so that WBAN lifetime is maximized. Further, transmit power levels and link likelihoods are updated only once major change in actions or postures is tracked. The algorithm is well-suited to WBAN monitoring applications with stationary actions and postures, the duration of which is significant compared to the packet transfer delay defined by QoS requirements, e.g., 250 msec. To the best of our knowledge, this is the first work that analytically formulates lifetime maximization for routing in IEEE802.15.4 WBANs. Further, LP which is used to calculate link likelihood factors for lifetime maximization and balanced energy depletion works in conjunction with transmit power control which significantly lowers communication overhead in order to achieve maximum WBAN lifetime.

Design of energy efficient routing protocols that improve network lifetime is one of the major challenges in WBANs since energy resource constraints are more severe compared to other conventional types of WSNs and also due to limited access to batteries [94]. Further, as opposed to conventional WSNs, scalability is less of an issue for WBANs than energy consumption because most of these networks consist of relatively low number of sensors and actuators that perform a variety of functions [51]. These characteristics cause most WBAN routing techniques to be case specific since there is no straightforward design in terms of multi-hop networking that could encompass all applications and situations [93]. In general, however these protocols are classified into temperature-based, cluster-based, and link-state routing protocols with the latter two being more focused on energy efficiency, therefore more relevant to our work.

Cluster-based routing protocols aim to increase lifetime by decreasing inter-cluster transmission distances and switching CHs to guarantee balanced energy depletion among nodes. The CHs are responsible for aggregating data from cluster nodes and send it to a BS [42–44, 54, 55]. The energy efficiency of these protocols mostly lies in the assumptions regarding channel and transceiver characteristics. Further, the power-law attenuation model makes these hierarchical routing protocols suitable mostly for static WSNs deployed in large environments rather than WBANs with small number of sensors which experience very dynamic link behaviour.

The majority of networking techniques that aim to address energy efficiency in WBANs are link-state routing protocols. In these protocols, a cost function that incorporates link connectivity, the remaining energy of the nodes, or both, is assigned to the links so that routing tables are updated in a way that energy depletion in sensors is balanced. A probabilistic routing protocol, PROPHET, proposed for WSNs [95] has inspired several WBAN link-state protocols published afterwards [49–51, 96, 97]. In PROPHET, a metric called *delivery predictability* is updated based on the frequency at which neighbouring nodes encounter each other and consequently messages are forwarded on paths with higher destination connectivity. In [49], Quwaider et al. defined *link likelihood factor* (LLF) and proposed probabilistic routing with postural link costs (PRPLC) which takes history of the links and therefore the locality of neighbours, into account as well. An extension of PRPLC which integrates inertial measurement unit (IMU) sensors for better locality recognition is proposed in [50]. Later, Maskooki et al. proposed opportunistic routing which is based on store and forward routing with nodes storing data and waiting for neighbours with better connectivity to BS to become available [51]. The aforementioned works are more suited to intermittently connected and delay tolerant networks with ultra-short range RF transceivers where the network connectivity graph is constantly changing. Even though these techniques yield an acceptable PDR, energy consumption and delay are sacrificed due to high number of transmissions and packet storing nature of protocol respectively.

There are a number of link-state routing protocols that incorporate transmit power control as well [52, 98, 99]. Nabi et al. devised a similar approach to [51] except that transmit power adaptation (TPA) is integrated [52]. Further, the nodes keep track of neighbours and utilize transmit power control to consume minimal transmission power while maintaining a predetermined link quality. In [53], a centralized link-state routing protocol along with TPA is proposed. In every cycle, nodes measure received signal strength indication (RSSI) over the connected links, merge it into their remaining energy and forward it to a host. The host makes decision on transmit power level and routing table of each node based on updated link costs and Dijkstra's algorithm. The problem with this work and similar approaches is the excessive control message overhead required for link quality assessment at the end of each *transfer round*, i.e., duration after which sensors will have one round of data delivered to the sink, and also for sensors to transmit the control data to the BS. In addition to this, the computational complexity involved with running Dijkstra's algorithm in the beginning of every transfer round takes a toll on access point battery which is usually a personal digital assistant (PDA) or a cellphone. Therefore, a routing protocol that could achieve maximum lifetime without remarkable communication overhead and frequent link cost assignment is critical for low data rate, class 0, WBAN monitoring applications.

In this work, we introduce a suboptimal probabilistic link-state routing protocol with transmit power control that is well-positioned to maximize WBAN lifetime, i.e., the time span before the first sensor in the network dies. In the proposed protocol, based on assigned transmit power levels and remaining energy in the sensors, sink solves a LP problem to derive a traffic flow distribution matrix with its elements representing *link likelihoods*, i.e., the probability that each node would be assigned as next hop to the other node. To be more specific, our work is close to [49] from the LLF assignment stand of view, however as opposed to [49] where the objective is better end-to-end connectivity, in our work likelihoods are derived so that network lifetime is maximized. To the best of our knowledge, this is the first work that formulates lifetime maximization problem as a LP with MAC layer and transceiver radio characteristics integrated into formulation. The algorithm is particularly useful for realistic mobility scenarios with subject person doing an action or holding onto a posture for long amount of time compared to transfer round duration, i.e., stationary actions. This is a realistic mobility model for many daily activities since most postures and actions involved in WBAN monitoring context, e.g., fitness or patient monitoring are stationary, i.e., last relatively long and follow a repetitive pattern as well. Despite low communication overhead, the proposed algorithm achieves lifetime maximization by:

- engaging in new transmit power selection only when significant variations in *expected weighted moving average* (EWMA) of path loss samples over limb-torso links is detected,
- updating traffic flow distribution matrix only when transmit power levels are updated.

We call the duration between the transmit power level and traffic flow distribution updates, the *transmit power update window*. Moreover, based on data collected during our measurement campaigns, we learned that the EWMA of path loss samples over limb-torso links is a strong measure of change of action or posture and starting the new transmit power update window, whereas the variations over limb-limb or torso-torso links is a lot milder.

The remainder of this chapter is organized as follows; In Section 2.2, we present a brief background on system model including IEEE802.15.4 MAC layer specifications, a radio model for RF transceivers and data delivery model for WBAN applications, afterwards proceed with lifetime maximization problem formulation. In Section 2.3, we present the steps that lead up to the algorithm which solves the problem formulation derived in Section 2.2. Evaluation of our algorithm for a specific monitoring WBAN consisting of pulse, blood flow, respiration, electrocardiography (ECG), temperature and glucose sensors during fitness activities is conducted in Section 2.4. We finish the paper in Section 2.5 with conclusions regarding effectiveness of the proposed algorithm and its limitations.

2.2 Concepts

We present our system model in Section 2.2.1 which forms the basis for the WBAN lifetime maximization problem formulation derived in Section 2.2.2.

2.2.1 System Model

In this section, we present the system model in terms of MAC layer and radio characteristics, data delivery model and QoS requirements. These features play a key role in problem formulation and the proposed routing algorithm.

IEEE802.15.4 MAC Layer: IEEE802.15.4 defines the physical and MAC layer specification for low data rate WSNs [12]. MAC layer in IEEE802.15.4 is defined within beacon-enabled and non-beacon-enabled modes. In non-beacon-enabled mode, the nodes in the network compete based on non-slotted carrier sense multiple access with collision avoidance (CSMA/CA), whereas in beacon-enabled mode, they operate based on superframe structures which are bound within beacon packets. Time division multiple access (TDMA) and contention-based communication are supported via contention free period (CFP) and contention access period (CAP) respectively. Beacon-enabled mode allows adaptation of low duty cycle frames, i.e., nodes can sleep during inactive period for energy conservation. The superframe structure of beacon-enabled mode is illustrated in Figure 2.1. Considering the periodic nature of the WBAN monitoring applications and the fact that the size of such networks are relatively small, we adopt the beacon-enabled mode of the MAC layer so that TDMA feature of the specification with GTS is supported [15]. Beacon interval (BI) and

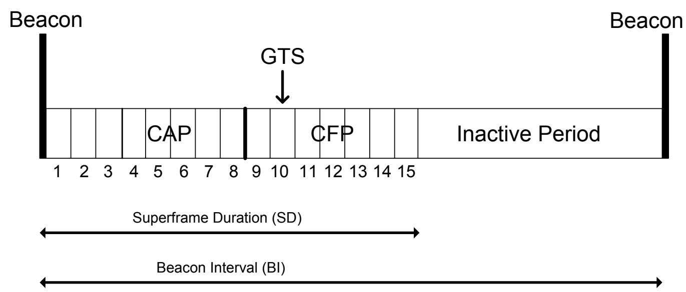

Figure 2.1: Superframe structure of IEEE802.15.4 MAC layer protocol

superframe duration (SD) are adjusted using beacon order (BO) and superframe order (SO) respectively, where

$$\begin{aligned} &BI = BaseSuperFrameDuration^{BO}, \\ &SD = BaseSuperFrameDuration \times 2^{SO}, \\ &BaseSuperframeDuration = BaseSlotDuration \times NumSuperframeSlots, \end{aligned} \tag{2.1}$$

and $0 \leq SO \leq BO \leq 14$, and BaseSlotDuration=15.36 msec. Therefore, superframe duration and beacon interval could vary between 15.36 msec. and 251.7 sec. based on application and networking requirements. Note that BI is adjusted based on the WBAN transfer round which was introduced in Section 2.1 and is determined based on QoS requirements that will be explained later in this section.

Radio Model: The transmitter and receiver power consumption model plays a key role in energy expenditure of the nodes and consequently network lifetime. Wang et al. [100] have proposed a power consumption model for CC2420 modules, that are widely used in IEEE802.15.4 studies. The transmitter power consumption, $P_t(d)$, denotes power consumption of the transmitter's radio in order to meet the desired Signal-to-noise ratio (SNR) at distance d while P_r is the receiver's radio power consumption. These parameters are modelled by

$$\begin{aligned} P_t(d) &= P_{elec} + P_a(d), \\ P_r &= \text{const}, \end{aligned} \tag{2.2}$$

where P_{elec} is a constant term representing the power dissipated in the electronic circuit of the module. The power consumed at power amplifier is denoted by $P_a(d)$ and is a function of transmit power shown by $P_{tx}(d)$ that represents required transmit power in order to meet the desired SNR at distance d,

$$P_a(d) = P_{tx}(d)/\eta, \tag{2.3}$$

where, η denotes power amplifier efficiency.

Data Delivery Model: Depending on the application, the data delivery model for WSNs can be continuous, event-driven, query-driven or hybrid [5]. WBAN monitoring applications work based on continuous data delivery model since sensors send data to the sink at a determined rate and in a continuous manner. In terms of data rate, WBAN applications are divided into three groups [40];

- Class 0: Low grade data; applications such as temperature monitoring, respiratory, and pulse,
- Class 1: Medium grade data; applications such as ECG, electroencephalography (EEG) and blood pressure, and,
- Class 2: High grade data; applications such as medical imaging, video, and electromyography (EMG).

This work is focused on Class 0 and low data rate Class 1 applications with continuous data delivery model.

Quality of Service: WBANs are very diverse with different applications having different QoS requirements in terms of latency, throughput and PER. In this work, our focus is on WBAN monitoring applications for Class 0 data rates. According to the relevant literature, $PER = 0.01$ and packet transfer delay of 250 msec meet the QoS requirements [101], while throughput is different for each WBAN application. The throughput required for the applications studied in this work are tabulated in Table 2.2. In the next section, we formulate the lifetime maximization problem.

2.2.2 Problem Formulation

In this section, we formulate WSN lifetime maximization as a mixed integer linear programming (MILP) problem. Further, based on the selected transmit power level and remaining energy in the sensors, our objective is to derive the data flow distribution, i.e., the matrix consisting of link likelihood elements, so that WSN lifetime will be maximized. Various network lifetime definitions have been proposed in the WSN context [102]. In this work, we define network lifetime as the duration until the first sensor dies, as this is most consistent with the requirements of WBAN applications. Moreover, as stated in Section 2.1, in contrast to more conventional WSNs where a large number of sensors are sampling the same feature, in WBAN monitoring applications, each sensor is responsible for observing a different parameter, e.g., pH, pulse and respiration [51]. Therefore, failure of any of these sensors will disrupt performance of the entire network.

Formulation of lifetime maximization problem is influenced by two specific features of IEEE802.15.4 MAC layer for TDMA-based communication. First, the transmitting node stays *on* during the whole allocated time slot, GTS, even after completion of packet transmission except that it starts to only consume the circuitry power P_{elec} rather than $P_{elec}+P_{tx}/\eta$. Second, the receiving node stays *on* during the whole allocated GTS and keeps consuming P_r even after completion of packet reception.

Now, let us assume a network consisting of N *on-body* nodes including $N-1$ sensor nodes and one sink node represented by $\mathbb{S} = \{S_1, \dots S_{N-1}\}$ and S_N respectively. Our objective is to derive link likelihoods in a way that the duration until the first node dies is maximized. Let $P_t^{(i,j)}$ denote the transmit power consumption in the i-th node when transmit power level $P_{tx}^{(i,j)}$ is adopted for communication between i-th and j-th nodes. Let $t_l^{(i,j)}$ correspond to communication duration between i-th and j-th nodes during l-th transfer round, and $E_{tr,l}^{(i,j)}$ denote the random variable associated with transmit energy consumption of i-th node when communicating with the j-th node, i.e.,

$$
\begin{aligned}
E_{tr,l}^{(i,j)} &= P_t^{(i,j)} t_l^{(i,j)} + \mathcal{I}_l^{i,j} P_{elec}(T_s - t_l^{(i,j)}),\\
\mathcal{I}_{i,j} &= \begin{cases} 1 & t_l^{(i,j)} \neq 0, \\ 0 & t_l^{(i,j)} = 0 \cdot \end{cases}
\end{aligned}
\tag{2.4}
$$

In (2.4), T_s represents the duration of each time slot. Electronic circuit energy $P_{elec}(T_s - t_l^{(i,j)})$ is only consumed when the l-th time slot is allocated to communication between i-th and j-th nodes. Otherwise $t_l^{(i,j)} = 0$, $E_{tr,l}^{(i,j)} = 0$ because the i-th node is turned off for energy conservation. The second term in the right hand side of (2.4) is associated with IEEE802.15.4 MAC layer characteristics that are explained in the beginning of this section. Similarly, the receive power consumption of the i-th node when listening to k-th node is given by $E_{r,l}^{(k,i)} = \mathcal{I}_l^{k,i} P_r T_s$ which implies that the i-th node listens during the whole GTS duration T_s in case the slot is allocated to the communication between i-th and k-th nodes.

The total transmit energy expended by the i-th node to communicate with the j-th node over the network lifetime of n transfer rounds is given by $E_{tr,Tot}^{(i,j)} = \sum_{l=1}^{n} E_{tr,l}^{(i,j)}$ and is calculated by $E_{tr,Tot}^{(i,j)} = (P_t^{(i,j)} - P_{elec})T^{(i,j)} + n_{i,j} P_{elec} T_s$, where $n_{i,j}$ is the total number of transfer rounds, i-th node spends forwarding its aggregated data to j-th node and $T^{(i,j)}$ represents the total time i-th node spends forwarding packets to j-th node. Similarly total receive energy consumption in i-th node to receive packets from k-th node is given by $E_{r,Tot}^{k,i} = n_{k,i} P_r T_s$, where $n_{k,i}$ denotes the total number of transfer rounds i-th node spends listening to k-th node. Therefore total energy consumption of i-th node after n transfer rounds is calculated by

$$E_{i,Tot} = \sum_{j \in \{1,\ldots N\} \setminus i} [(P_t^{(i,j)} - P_{elec})T^{(i,j)} + n_{i,j} P_{elec} T_s] + \sum_{k \in \{1,\ldots N-1\} \setminus i} n_{k,i} P_r T_s. \tag{2.5}$$

The MILP formulation of the lifetime maximization problem is

$$\begin{aligned}
\underset{\substack{T^{(i,j)}, n_{i,j} \\ i \in \{1,\ldots N-1\}}}{\text{maximize}} \quad & n, \\
\text{subject to} \quad & E_{i,Tot} \leq E_{init}^{(i)}, \\
& \sum_{j \in \{1,\ldots N\} \setminus i} [T^{(i,j)} - n_{i,j} h] - N_i Q_i = \sum_{k=1}^{N} [T^{(k,i)} - n_{k,i} h], \\
& \frac{n}{\alpha_i} \leq \sum_{j \in \{1,\ldots N\} \setminus i} n_{i,j} \leq n, \\
& T^{(i,j)} \leq n_{i,j} T_s,
\end{aligned} \tag{2.6}$$

where the first constraint ensures that all nodes still have energy left after n transfer rounds. In fact (2.6) translates to the duration after which the first node dies. The second constraint is the flow conservation in which N_i is number of transfer rounds during which, i-th node has generated data whereas h is a fixed term accounting for duration of the footer and header that is merged with each data packet and Q_i denotes duration of the data i-th sensor generates after a specific number of transfer rounds. The third constraint ensures that aggregate number of transfer rounds allocated to a node to forward data does not exceed the network lifetime. Moreover high data rate sensors generate data at every transfer round whereas low data rate sensors generate data periodically after a fixed number of transfer rounds. Therefore, for high data rate sensors $\alpha_i = 1$ and $\sum\limits_{j \in \{1,\ldots N\} \setminus i} n_{i,j} = n$ since each sensor has at least its own generated data to transfer in each transfer round. On the other hand, low data rate sensors may forward data of other sensors even during transfer rounds they have not generated that of their own. Fourth constraint guarantees that the amount of time assigned to data transmission from i-th to j-th node does not exceed T_s. Due to combination of discrete and continuous variables, (2.6) is a MILP problem. In Section 2.3, we explain our methodology to solve the lifetime maximization problem derived in (2.6).

In the next section, we explain transmit power adjustment algorithm in order to meet QoS requirements in terms of PDR. This in fact yields new $P_t^{(i,j)}$ coefficients in (2.5), and results in a new MILP which is to be solved based on new coefficients. Therefore, next hops and inter-node communication durations are reassigned every time new transmit power levels are adopted. The structure of the transmit power update window is illustrated in Figure 2.2. In the beginning of each update window, transmit power levels and consequently link likelihoods are reassigned.

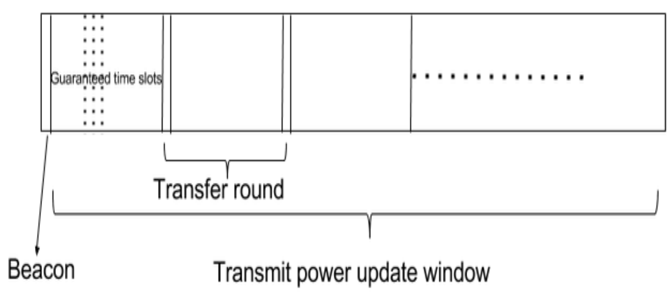

Figure 2.2: Transmit power update window: each transmit power update window is made up of several transfer rounds. In each transfer round, one round of data delivery to the sink is completed. Each round contains time slots which are allocated to nodes for data transmission. The structure of a transfer round is illustrated in Figure 2.1. Every node is allocated at most one time slot in each transfer round.

2.3 Solution of the Lifetime Maximization Problem

In this section, we explain the procedure to solve the lifetime maximization problem given in (2.6). As explained in Section 2.2.1, in WBAN monitoring applications, $PER \approx 1\%$ is required to meet QoS requirements. Therefore, transmit power levels in (2.5) and consequently the lifetime maximization problem in (2.6) must be adjusted so that the requirements in terms of PDR are met.

2.3.1 Transmit Power Adjustment Algorithm

Several works have discussed power management techniques in WBANs [52, 53] based on adapting the level of transmission power to the variable nature of the channel caused by shadowing and node movements by exploiting real-time link assessment. However, the fast and abrupt nature of fitness activities make the real time link assessment overwhelming in terms of communication overhead. In order to avoid the communication overhead involved in real-time link assessment and transmit power control, we suggest to update the required transmit power levels only when major variations over EWMA of RSSI samples over limb-torso links are observed. Further, as will be explained in Section 2.3.3, our measurements show that this feature is a suitable measure for action or posture variation in WBANs. The purpose from power management is to assign required transmit power level $P_{tx,l+1}^{(i,j)}$ for communication between i-th and j-th sensor nodes during the upcoming, $(l+1)$-th, update window, W_{l+1}, so that specific PER requirements are met. Once the required transmit power levels are updated, the traffic flow distribution matrix is renewed based on (2.6). Each update window consists of multiple transfer rounds. During each round, one set of data is delivered to the sink. Accordingly, the proposed transmit power control algorithm is composed of two entities: action variation recognition and transmit power selection.

Action Variation Recognition: The goal of this entity is to determine whether transmit power levels need to be updated, and new update window to start thereof. As stated in previous sections and as will be seen in Section 2.4, our measurements show that EWMA of path loss variation over limb-torso links during change of actions is remarkably larger than that of limb-limb or torso-torso links. Further, we introduce the EWMA for tracking RSSI large fluctuations that result from action variations so that the transmit power levels would be reassigned. Let $r_{l,m}^{(i,j)}$ and $r_{l,m-1}^{(i,j)}$ denote EWMA of RSSI at the j-th node in the m-th and $(m-1)$-th transfer rounds, respectively, when i-th node is transmitting, while $rss_{l,m}^{(i,j)}$

denotes the observed RSSI value during m-th transfer round and l-th update window; and α is a real weighting factor between 0 and 1. The EWMA update of RSSI is represented by

$$r_{l,m}^{(i,j)} = (1-\alpha).r_{l,m-1}^{(i,j)} + \alpha.rss_{l,m}^{(i,j)}. \tag{2.7}$$

The purpose of this procedure is to end the window W_l and reassign transmit power levels when EWMA function drops or spikes more than a predetermined threshold, e.g., 5 dB. Note that smaller α causes more delay in recognition of variations while less importance is given to spontaneous path loss variations which happen very frequently even for fixed actions and postures. Therefore, a small weighting factor amount, e.g., $\alpha = 0.05$, allows us to ignore posture variations of short duration. Moreover, as stated in Section 2.1, our focus is to capture the stationary actions which continue for a large amount of time compared to transfer round size duration. The performance of this action variation recognition strategy on real collected data will be described in Section 2.4.

Transmit Power Level Selection Strategy: Once change of actions or postures is recognized, the transmit power levels required to support communication over each link needs to be updated. Furthermore, transmit power levels $P_{tx,l+1}^{(i,j)}$ corresponding to the $(l+1)$-th update window are selected based on path loss instances experienced over the preceding link assessment window $W_l^{(test)}$ which is conducted at the end of the current update window W_l. The transmit power is selected so that the average probability of a packet drop based on path loss values observed over this link assessment window is below a specific threshold, hence PDR remains above the threshold PDR$_{th}$ allowed by QoS requirements, e.g., PDR$_{th}$= 99%. The implementation considerations of this phase is explained in Section 2.3.3 and Algorithm 1.

Let link assessment window $W_l^{(test)}$ contain $w_l^{(test)}$ RSSI samples, and $P_{tx,l+1}^{(i,j)}$ denote the assigned transmit power for communication between i-th and j-th nodes over W_{l+1} which remains fixed over the entire upcoming window. Let $pl_{l,n}^{(i,j)}$ denote the n-th path loss sample in $W_l^{(test)}$. Based on Figure 2.3, assuming that $L(r)$ denotes packet loss probability when $RSSI = r$, we select $P_{tx,l+1}^{(i,j)}$ so that

$$\begin{aligned} P_{tx,l+1}^{(i,j)} &= \underset{P_{tx}}{\operatorname{argmin}} \left(\frac{1}{w_l^{(test)}} \sum_{n=1}^{w_l^{(test)}} L(P_{tx} - pl_{l,n}^{(i,j)}) < 1 - PDR_{th} \right), \\ pl_{l,n}^{(i,j)} &= P_{tx,l}^{(i,j)} - rss_{l,n}^{(i,j)}. \end{aligned} \tag{2.8}$$

In (2.8), $rss_{l,n}^{(i,j)}$ represents the n-th RSSI sample in l-th link assessment window $W_l^{(test)}$. Note that in (2.8), the transmit power P_{tx} is selected so that mean packet loss would have remained below the threshold over the past test window in case P_{tx} was selected.

Figure 2.3 presents the measurements and shows PDR as a function of RSSI for micaZ CC2420 motes. The experiment involved more than 40,000 packets, 44 bytes long each, sent from the different pairs of sensors illustrated in Figure 2.4 with 8 transmit power levels between -25 dBm and 0 dBm. The results are consistent with [103] which reports PDR= 85% for RSSI=-87 dBm.

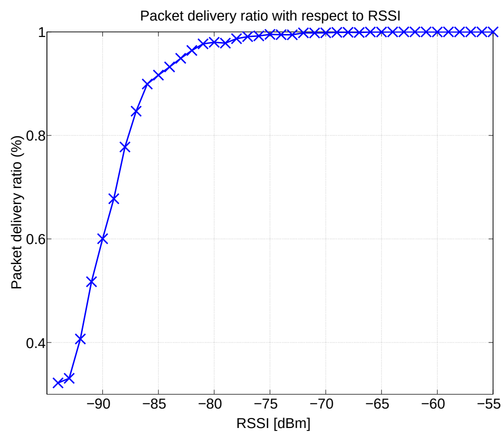

Figure 2.3: PDR with respect to RSSI [dBm]; PER=1% is achieved for RSSI=-78 dBm with user doing different actions and transmit power level taking 8 different levels between -25 dBm and 0 dBm

2.3.2 LP Relaxation

As explained in Section 2.2.2, because MILP problems are NP-complete, we apply LP relaxation in order to cause the discrete variables n_{ij} adopt real values. Afterwards, derived transfer round values n_{ij} are rounded to make the problem P-complete and therefore solvable in polynomial time. Let M_{opt} and M_{real} represent the solution to MILP and relaxed LP problem respectively. In an integer LP maximization problem, the integrality gap with minimum value of 1, is a measure of the efficiency of the LP approximation and is defined as the ratio between the optimum and the relaxed derived maximum values, $IG = \frac{M_{real}}{M_{opt}}$. Considering that the rounding algorithm uses solution of the relaxation to achieve M_{round}, the $\frac{M_{real}}{M_{round}}$ ratio, upper bounds the IG. The relationship between M_{real}, M_{opt} and M_{round}

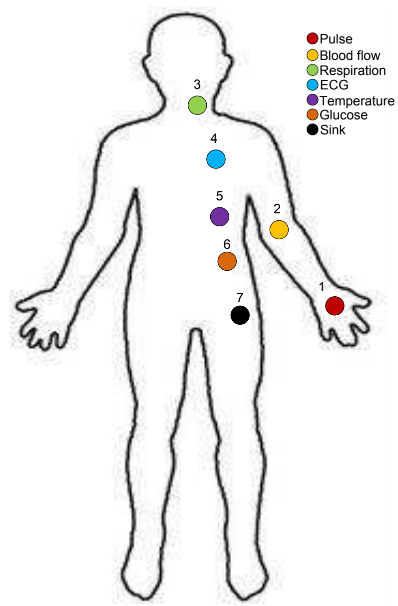

Figure 2.4: On-body sensor placement; 1st, 2nd, 3rd and 4th sensors must be mounted at specific locations. The 5th and 6th sensors are not restricted and have been placed close to the sink for relaying purposes

is depicted in Figure 2.5. In Section 2.4, we apply LP relaxation to (2.6) so that discrete variables are allowed to take on real values. The optimal value of this LP relaxation yields an upper bound to the optimal value of the MILP model. We will see that suboptimal MILP solution that results from rounding the variables in LP relaxation is fairly close to this achieved upper bound, therefore close to MILP optimal solution.

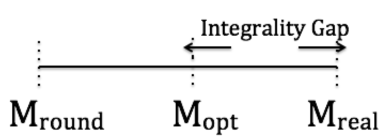

Figure 2.5: The relationship between integrality gap (IG), M_{opt}, M_{round} and M_{real} is illustrated. $\frac{M_{real}}{M_{round}}$ provides an upper bound to $IG = \frac{M_{real}}{M_{opt}}$.

2.3.3 Implementation Considerations and Routing Algorithm

As explained in Section 2.3.1, each transmit power update window consists of two phases; the *transmit power selection* and *data transmission*. Here, we explain the mechanism of each phase.

Transmit Power Selection

As described in Section 2.3.1, when a transmit power update window starts, the nodes attempt to update the required transmit power level for a reliable communication with other nodes in the WBAN. Since link assessment starts in the beginning of each update window, sink broadcasts a beacon and allocates GTS to nodes for transmission and reception of test packets. Each recipient node adds the RSSI of the received packet to the array which is designated for link assessment over the link between the two corresponding nodes. The hidden terminal problem is not an issue because all nodes hear each other at maximum transmit power level. Due to energy efficiency and latency considerations, a set of nodes denoted by $\mathbb{S}_t$, engage in transmission of link assessment packets. We pursue this approach because: 1) channel symmetry in terms of required transmit power over a specific link which is different from symmetry in terms of RSSI. Moreover, considering transmit power update in (2.8) channel symmetry of our interest translates to $P^{(i,j)}_{tx,l+1} = P^{(j,i)}_{tx,l+1}$ and 2) required transmit power to meet PER requirements between pairs of nodes whose distance and line-of-sight (LOS) degree are fixed with respect to each other, is not sensitive to the type of activity. For example, minimum transmit power level, -25 dBm, always suffices to meet PER=1% over links between 1st-2nd, 4th-5th, 4th-6th, and other similar pairs in Figure 2.4.

The procedure continues for a predetermined duration before nodes stop broadcasting link assessment packets to each other. At this point, nodes broadcast packets consisting of RSSI arrays so that they are collected by the sink. The sink calculates transmit power levels based on (2.8) and consequently derives the traffic flow distribution matrix $M^{(l)}_{dist}$ according to the solution to (2.6). Based on $n_{i,j}$ values derived in l-th update window, the sink makes a traffic flow distribution matrix $M^{(l)}_{dist}$ whose elements m_{ij} represent the probability that the i-th node is assigned as next hop to the j-th node, $\sum\limits_{i\in\{1,\ldots N\}\setminus j} m_{ij} = 1$. Consequently, in the beginning of every transfer round, along with the beacon packet which is broadcast for synchronization purposes, the next hop for every sensor is randomly selected based on $M^{(l)}_{dist}$ and is transmitted along with the beacon. The distribution matrix is used until the next update window starts, transmit power levels are updated and the new flow distribution matrix $M_{dist}^{(l+1)}$ is derived.

The sink thereafter broadcasts calculated transmit power levels which are used by nodes over the data transmission phase of the update window. During the transmit power selection period, nodes still transmit their main data packets in allocated GTS slots. However, this is done in single-hop manner because maximum transmit power level, P_{tx}=0 dBm, suffices for PDR=99% for all the nodes considered in this study, whereas data end-to-end transfer delay is 250 msec.

Data Transmission

This phase starts once the sink calculates the transmit power levels and the corresponding lifetime maximizing link likelihoods. At this stage, beacons broadcast by the sink in the beginning of each beacon interval (transfer round) are used for synchronization purpose and random assignment of the next hops to each sensor based on likelihood elements m_{ij} in $M_{dist}^{(l)}$. Pseudocode of the proposed algorithm is presented in Algorithm 1.

2.3.4 Measurement Campaign and Simulation Setup

In this section, we first summarize the essential aspects of our data collection tool and measurement campaign to collect path loss samples over on-body links for specific activities, i.e., running, jumping jack, lateral pull downs and rowing. The collected data is used to simulate different components of the proposed algorithm. Further, the action recognition variation explained in Section 2.3.1 in addition to power adjustment which results from Figure 2.3 and our discussion in Section 2.3.1, are simulated based on real collected data. Afterwards we proceed with simulation setup and scenarios that are going to be simulated in Section 2.4.

micaZ Motes: One of the very commonly used transceivers for IEEE802.15.4 WBAN monitoring applications is the micaZ mote developed by Crossbow Technology. The mote contains two major sources of power consumption, the CC2420 transceiver and the MSP430 CPU. The amount of current drawn in different radio modes is given in Table 2.1 [104]. In the next part, we explain the measurement campaign which underlies the evaluation of our proposed algorithm.

Algorithm 1 Pseudocode of the proposed probabilistic link-state routing protocol

BI=250 msec, SD=50 msec

Phase 1: Transmit power selection;

- link assessment
  Packet length=17 bytes, P_{tx}=0 dBm
  For each GTS, sink chooses a transmitter from $\mathbb{S}_t$, whereas nodes $\mathbb{S} \setminus \mathbb{S}_t$ listen $\forall S_i \in \mathbb{S}_t$, $t \leq T_{phase1}$
  - Nodes S_i broadcasts link assessment packets in the allocated GTS
  - $\forall S_j \in \mathbb{S} \setminus \mathbb{S}_t$, S_j adds $RSSI_{ij}$ to the corresponding RSSI array
- power selection
  - $\forall S_i \in \mathbb{S} \setminus \mathbb{S}_t$, S_i forwards RSSI arrays to the sink
  - Sink applies (2.8), calculates vector $P_{tx,l}^{(i,j)}$ $\forall j \leq N, j \neq i$

Phase 2: Data communication;

packet length=85 bytes, Transmit power levels $P_{tx,l}^{(i,j)}$

After LP relaxation, sink solves the MILP in (2.6) and derives $M_{dist}^{(l)}$.

Based on link likelihood elements m_{ij} in $M_{dist}^{(\mathrm{l})}$, sink assigns next hops and allocates time slots for the upcoming transfer round

Communication starts

RSSI EWMA is monitored over limb-torso links

1. If $\left| r_{l,m}^{(i,j)} - r_{l,m-1}^{(i,j)} \right| > 5\ dB$ go back to Phase 1
2. else go back to line 2 in Phase 2

Measurement Campaign: Here, we describe the measurement campaign used to characterize the path loss between different pairs of nodes during different actions. The measurement campaign has two goals;

1. Derive path loss samples between pairs of nodes in Figure 2.4 during doing five actions and postures of study; jumping jack, running, lateral pulldowns, sit-ups and standing still. These samples will be used to simulate the routing algorithm explained in Section 2.2.2.
2. Derive PDR for different RSSI levels as illustrated in Figure 2.3. This function helps

Table 2.1: micaZ Radio+CPU power consumption

Transceiver mode	Drawn current (Radio+CPU)	Drawn current (Radio)
RX	22.8 mA	18.8 mA
TX, P_{tx}= 0 dBm	21.7 mA	17.4 mA
TX, P_{tx}=-1 dBm	20.3 mA	16.5 mA
TX, P_{tx}=-3 dBm	19 mA	15.2 mA
TX, P_{tx}=-5 dBm	17.3 mA	13.9 mA
TX, P_{tx}=-7 dBm	16.3 mA	12.5 mA
TX, P_{tx}=-10 dBm	14.9 mA	11.2 mA
TX, P_{tx}=-15 dBm	13.6 mA	9.9 mA
TX, P_{tx}=-25 dBm	12.1 mA	8.5 mA

us carry out the transmit power control strategy in (2.8).

As illustrated in Figure 2.6, the study is done for specific activities, including running on the treadmill, jumping jacks, lateral pulldowns, standing still and sit-ups. At the time of data collection, the subject who is the second author of this paper, was a 30-year-old male with an athletic build, 178 cm height and 78 kg weight. Measurements were done with CC2420 RF modules in a middle size fitness room sparsely filled with fitness equipment. The links between every pair of nodes illustrated in Figure 2.4 in addition to a mote mounted on ankle, were tested with 8 different transmit power level shown in Table 2.1 and for 2 minutes allocated to each action. The motes were set to transmit 44 byte packets with 27 bytes allocated to payload and 17 bytes to the header as in [105]. The test repeats for each link, with transmit power levels taking turn in a round-robin manner, and RSSI values being recorded at a maximum frequency of 200 sample/sec with PER values calculated from the logged data.

Sensor Placement and Simulation Setup: Despite conventional WSNs, in WBAN monitoring applications most sensors are constrained to be mounted on specific human body points because some vital features need to be collected from certain points at torso or limbs. In this study, we consider six sensors; ECG, pulse, respiration, glucose, blood flow and temperature which are frequently used in WBAN monitoring applications. As explained earler, apart from temperature and glucose, other four sensors are placed on certain points as illustrated and tabulated in Figure 2.4 and Table 2.2 respectively. Lack of placement constraint for temperature and glucose sensors and the fact that their required sampling rate is well below other sensors help us utilize them as intermediate relays to increase lifetime, as seen in Figure 2.4.

The sink is a ZigBee Coordinator (ZC) whereas every other node is a ZigBee Router (ZR), i.e, is capable of aggregating and relaying data of other sensors. The energy consumed for computation, sensing, generating and aggregating data is not significant compared to the energy consumed by receiver and transmitter radio circuits [106]. For every specific fitness activity, the i-th sensor node adopts a fixed transmit power level, $P_{tx,l}^{(i,j)}$, through the procedure explained in Section 2.2.2 to communicate with the j-th sensor node which is the power required to achieve PER $< 1\%$. In order to accommodate latency requirements, the beacon interval is chosen to be 250 msec which is the duration taken by the sensors to complete one round of data delivery to the sink. In the next section, we explain the results regarding on-body link path loss studies from our measurement campaigns and proceed with numerical study of Algorithm 1 in addition to comparison with existing routing algorithms.

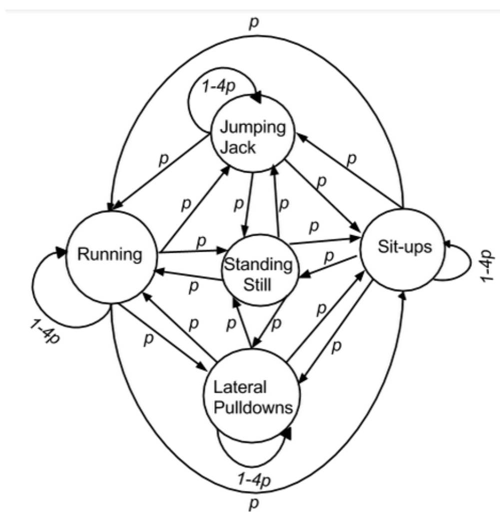

Figure 2.6: Mobility model for simulations; Markov graph of transition probabilities between actions is illustrated. Higher p values translate to shorter duration for a specific action. The case $p = 0.004$ which translates to average duration of 1 minute for each action is considered as a realistic case for patient or fitness monitoring applications

Table 2.2: Monitoring wireless body area network

Sensor number	Sensor type	Placement	Sampling rate (per second)
1	Pulse	palm	1
2	Blood flow	middle arm	20
3	Respiration	neck	80
4	3-lead ECG	chest	200
5	Temperature	upper torso	0.1
6	Glucose	lower torso	0.01

2.4 Results

In this section, we begin by studying the link behaviours observed during our measurement campaign and proceed to evaluate a case of monitoring application introduced in Section 2.3.4 where sensors with different sampling rates are mounted on the upper human body; a WBAN consisting of pulse, blood flow, respiration, ECG, temperature and glucose sensors is shown in Table 2.2. For the sake of simplicity and without lack of generality, we assume that only one ECG lead is being used, even though we can generalize it to the 3-lead case given that packet size will change accordingly to accommodate the corresponding data. As stated in the action variation recognition strategy in Section 2.3 and depicted in Figures 2.7 and 2.8, *limb-torso* links are a suitable indicator in order to tell action variations and trigger transmit power selection phase.

In order to illustrate this phenomenon, two links during a variety of actions with fixed power level $P_{tx} = 0$ dBm are depicted in Figure 2.7. As seen in Figure 2.7b, specific change of actions may impose remarkable path loss variations over limb-torso links. In Figure 2.8, larger variations of path loss over limb-torso links during the course of one action, i.e., Figure 2.8a, and also larger path loss difference among multiple actions over these links, i.e., Figure 2.8b are illustrated.

As shown in Figure 2.9, the minimum transmit power level, P_{tx}=-25 dBm, suffices to achieve PER $\approx 1\%$ for *limb-limb* or *torso-torso* links that exist in Figure 2.4. However, these plots are not shown since they lie on the zero PDR level. In contrast to these links, much higher transmit power levels are needed for limb-torso, e.g., links from 1st and 2nd sensor nodes to the sink in Figure 2.4. Moreover, actions and body movements result in increased shadowing over limb-torso links and demand higher fixed transmit power level in order to meet QoS requirements.

In Section 2.3.2, we described the LP relaxation applied to the MILP problem expressed

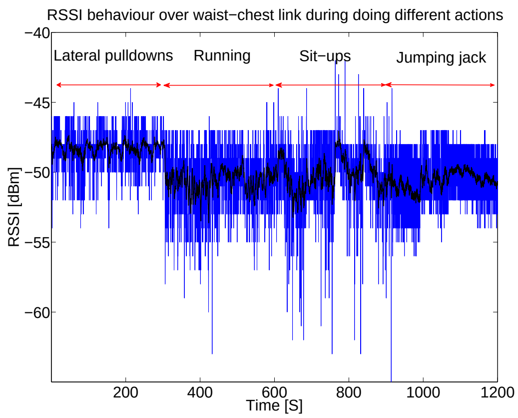

(a) waist-chest

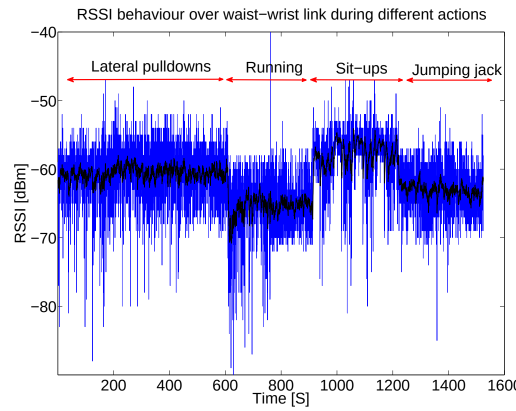

(b) waist-wrist

Figure 2.7: RSSI behaviour over waist-chest link on the subject person during four actions of lateral pulldowns, running, sit-ups and jumping jack with $P_{tx} = 0$ dBm is shown in (a), while waist-wrist link for the same round of actions is illustrated in (b). Black function shows the EWMA with $\alpha = 0.05$ over RSSI behaviour; As could be seen, RSSI over limb-torso link is a better indicator of action variations.

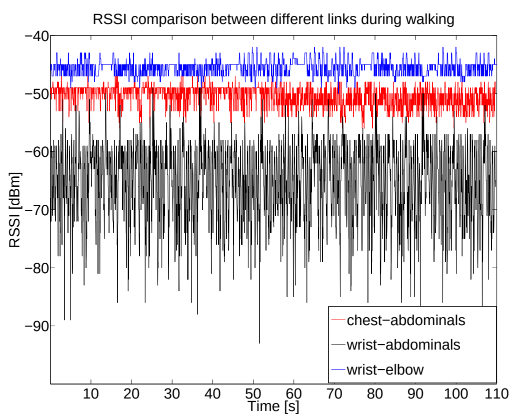

(a) RSSI comparison for different links during running

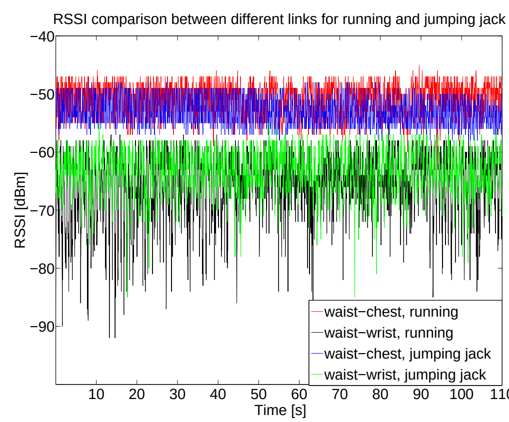

(b) RSSI comparison for different actions and links

Figure 2.8: RSSI behaviour on limb-limb, torso-torso or limb-torso links for $P_{tx} = 0$ dBm are shown during walking in (a) and during jumping jacks in (b). When action changes, most RSSI variations occur on limb-torso links rather than torso-torso or limb-limb links.

in (2.6) and also introduced the parameter IG. In Figure 2.10, we show that applying the relaxation even when the energy remaining in the sensors is small, e.g., 1 J, yields an acceptable approximation error, i.e., around 1%. For this scenario, the activity type is randomly

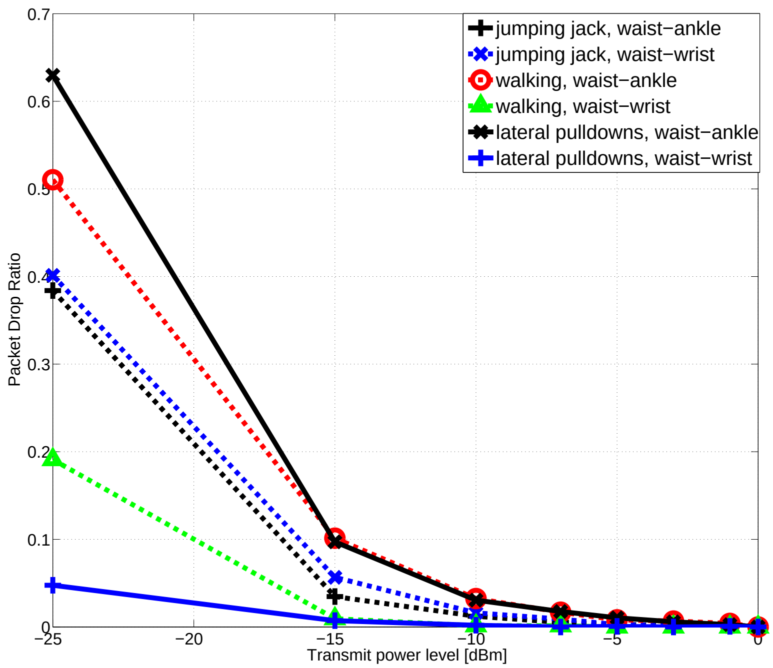

Figure 2.9: PER with respect to transmit power level for different on-body links and fitness activities; Higher transmit power level is required to achieve the desired PDR on limb-torso links compared to torso-torso or limb-limb links

chosen every 60 seconds out of five activities of interest. Even for small energy remaining in the sensors, n_{ij} values are either 0 or fairly large, of the order of 10^3, hence relaxation and rounding do not sacrifice any remarkable accuracy. As defined in Section 2.2.2, the traffic flow distribution matrix $M_{dist}^{(l)}$ gives the ratio of transfer rounds in the update window, that each node must spend communicating with other nodes so that network lifetime becomes maximized. In order for energy depletion to be totally balanced, size of update window W_l should be large enough compared to transfer round size so that probabilistic selection of next hops based on $M_{dist}^{(l)}$ result in next hop ratios which actually comply with elements m_{ij} in $M_{dist}^{(l)}$. Moreover, the ideal case is for the whole network lifetime to consist of only one update window so that the n_{ij} values derived in (2.6) are deterministically applied.

In Figure 2.11, the communication overhead of transmit power selection phase, PER and energy depletion in sensors with respect to action transition probability p for the pro-

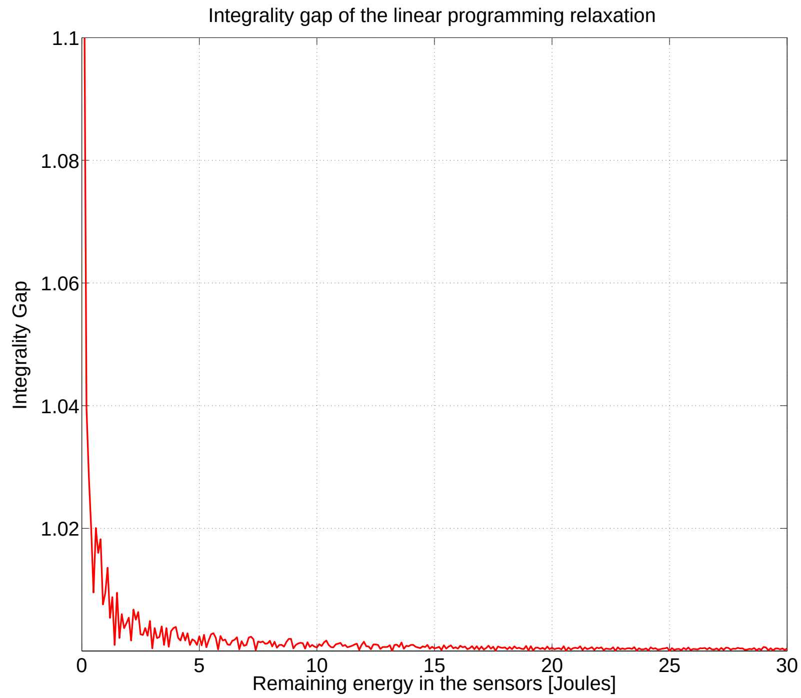

Figure 2.10: IG with respect to remaining energy in the sensors; It can be seen that applying relaxation to (2.6) results in approximation error below 1% even for relatively small values of remaining energy, $\approx 1\ J$

posed routing protocol are illustrated. We define communication overhead as the ratio between energy consumed in Phase 1 of the routing protocol proposed in Algorithm 1 and total energy consumption in the network. As a more realistic WBAN scenario, we assume the case $p = 0.004$ for the mobility model shown in Figure 2.6 which translates to average duration of 1 minute for each action. Figure 2.11b shows balanced energy depletion of sensors under this condition.

In Table 2.3, link-state and cluster-based WBANs are benchmarked in terms of relative advantages and drawbacks. In Dijkstra-based routing algorithm [53], remarkable additional reception energy consumption is expended in nodes since each node listens to beacon packets transmitted by all other nodes in the beginning of a transfer round. However, in terms of connectivity, the algorithm is powerful due to its frequent link assessments. In PRPLC [49], transmit power is fixed and next hop is chosen based on its probabilistic connectivity to the

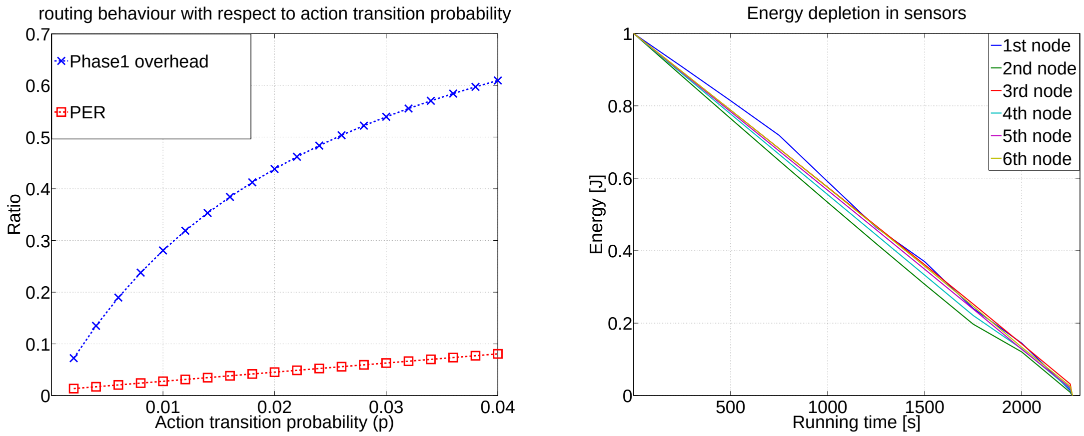

(a) (b)

Figure 2.11: Performance of the proposed link-state routing protocol; (a) shows communication overhead and PER with respect to action transition probability. The larger frequency in action variations translates to less energy efficiency of the proposed protocol. Balanced energy depletion in sensors is depicted in (b).

Table 2.3: Benchmark of different link-state and cluster-based routing protocols in terms of networking metrics

Routing protocol	PRPLC	Dijkstra-based	HIT	Probabilistic link-state
Pros	1-very good connectivity 2-useful for ultra-short range transceivers and delay tolerant applications	1-very good connectivity, delay 2-very good lifetime for high data rate applications	good lifetime for line networks on a single limb or torso and immobile scenarios where log-distance path loss model applies	1-Very good network lifetime 2-Acceptable connectivity for continuous actions 3- Very low control message overhead
Cons	1-high control message overhead, 2-high delay and poor lifetime	1-large control message overhead for low data rate applications 2-poor lifetime for low data rate applications	1-Low network lifetime for mobile scenarios	1-poor connectivity for short actions and postures, 2-high control message overhead for short actions

sink. Even though PRPLC beats our algorithm in terms of connectivity, balanced energy consumption is not achieved. Further, PRPLC is best suited to intermittently connected WSNs which are either made up of ultra-short range transceivers or work based on minimum transmit power level on CC2420 transceivers and for applications with high delay tolerance.

Comparison with Cluster-based Routing Protocols: LEACH [54] and PEGASIS [55] are the two most popular cluster-based WSN routing protocols. Further, LEACH and PEGASIS work based on forming clusters and chains of nodes respectively and having a cluster head (CH) aggregate the data and forward it to the BS. Intra-cluster and intra-chain communication in LEACH and PEGASIS are performed in multi hop and direct manner respectively. These protocols have inspired more energy efficient extensions such as Energy-LEACH (E-LEACH), Multihop-LEACH (M-LEACH) [107], and techniques like Anybody [42], Hybrid Indirect Transmission (HIT) [43] that are specifically devised for WBANs. HIT is a combination of LEACH and PEGASIS in the sense that in every cluster, packets are forwarded to the CH in a multi hop manner and the aggregated data will be transmitted to the BS afterwards [43].

Table 2.4: Lifetime comparison between the proposed probabilistic routing protocol and cluster-based algorithms with 100 J energy available for each sensor

Action \ Different techniques	HIT	E-LEACH	Single hop	proposed probabilistic routing
Walking	28h	40h	57h	65h
Jumping Jack	29h	41h	57h	69h
Rowing	29h	40h	57h	71h
Lateral Pulldowns	29h	40h	57h	71h

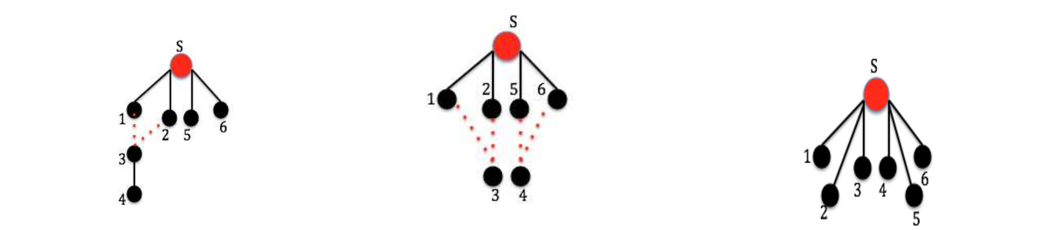

(a) Spanning tree with three levels
(b) Spanning tree with two levels
(c) Spanning tree with one level

Figure 2.12: Simulating the algorithm for running activity; LP results in 12 spanning trees with one, two and three levels; some of which are illustrated. Solid lines are fixed in every graph whereas dotted lines show the alternatives each node could forward the data to.

In both HIT and E-LEACH, a gateway is designated at each transfer round to aggregate data from all other sensors and forward them to the sink. Further, in E-LEACH and HIT implementations, the portion of transfer rounds each node takes up as gateway is chosen so that network lifetime is maximized with the constraint being put on the structure of the spanning trees which are assigned. As can be seen from the position of non-zero elements

(a) E-LEACH spanning tree (b) HIT spanning tree

Figure 2.13: General spanning tree topologies resulted from HIT and E-LEACH techniques; E-LEACH yields two level trees whereas HIT which is inspired by PEGASIS yields 4 level trees. In both cases one gateway is responsible for data aggregation and forwarding it to the sink whereas nodes become gateway in a round-robin manner

$$M_{dist}^{(\text{walking})} = \begin{pmatrix} 0 & 0 & 0.23 & 0 & 0 & 0 \\ 0 & 0 & 0.18 & 0 & 0 & 0 \\ 0 & 0 & 0 & 0.07 & 0 & 0 \\ 0 & 0 & 0 & 0.25 & 0 & 0 \\ 0 & 0 & 0 & 0.35 & 0 & 0 \\ 1 & 1 & 0.59 & 0.32 & 1 & 1 \end{pmatrix} \quad M_{dist}^{(\text{jumping jack})} = \begin{pmatrix} 0 & 0 & 0.18 & 0 & 0 & 0 \\ 0 & 0 & 0.13 & 0 & 0 & 0 \\ 0 & 0 & 0 & 0.03 & 0 & 0 \\ 0 & 0 & 0 & 0.25 & 0 & 0 \\ 0 & 0 & 0 & 0.29 & 0 & 0 \\ 1 & 1 & 0.69 & 0.43 & 1 & 1 \end{pmatrix}$$

$$M_{dist}^{(\text{rowing})} = \begin{pmatrix} 0 & 0 & 0.18 & 0 & 0 & 0 \\ 0 & 0 & 0.13 & 0 & 0 & 0 \\ 0 & 0 & 0 & 0.03 & 0 & 0 \\ 0 & 0 & 0 & 0.25 & 0 & 0 \\ 0 & 0 & 0 & 0.29 & 0 & 0 \\ 1 & 1 & 0.69 & 0.43 & 1 & 1 \end{pmatrix} \quad M_{dist}^{(\text{lateral pulldowns})} = \begin{pmatrix} 0 & 0 & 0.18 & 0 & 0 & 0 \\ 0 & 0 & 0.13 & 0 & 0 & 0 \\ 0 & 0 & 0 & 0.03 & 0 & 0 \\ 0 & 0 & 0 & 0.25 & 0 & 0 \\ 0 & 0 & 0 & 0.29 & 0 & 0 \\ 1 & 1 & 0.69 & 0.43 & 1 & 1 \end{pmatrix} \tag{2.9}$$

in (2.9), the distribution matrices that result from applying our proposed algorithm to different actions are very similar. Furthermore, for the four shown actions, in every assigned tree, 1st, 2nd, 5-th and 6-th nodes directly communicate with the sink whereas 3rd and 4-th nodes have other alternatives as well. Distribution matrices derived in (2.9) translate into 12 spanning tree graphs some of which are illustrated in Figure 2.12. As observed in derived matrices in (2.9), the highest probability is assigned to the 1-level graph therefore the mean hop count a packet takes to reach the sink is close to one whereas energy depletion is balanced as illustrated in Figure 2.11b.

On the other hand, general spanning tree structure of HIT and E-LEACH is illustrated in Figure 2.13. As can be seen in E-LEACH all spanning trees are two level with nodes taking turn to adopt gateway role (3rd node is the gateway in Figure 2.13) whereas in HIT, trees could have different number of levels based on the node which has been assigned as gateway, e.g., 6-th node being assigned as gateway results in a 6-level tree. Therefore, due to the general structure of the spanning trees defined for these techniques, the mean hop count is higher than that of single hop communication and the proposed probabilistic routing algorithm.

As stated in Table 2.3, even though HIT yields suitable lifetime for log-distance path loss model where transmission to the closest neighbour saves energy, it is not necessarily an energy-efficient option for mobile scenarios and transceivers with high reception power. Note that even though balanced energy depletion is achieved in these techniques, mean hop count that each packet takes in order to reach the sink is high and lifetime is far from maximum as well. In Table 2.4, our proposed algorithm is compared to classic and popular cluster-based routing protocols in terms of network lifetime. Since our proposed transmit power control can be used in complementary with these cluster-based protocols, in order for the comparison to be fair and only be focused on the impact of routing and assigned routing spanning trees, we have applied the same transmit power control strategy to E-LEACH and HIT. The reason these protocols perform worse than single-hop communication is the structure of their assigned routing spanning tree which does not allow direct transmission which is a suitable communication form due to relatively high reception energy of CC2420 transceivers. In Figure 2.14, applicability range of the proposed routing algorithm is shown. As can be seen the number of sensors is limited by characteristics of TDMA-based IEEE802.15.4 MAC layer. The step function is the result of fixed maximum number of guaranteed time slots in a IEEE802.15.4 superframe illustrated in Figure 2.1. Further for a larger number of sensors, one should consider using contention-based portion of the superframe as well.

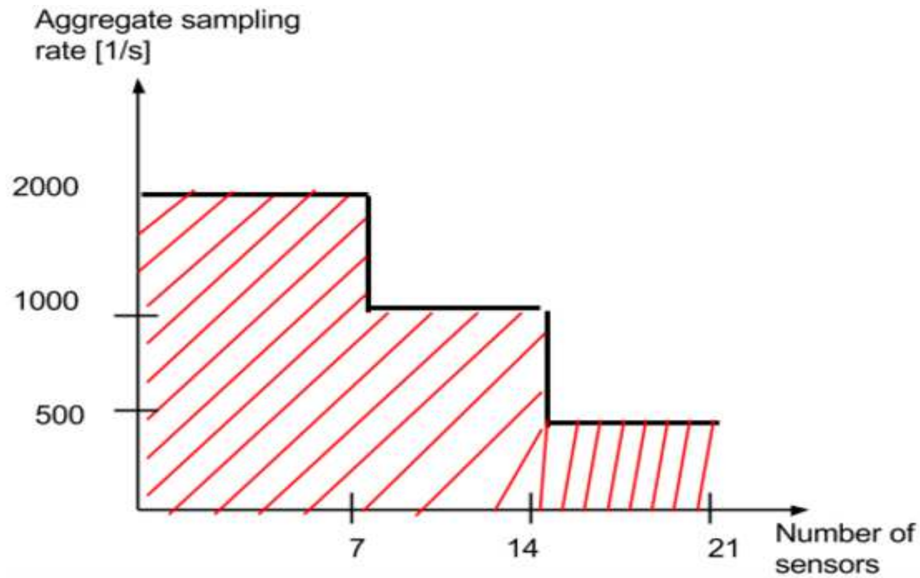

Figure 2.14: Approximate applicability range of the proposed routing algorithm; Shaded region shows the aggregate sampling rate (bandwidth) achievable for different number of sensors

2.5 Discussion

In this chapter, we have proposed a link-state routing protocol that uses LP techniques and transmit power adjustment to maximize WBAN lifetime. The algorithm is best suited to maximizing WBAN lifetime, and addresses connectivity in monitoring applications and mobility models which involve stationary postures associated with routine daily activities. In our proposed algorithm, we overcome communication overhead imposed by real time link assessment, calculation complexity caused by routing table calculation, and address lifetime maximization by: 1) monitoring RSSI in a dynamic and distributed manner on data packets communicated over links, therefore performing link assessment and changing the transmit power levels only when sharp fluctuations in EWMA of RSSI is observed, 2) only accounting for limb-torso links in the link assessment process because RSSI variations over limb-limb or torso-torso links are not remarkable in terms of the required transmit power level, 3) using LP to derive link likelihoods.

The proposed routing protocol is suboptimal for two reasons; 1) the limited duration of each action which results in the algorithm not fulfilling the exact derived link likelihoods since the number of transfer rounds within an update window is limited, 2) LP relaxation; the lifetime maximization problem is in fact a MILP. In the work proposed here, specific characteristics of IEEE802.15.4 MAC are taken into account to derive LP formulation of the lifetime maximization. Accordingly, this work applies to WBANs which are built upon IEEE802.15.4 MAC layer. As a future practice, deriving lifetime maximization LP for other standards, e.g., IEEE802.15.6 would be very useful. Moreover, IEEE802.15.6 mostly supports one and two hop star networks, therefore new design constraints are needed. Note that due to the limitations of TDMA-based IEEE802.15.4 MAC which mandates that all time slots have equal durations, the proposed algorithm may not be efficient in terms of bandwidth utilization. Therefore, design of MAC protocols with dynamic time slot duration and variable time slots throughout a transfer round would help to ensure more efficient utilization of bandwidth should larger number of sensors are deployed.

Chapter 3

Periodic Connectivity in Body Area Networks and Its Implications for Scheduling

3.1 Introduction

In this chapter, we propose an energy efficient scheduling algorithm for a particular class of actions so-called periodic actions and a specific class of applications which are delay tolerant. That is: 1) Firstly, we show that a group of actions (particularly fitness) are periodic in the sense that some links (extremity-torso) show periodic and predictable connectivity behaviour, 2) Secondly, we propose a scheduling technique along with transmit power adjustment to take advantage of predictability over these links for lower energy consumption. Moreover, the periodicity of on-body links is employed to predict the future behaviours of links so that energy-efficient communications between on-body nodes is established, thereby network lifetime is elongated. This scheduling technique can be used in complementary with WBAN routing protocols such as the proposed work in Chapter 2. Moreover the periodicity enables single-hop communication with sink at low transmit power, hence saves remarkable energy.

WBANs, as also defined in Chapter 1, are a subclass of WSNs which consist of a set of sensing nodes worn on the human body or implanted into the tissues. After the observations are made by the sensing nodes, they are sent to a centralized data monitoring and processing centre, i.e., an off-body base station or an on-body sink node usually mounted on the left waist, by means of wireless communications so that relevant decisions are made or data is logged. As mentioned in Chapter 1, in WBANs frequent replacement of the batteries should be avoided as battery replacement particularly for implanted sensors is not an easy task to accomplish. Therefore, it is necessary to lower the power consumption in the WBAN. Wireless communication is the most energy consuming task performed by the sensor nodes

[108]. This causes development of energy-aware communication protocols and mechanisms to contribute the most to elongating batteries lifespan. Improvements in battery longevity can be achieved with several means among which lowering transmit power level is significantly important.

In general, several scheduling techniques have been proposed for WBANs. Store and forward scheduling techniques [56, 57] increase likelihood of a packet reaching its destination by storing the packet at multiple hops which however heavily increases energy consumption [53]. Transmit power control strategies [52] that work along with some of these techniques still result in high overhead due to frequent link assessments associated with transmit power adjustment. Opportunistic scheduling techniques [58–60] which uses temporal and spatial diversity of the channel to allocate bandwidth to the user with a more suitable channel state also suffer from communication overhead. Most of the opportunistic techniques are designed to maximize resource utilization in the network while providing fairness among users. Only a few of the opportunistic scheduling studies consider the power constraints in the design of their algorithms [80, 81]. In these studies, the transmission power is adjusted to the condition of the underlying fading channel for achieving a desirable data rate. However, the continuous link assessment make these techniques incompatible with WBANs where nodes ideally turn their radio off as an energy-saving measure until it is their turn to transmit. Another class of WBAN scheduling techniques focus on adaptive or optimized GTS allocation in IEEE802.15.4 WBANs in order to meet latency and fairness requirements or to make best use of bandwidth [61, 62, 109]. The idea in power management techniques [56, 98, 105, 110] is to exploit real-time link assessment in order to adapt the level of transmission power to the variable nature of the channel caused by shadowing. In real time link assessment the transmission power level is adapted to the current condition of the links. All these studies only focus on the cases with fixed or very slow moving nodes. However, in most daily activities WBAN is a highly dynamic network and the on-body links are highly dynamic, thereby the aforementioned acknowledgement-based schemes yield significant power control traffic which is not power efficient.

Furthermore, in most of these works, emphasis is on latency and bandwidth requirements rather than to increase energy efficiency. One of the intrinsic characteristics of WBANs that the aforementioned studies do not take advantage of is periodicity of most prolonged body actions. Lots of daily routine activities, e.g., walking, running and fitness activities involve periodic body movements which result in periodic connectivity of some links as a result of severe shadowing caused by limbs obstructions or internode distance variation. We believe that the periodic nature of the actions can be exploited in the design of scheduling techniques as an effective approach towards power efficiency in WBANs. For applications with looser deployment requirements, i.e., in terms of latency, priority and node placement, action recognition along with predictability of connectivity over specific limb-torso links during periodic actions are exploited to propose a scheduling algorithm along with transmit power adjustment in order to achieve high energy efficiency.

In this chapter we propose a novel action-based scheduling technique in order to reduce energy expenditure. Further, we show that direct, i.e., single hop, transmission with low transmit power level is possible over many links which suffer from a high degree of shadowing, in case we make use of predictable behaviour of these links during specific actions. In the proposed algorithm, RSSI levels of on-body links are measured in a real time manner and are subsequently used by the naive Bayes algorithm for action recognition. Once the action is recognized, given that periodic behaviour of specific links is known to sink, GTS allocation is carried out so that single hop transmission over periodic links with low transmit power levels becomes possible. To the best of our knowledge, this is the first time that a scheduling technique exploits the periodic behaviour of on-body links for packet transmission.

The remainder of this chapter is as follows: in Section 3.2 we explain concepts such as connectivity, periodic and non-periodic links, action recognition and also energy consumption lower bound, i.e., given that complete global knowledge about future behaviour of path loss is available. The lower bound provides us with a benchmark to assess our proposed technique. In Section 3.3, we explain mechanism of our RSSI-based action recognition technique which does not need any IMU sensor in addition to our scheduling technique. Finally we do the performance evaluation and explain the results in Section 3.4, and wrap up the chapter with conclusion in Section 3.5.

3.2 Concepts

In this section, we define some key concepts and terminologies in addition to nature of the scheduling problem that will be used in the rest of the chapter. Note that system model in terms of radio model and MAC layer characteristics is the same as Section 2.2.1 discussed in Chapter 2. However in terms of data delivery model, the technique discussed in this chapter is mostly suited to query-driven applications or continuous application with large delay tolerance. Further, as discussed in Section 3.1, the proposed technique is well-suited to delay tolerant applications where periodic links wait for their allocated GTS to arrive during their good channel state behaviour. In the following, we first explain periodic actions, and go on to define connectivity, periodicity and classification of links into periodic and non-periodic types.

3.2.1 Periodic Actions

Periodic actions have been recognized in the literature for a long time [111, 112]. In fact classification of actions into periodic and non-periodic has been done in [111], while the periodicity attribute has been used for action recognition in both works. Activities such as walking, running, swimming, sit ups and many more daily activities particularly in fitness context which follow a repetitive pattern in motion are known as periodic actions. Even though periodicity has been used for action recognition, using this important characteristic to achieve energy efficiency in WBANs has widely been ignored.

3.2.2 Connectivity, Periodicity and Link Classification

Assuming that transmit power level is employed in a discrete manner which is the case for most IEEE802.15.4 compliant modules, connectivity function $C_{kj}(t)$ for k-th link and j-th transmit power level $P_{Tx} = P_{tx}^{j}$ is defined as

$$C_{kj}(t) = \begin{cases} 1 & ; \; P_{Rx} > \gamma, P_{Tx} = P_{tx}^{j} \\ 0 & ; \; P_{Rx} < \gamma, P_{Tx} = P_{tx}^{j} \end{cases}, \tag{3.1}$$

where γ is the minimum required received packet power which can be determined so that the successful reception of the packet is guaranteed. In our performance analysis, we define the threshold as $\gamma = -85$ dBm because it guarantees high packet delivery ratio and also lies within the required threshold range derived in [56]. k-th link is periodic when there exists at least one j that renders the connectivity function C_{kj} periodic with action period T, $C_{kj}(t) = C_{kj}(t+T)$. On the other hand non-periodic links follow more random path loss behaviour. The links studied in Chapter 2 were treated as non-periodic links because we only took advantage of their stationarity for transmit power adjustment.

3.2.3 Scheduling for Periodic Actions

In IEEE802.15.4 WBAN context, the purpose from scheduling is to allocate time slots to nodes so that applications requirements in terms of latency and bandwidth are met. As discussed in Section 3.2.2, specific links show periodic behaviour during specific actions. This adds extra amount of predictability to stationary actions studied in Chapter 2. Further, in Chapter 2 we only took advantage of stationarity of links for transmit power adjustment. However, in this chapter, we show that periodic connectivity of links helps us adopt single-hop communication with low transmit power levels, therefore save more energy. The key to such a time slot allocation is action recognition so that sink becomes aware of periodic links and does the power adjustment accordingly. Moreover, in this work we assume that action's period is fixed and once the action is known, the periodic links along with their connectivity behaviour are known. This may not be a realistic assumption for real world scenarios, however it serves as a case study in order to prove the energy efficiency that can be achieved over periodic links. In the next section, we explain our action recognition technique.

3.2.4 Action Recognition

Action recognition is the first step en route to our WBAN scheduling technique. Several works have been previously done on action recognition using on-body sensors [113–115]. In these works, IMU sensors are used to capture limbs acceleration and angular velocity in two directions: inclination angle θ and azimuth angle ϕ. Features, e.g., mean, standard deviation, root mean square, first and second derivatives [115] are then extracted from the collected parameters in different time segments. They are subsequently transmitted to the sink so that the action is decided based on hidden Markov model (HMM). In [113], angular velocity and acceleration parameters in time windows of certain size are transmitted to a BS which uses a set of training motion sequences to classify the actions. The action recognition technique proposed here, is more economical because sensor nodes are not required to be equipped with accelerometers.

Our technique is also superior in terms of classification time which means it only takes one action period to do action recognition. In most periodic fitness activities, some torso-limb links are likely to experience periodic connectivity bevahiour, e.g., wrist-waist during jumping jack or ankle-waist during running. We can use these torso-limb links to extract features such as path loss mean and standard variation. Assuming that these features are independent, naive Bayes algorithm is used as the classification tool. Even though naive Bayes classification is meant to be working for independent features, it often shows a good performance for more complex situations as well [116]. The algorithm is linear in time for both training and testing, therefore has optimal time complexity [117]. Even though in our setup we only use two on-body links, i.e., wrist-waist and ankle-waist for action recognition, it can be easily and intuitively observed that applying more links help us recognize more actions and with better accuracy. Action classification setup will be explained in Section 3.3.1.

3.2.5 Energy Consumption Lower Bound

In this section, we explain how to derive a lower bound on energy consumption of an arbitrary network which consists of n links that are going to be provided with time slots for TDMA communications. The lower bound in fact enables us to discover how the suggested scheduling and power adjustment technique helps us reach closer to the power consumption lower bound on so called periodic links than over non-periodic links. Moreover the purpose from this derivation is to observe how close the periodic link behaviour helps us get to the case where future behaviour of the link is totally known. In order to derive such a lower bound, the BS is assumed to be aware of channel behaviour on both types of links. Moreover there exists a global awareness about channel behaviour of on-body links. Therefore even though no real-time channel assessment is conducted, packet failures and retransmission do not occur over the links. Note that even though this is not a realistic assumption in the real world scenarios, it provides us with a useful benchmark for the comparison conducted in Section 3.4.

Let P_{ki}^{j} represent the power drawn from the transceiver battery when transmit power $P_{Tx} = P_{tx}^{j}$ is employed whereas P_{tx}^{j} is the minimum level required to have a successful packet transmission at i-th time slot over k-th link. Suppose r_k is the required data rate for k-th link and m is the data packet length in bits for each transmitted packet while R denotes transmission bit rate of the standard, e.g., IEEE802.15.4. This demands for $n_k = \frac{r_k.T}{m}$ time slots per action period to be allocated to k-th link, where T is period of the action. We need to allocate time slots and transmit power levels to the nodes so that

- only one node is permitted to transmit during a particular time slot,
- required data rate over both links is met,
- aggregate power consumption of transceivers is minimized.

This translates to the following optimization problem:

$$\min\Big(\sum_i \sum_k \alpha_{ik} P_{ki}\Big) \text{ subject to}$$
$$\begin{cases} \sum_{i=1}^{n} \alpha_{ik} > n_k & ;\ \forall k = 1, 2 \\ \alpha_{ik} \in \{0, 1\} & ;\ \forall i = 1, 2 \cdots, n, \forall k = 1, 2 \\ \alpha_{i1} \wedge \alpha_{i2} = 0 & ;\ \forall i = 1, 2 \cdots, n \end{cases}, \tag{3.2}$$

where α_{ik} denotes channel access permission factor for the kth link at i-th time slot. Moreover, $\alpha_{ik} \in \{0, 1\}$ is a bit which takes on 1 if access at i-th time slot is given to the k-th link, takes on 0 when permission is not granted. In (3.2), P_{ki} is the power drawn from battery which is associated with minimum transmit power level that guarantees connectivity on k-th link at i-th time slot, i.e., condition $P_{Rx} > -85$ dBm is met. Note that transmitter's power consumption with respect to transmit power level, as also described in Section 2.2.1, is an increasing function [118]. In the third constraint, $\wedge$ operator denotes logical AND. Second and third constraints force only one packet transmission during a single time slot and prevent simultaneous transmission on links as it causes interference. Note that even though in (3.2) we are concerned with energy consumption, time slot duration is not involved because it is assumed to be fixed over the whole action period and is one packet long in terms of transmission duration. It is again worth mentioning that (3.2) denotes aggregate energy consumption where single-hop communication is adopted for all nodes. Our measurements help us determine P_{ki} values. This optimization is a binary integer linear programming which is a NP-hard problem and can be solved with MATLAB for different required data rate vectors $\mathbf{r_k}$. Note that the calculated lower bound is not practically obtainable since transmitter is oblivious to future link behaviour. In the next section, we explain our methodology that leads to our proposed scheduling algorithm in addition to the measurement campaign and simulation setups that are going to be numerically studied in Section 3.4.

3.3 Methodology

In this section, we explain practical considerations regarding implementation of our proposed scheduling algorithm. Further, we explain how the action recognition and transmit power adjustment phases work on a IEEE802.15.4 WBAN.

3.3.1 Proposed Scheduling Technique

As stated in Section 3.2.2, we divide on-body links into two types of periodic and non-periodic. In this section, we exploit our proposed link classification in order to devise a scheduling technique that works without frequent link assessments. The technique works based on periodicity and predictability of periodic links introduced in this chapter and stationary behaviour of non-periodic links which were discussed in Chapter 2. Note that, in ideal circumstances in terms of bandwidth utilization for TDMA-based communication, there should be no overlap among connected sessions of periodic links so that maximum number of time slots is granted to each node. However, this may not be possible as number of nodes increases in realistic real world scenarios. In case, we are not looking to take advantage of periodic behaviour, the transmit power adjustment proposed in Chapter 2 along with scheduling formulation in (3.2) can be used for time slot allocation.

This work is a case study and only serves as a proof of concept for energy efficiency that is achievable over periodic links which suffer high shadowing. Therefore, scheduling for multiple periodic links to maximize bandwidth utilization remains as a future work and is out of scope of this chapter. In this work, we assume there are only two single hop links from extremities to sink which is mounted on waist is available. As a scheduling strategy, we suggest using the connected session of the periodic link with low transmit power levels whereas the other part of the action cycle, i.e., during which the periodic link is not available, is allocated to the stationary non-periodic link with adopting fairly high transmit power levels, i.e., with power adjustment strategy proposed in Section 2.3.1.

Let $\delta_k(j)$ denote probability of packet reception failure on k-th link when $P_{Tx} = P_{tx}^j$, $\delta_k(j) = P(P_{Rx} < -85 \text{ dBm} | \mathrm{P_{TX}} = \mathrm{P_{tx}^j})$, where $P(\cdot)$ denotes probability function. We summarize the criteria for choosing index j in P_{tx}^j as follows;

$$j : \begin{cases} \underset{j}{\operatorname{argmin}} \, (P_{tx}^j | C_{kj}(t) = C_{kj}(t+T)) \ ; \ \text{periodic links} \\ \text{same as Section 2.3.1} \ ; \ \text{non-periodic links} \end{cases} . \tag{3.3}$$

We solve (3.3) separately for both links, while the idea is to choose suitable fixed transmit power levels that can satisfy (3.3). As noted earlier, power adjustment technique expressed in (3.3) has been justified in Sections 3.2, 2.3.1. After any action variation trigger, allocated time slots and required transmit power levels will be sent along with the beacon that sink broadcasts for synchronization purposes at the end of each transfer round.

Action Recognition: As explained in Section 3.2.4, action classification is one of the major components of our study. Furthermore, we assume that once the action is known, the behaviour of periodic links in terms of connected sessions is known whereas behaviour of non-periodic links in terms of their stationary behaviour is recognized as described in Chapter 2. An important issue to be considered in the design of our algorithm is that sink is able to recognize when one action is cut and another has started so that it can reschedule the links. Trigger of the action recognition phase is done based on the procedure explained in Chapter 2, i.e., Section 2.3. The transceivers mounted on extremities will then be triggered to stop data transfer whereas sink runs action recognition test again. Sink node sends short test packets, i.e., 17 byte long packets which is PHY/MAC header size and the minimum ZigBee packet size, to wrist and ankle nodes during a single period of the action that is known. These nodes read the RSSI levels, extract mean and standard deviation and send them back to the sink where naive Bayes algorithm is run to classify the actions. Once the action is recognized, the time slot allocation is determined based on the scheduling technique described in Section 3.3.1.

Training and Test Set: As discussed in Section 3.2.4, naive Bayes classification method is used for action recognition in this chapter. As will be explained in the next section, our data set is composed of four actions, 3 minute long each. With action period being 1 second, there are 180 mean and standard variation feature points available for each action. We allocate 135 and 45 points per action to training and test sets respective. Gaussian model for the training feature set in each class is calculated for mean and standard variation of the observed path loss points. Maximum a posteriori (MAP) decision rule is then applied to classify the test set. Accuracy of our action recognition technique will be discussed in Section 3.4.

3.3.2 Measurement Campaign and Simulation Setup

In order to proceed with numerical study of the proposed action recognition and scheduling, we need to capture path loss behaviour of the studied on-body links. In this work we study four periodic fitness actions: jumping jack, running, rowing and lateral pulldowns, with two *on-body* links of wrist-waist and ankle-waist. The reason to choose this node placement setup is its diversity in providing suitable features and various combination of periodic links needed for the proposed action recognition and scheduling technique which will be explained later. Even though we have only studied four actions in this chapter, the same discussion holds for other periodic actions as well. Our measurement tool, as also described in Section 2.3.4, is micaZ CC2420 mote which is widely used in IEEE802.15.4 WSN research studies. The mote is a IEEE802.15.4/ZigBee compliant RF transceiver for low-power wireless applications. We keep the action's period unchanged during the measurements as periodicity plays the major role in our proposed scheduling technique. The period of all four actions of interest is also the same. The subject person is a 29 year old lean male with 178 cm height and 78 kg weight. For each action of interest, waist transceiver is set to send 17 byte length packets within every 5 msec with the maximum power, 0 dBm. The test goes on for three minutes per action with RSSI values being recorded in the extremity transceivers. Note that for micaZ CC2420, received signal power has a linear relationship with RSSI values [118]. In Section 3.4 behaviour of periodic links will be illustrated whereas link classification, i.e., periodic and non-periodic, will be tabulated.

Sensor Placement and Simulation Setup: In terms of simulation setup, the simulated scenarios are very similar to Chapter 2, i.e., explained in Section 2.3.4. However four actions of study are running, jumping jack, rowing and lateral pulldowns. Whereas as opposed to Chapter 2 where several positions for node placement is considered, in this chapter only wrist and ankle have been designated for node placement, while waist is still the candidate for sink's position. In addition to higher diversity and independence in terms of features that would benefit us for simple action recognition explained in Section 3.3.1, this node placement serves our objective which is to show how periodic links help achieve more energy efficiency compared to non-periodic links. In terms of simulation scenarios for studying action classification accuracy and energy efficiency of the scheduling algorithm, the four actions of interest are randomly chosen and each continue for one minute before the new action starts. In the next section, behaviour of periodic links, classification of links for the studied actions, performance of the proposed action recognition technique and energy efficiency of the proposed scheduling technique are illustrated and explained.

3.4 Results

In this section, we present the results regarding behaviour of periodic links, performance of action recognition, and proposed scheduling algorithm in terms of energy efficiency. As observed in our measurement campaign, periodic links in four actions of interest, running (RN), jumping jack (JJ), rowing (RW) and lateral pulldowns (LPD) are tabulated in Table 3.1, while behaviour of two periodic links are illustrated in Figures 3.1 and 3.2. In Table 3.1, we refer to waist-wrist, and waist-ankle with *wrist* and *ankle* links respectively as the waist end is common between them, because sink is usually mounted on waist. As illustrated in Figures 3.1, and 3.2, fairly low transmit power levels result in periodic connectivity sessions over periodic links during jumping jack and running.

Table 3.1: Actions of interest and periodic links

Action	RN	JJ	RW	LPD
Periodic link	Ankle	Wrist	Wrist, Ankle	Wrist

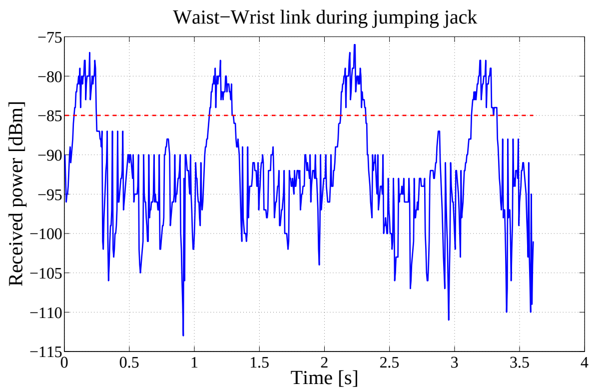

Figure 3.1: Received power over waist-wrist link with $P_{Tx} = -25$ dBm; redline shows the connectivity threshold which occurs when $P_{Rx} = -85$ dBm

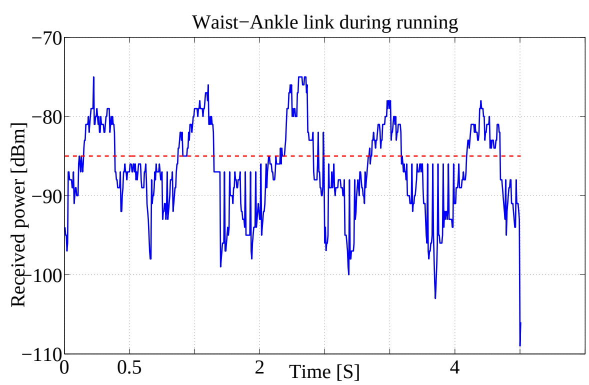

Figure 3.2: Received power over waist-ankle link with $P_{Tx} = -20$ dBm; redline shows the connectivity threshold which occurs when $P_{Rx} = -85$ dBm

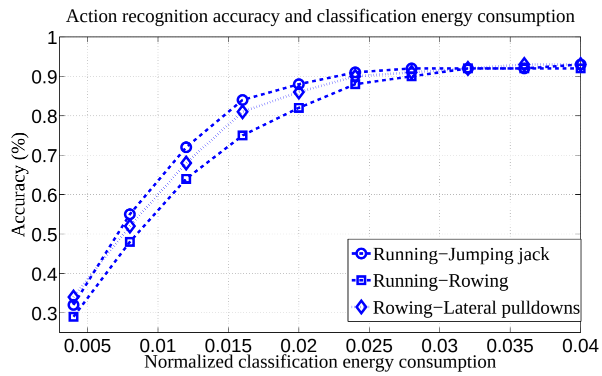

Figure 3.3: Action recognition accuracy with respect to classification energy to aggregate energy consumption ratio for $r = 1kB/s$ with two actions done in a row

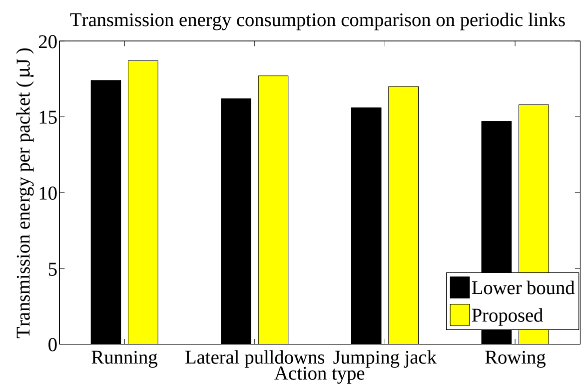

Figure 3.4: Per packet energy consumption comparison between proposed scheduling and lower bound on periodic links

In Section 3.2.4, we described how action recognition in our study works. Classification energy consumption is an important issue because it increases the aggregate energy consumption in the network. Classifier accuracy with respect to normalized classification energy consumption is depicted in Figure 3.3, while the normalizing constant is aggregate energy consumption. The simulation scenario is composed of various combinations of two actions being done in a row for one minute each and with 37 slots/period having been allocated to both links when beacon order is 2, i.e., BO=2. Each point in Figure 3.3 corresponds to a specific rate at which RSSI levels are being sampled over one period for feature extraction. As mentioned earlier in Section 3.3.2, there exists a simple linear relationship between received signal power in terms of dBm and RSSI values. Furthermore, accuracy varies with how fast each link is sampled over each action period by test packets. Higher data packet

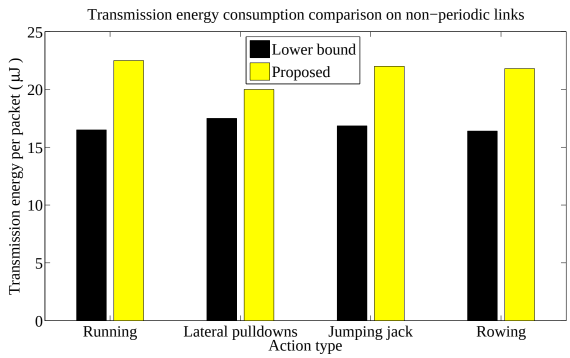

Figure 3.5: Per packet energy consumption comparison between proposed scheduling and lower bound on non-periodic links

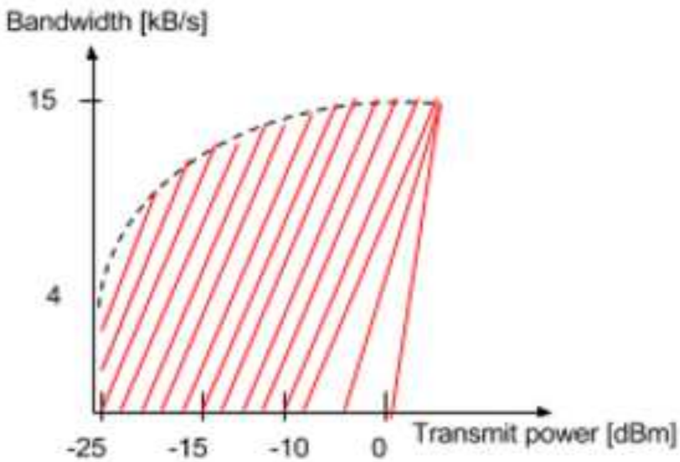

Figure 3.6: Approximate applicability range of the proposed scheduling algorithm; Shaded region shows the achievable bandwidth to meet PDR>95% over a periodic link for different transmit power levels

rates will obviously result in lower classification energy ratios for the same action duration. As seen in Figure 3.3, accuracy improves as number of samples increases. This makes sense because small number of samples does not capture the action properly, therefore causes error in action classification.

We have done a comparison between lower bound energy consumption explained in Section 3.2.5 and proposed scheduling technique in terms of energy consumption per packet for different actions and for both periodic and non-periodic links in the bar charts illustrated in Figures 3.4, and 3.5 respectively. Note that in all four actions, periodic link outperforms non-periodic link in terms of reaching energy consumption lower bound. The difference between the lower bound and proposed scheduling energy consumption originates from the completely retransmission free and minimized transmit power level adopted in the former case. This is not practical in the real world situation because global awareness of channel future behaviour does not exist. In fact, Figures 3.4, and 3.5 indicate that our scheduling technique over periodic links is more energy efficient in comparison to non-periodic links for which, there is no specific pattern present.

It is also trivial that our technique outperforms techniques that use real time channel assessment because it is a very energy consuming task in highly varying WBANs [108, 110]. As observed in Figure 3.5, in lateral pulldowns the energy consumption of proposed scheduling technique is very close to the lower bound. The reason for this is the fixed nature of the ankle-waist link during the action. It is noteworthy that wakeup, sleep, and processing power consumption are neglected in our analysis. As stated in Chapter 1 and reiterated in Chapter 2, this is a reasonable assumption since more than 80% of WSNs energy consumption is devoted to communications and the fact that wake up and sleep energy consumption is negligible compared to transmit and receive power consumption. In Figure 3.6, the approximate applicability range of our scheduling and power adjustment technique in (3.3) in terms of application bandwidth for periodic extremity-waist links is illustrated. Furthermore, the proposed technique allows us to achieve relatively high bandwidth and PDR at low transmit power levels, i.e., as seen in Chapter 2, 4 kB/s is adequate to achieve the desired bandwidth for most WBAN monitoring applications. Note that the illustrated range holds only for a situation when a single periodic link exists. Presence of more nodes and links requires further study in order to achieve the maximum bandwidth by adopting low transmit power levels.

3.5 Discussion

In this chapter, we proposed a scheduling algorithm that accounts for the periodic shadowing observed over many WBAN links and thereby reduce the transmit power required to transfer information and thereby enhance energy efficiency at the expense of latency. This technique helps us achieve single hop communication between some limb-torso links by adopting low transmit power levels which is not possible for stationary actions studied in Chapter 2. Periodic prolonged actions such as fitness activities cause on-body links to undergo periodic predictable connectivity sessions that can be exploited for low power communications. Beside periodicity which can be used for energy efficient communication, diversity of RSSI samples over such links provides us with mean and standard deviation features which makes simple real-time action recognition based on naive Bayes classification possible. One of the most important implications of our algorithm is placement of the nodes which are not constrained in terms of position and are not delay tolerant in terms of application. Further, since as discussed in Chapter 2 torso might be already occupied with restricted sensors in terms of placement, sensors with looser placement and latency requirements can be mounted on extremities, e.g., ankles and wrists, so that energy efficiency is achieved by single hop communication and low transmit power levels.

The main limitations of our study are: 1) action specificity of the algorithm from the perspective that its applicability to the actions not studied in this work needs to be evaluated, 2) being applicable to fixed pace periodic actions since any change in activity's pace results in additional packet drops, and 3) its dependence on subject person since training set for action recognition may be required based on a new subject.

One of the most fundamental future research areas is node placement and scheduling techniques to maximize throughput with low transmit power level for scenarios where several periodic links are available. Because here, as a case study, we studied energy efficiency and achievable bandwidth for a single link. However, in the real world, many nodes with looser placement requirements may exist. Placing these nodes on locations where their connected sessions have shorter overlap yields more bandwidth for higher data rate applications.

Chapter 4

RSSI-based Distributed Self-Localization for Wireless Sensor Networks in Precision Agriculture

4.1 Introduction

In this chapter, we propose a RSSI-based distributed Bayesian localization algorithm based on message passing to solve the approximate inference problem. The algorithm is designed for precision agriculture applications such as pest management and pH sensing in large farms where greater power efficiency besides communication and computational scalability are needed but location accuracy requirements are less demanding. Communication overhead which is a key limitation of popular non-Bayesian and Bayesian distributed techniques is avoided by a message passing schedule in which outgoing message by each node does not depend on the destination node, therefore is fixed size. Fast convergence is achieved by: 1) eliminating the setup phase linked with spanning tree construction which is frequent in belief propagation schemes, and 2) the parallel nature of the updates since no message needs to be exchanged among nodes during each update, which is called the *coupled variables* phenomenon in non-Bayesian techniques and accounts for significant amount of communication overhead. These features make the proposed algorithm highly compatible with realistic WSN deployments, e.g., ZigBee which are based upon the AODV where RREQ and RREP packets are flooded in the network during route discovery phase.

Since late 1990's, a wide range of indoor and outdoor localization techniques have emerged based on camera, infrared, wireless local area network (WLAN), ultra wide band (UWB), Bluetooth, and RFID [119, 120], while GPS technology has revolutionized outdoor localization. Localization techniques are developed for a wide variety of applications and are different in terms of accuracy, coverage, cost, responsiveness and adaptiveness to environmental changes [121, 122]. Even though GPS-based localization techniques are attractive in terms of accuracy, their impaired coverage in metropolitan environments and lack of cost-effective scalable solutions sparked emergence of IEEE802.15.4/ZigBee localization algorithms that work based on RSSI. These techniques have advantage over Bluetooth, UWB and Wi-Fi [123] due to their energy efficiency and capability to support high-range communication and mesh networking [124]. Further, even though RSSI-based techniques are less accurate compared to camera-based and infrared technologies, cost efficiency makes them ideal for large scale outdoor applications such as agricultural environments in which distance between nodes so called inter-node distance is relatively high and localization accuracy requirements are looser.

Precision agriculture is one of the rapidly growing WSN areas for outdoor environments which enhances crop management and yield through sophisticated management of soil, water resources and applied inputs [125]. WSNs are deployed to improve spatial data collection, precision irrigation, variable-rate technology and supplying data to farmers [17, 126–128]. This requires sampling of critical features such as soil pH, moisture, electrical conductivity in addition to deployment of actuators to trigger a wide variety of processes varying from drip irrigation to pest management, e.g., mating disruption. In order to provide meaningful feature maps that improve resource management and decision making, being aware of location of the sensors that have generated data is critical [129]. Loose accuracy requirements beside the cost involved with equipping all sensors with GPS, raise the need for localization algorithms which are low cost, and are compatible with COTS transceiver modules. This is particularly important for large WSNs such as precision agriculture and smart grid where faulty recordkeeping, i.e., human error in data logging, has been reported a lot and may even cause devices to get lost. Besides, the sensor boxes which contain battery, transceiver and other components as well are usually taken off in bulks before being taken for service and brought back for re-installation therefore operators need to be able to install them without having to necessarily mount them at their initial point. These make a localization algorithm that could seamlessly run and make each box aware of its location save a lot of time and resource.

In this work, we propose an anchor-based, probabilistic, distributed and range-based localization technique for static IEEE802.15.4 WSNs using RSSI samples. The algorithm is called *Bayesian model for information aggregation*, and is particularly suited to precision agriculture or applications with similar accuracy requirements, network size and node connectivity. Moreover, anchor-based localization algorithms make use of landmarks or anchor nodes to help localizing unknown nodes [130] and are divided into range-based and range-free techniques. Range-free algorithms do not take advantage of distance, angle or time measurements in order to execute localization [131]. These algorithms use connectivity information [132], distance in terms of number of hops [133, 134] or other measurement free metrics for positioning. On the other hand range-based algorithms exploit time of arrival (TOA) [135], angle of arrival (AOA) [136] or RSSI [137] to estimate inter-node distances. RSSI-based techniques [138–141] which are more attractive in the sense that no additional hardware is required in order to make the distance estimation, have been proposed for node localization in general context and precision agriculture applications as well [142]. On the other hand, distributed or cooperative techniques [9, 82] are attractive for large scale problems since processing burden is divided between nodes and are classified as Bayesian and non-Bayesian schemes. The algorithm proposed in this work belongs to Bayesian distributed techniques where cooperative schemes are proposed to solve Bayesian estimators such as minimum mean square error (MMSE) and MAP. In most distributed Bayesian techniques message passing algorithms such as belief propagation (BP), nonparametric belief propagation (NBP) and their variants are proposed to estimate the marginalization over a Markov random field (MRF) that contains nodes location and pairwise distance estimates between them as variables and observations respectively [143–146]. Whereas, in non-Bayesian schemes techniques such as alternating direction method of multipliers (ADMM) [147], descent gradient [148–150] and sequential greedy optimization (SGO) [151] are applied to solve convex relaxation localization problems, i.e., semidefinite programming (SDP) and second-order cone programming (SOCP) [152, 153], or directly to solve the non-convex problem in a distributed manner.

BP-based techniques are vulnerable to loopy graphs which cause them either not to converge at all or converge only under specific circumstances in terms of number of loops [154]. Therefore these techniques are mostly used for the scenarios where a few slowly moving or static nodes along with relatively high number of anchors, and all equipped with short range transmitters, render the statistical graph spanning tree or have few number of loops. Further, multi-hop communication, at least $O(N)$ communication cost, is required both in order to form the statistical graph or the spanning tree. On the other hand, distributed non-Bayesian techniques are more suited to localization for large static WSNs and the fact that a fairly large number of these techniques is proposed in the literature, serves as an evidence for that. Further, most of these techniques work based on single-hop communication and are not susceptible to loops in the network. However these works suffer from significantly high communication overhead which is associated with the information that is required to be exchanged among neighbouring nodes between consecutive update iterations. In the distributed optimization context, this phenomenon is called *coupled variables* or *complicating variables* where each node depends on information from other nodes to form its new optimization subproblem or update its outcome. Computational complexity which is linked with the tasks nodes are assigned during each iteration is another issue. On the other hand, in precision agriculture applications, relatively high number of connected unknown nodes, limited processing power of embedded microcontrollers and underlying IEEE802.15.4 WSNs which work in conjunction with route discovery phase of AODV routing protocols, call for a real-time, fast and power efficient algorithm which relies on local single-hop information exchange and is not susceptible to loops in the network.

Our proposed Bayesian framework is similar to state-of-the-art distributed non-Bayesian techniques from the perspective that nodes only communicate with their single-hop neighbours while it is inspired by graph theory in social networks context [155, 156]. Further, as opposed to message passing schemes for Bayesian estimation [143–146, 154, 157] where graph nodes represent random variables, our work is similar to [156] with the difference lying in the fact that in [156], nodes denote *agents* or *social sensors* whereas in our work nodes represent *physical sensors*. Moreover, we propose a Bayesian framework for information aggregation which has low and scalable communication cost, i.e., independent from number of neighbouring nodes, but still achieves desired accuracy for particular precision agriculture applications such as pest management and pH sensing. Features such as single-hop communication, same outgoing message to all neighbouring nodes, i.e., lack of coupled variables phenomenon, in addition to not having to use spanning tree construction techniques results in an algorithm which has low communication and computational complexity, therefore is scalable.

The proposed technique is well positioned to address self-localization in do it yourself (DIY) networks which run ZigBee or other proprietary networking protocols based upon IEEE802.15.4 specifications. This is associated with the fact that algorithm starts working in conjunction with route discovery phase of AODV-based routing protocols where RREQ packet originated from an arbitrary source node is flooded in the entire network. We derive a closed-form recursive relationship for message passing schedule that updates Bayesian estimation of nodes location at a time step during which one or multiple path loss samples are generated and therefore call the algorithm a Bayesian model for information aggregation. We prove that the location constraint resulted from a generated path loss sample is in fact convolution of path loss likelihood and the most recent location estimation of the generating node. Realistic assumptions regarding independence of RSSI samples and conditional independence of location updates of nodes are used to prove that location constraints resulted from dependent paths (loop forming paths) multiply. This makes the algorithm faster and more power efficient both by setup phase elimination and also nature of the recursive message passing schedule. Setup phase elimination includes omission of spanning tree construction, and intermediate node tracking which helps making use of location constraints resulted from the paths that are traversed by flooding RREQ packets. In fact, the algorithm's robustness against loops in the WSN connectivity graph is verified by extensive simulations. On the other hand the proposed message passing schedule results in parallel updates and fixed size outgoing message from each sensor. Moreover, as opposed to non-Bayesian distributed techniques, neighbouring nodes do not exchange additional information between iterations while outgoing message size is fixed and independent of destination node, therefore does not scale and grow with number of neighbouring nodes.

Since our goal is to devise an algorithm that can work in conjunction with COTS transceiver modules, we characterize path loss at 2.45 GHz ISM band. Our measurement campaign helps us 1) show log-distance path loss model provides a good fit to our collected data corresponding to below and above canopy level communication, 2) derive path loss likelihood function conditioned on inter-node distance which is a fundamental part of the proposed algorithm, 3) study shadowing correlation along different directions which helps us conclude upon conditional independence of measured path loss samples that lead to the proposed message passing schedule, and 4) generate random independent path loss samples and evaluate our algorithm since lognormal path loss model and shadowing independence is verified. Further, our measurement campaign gives us advantage over previous works which simply assume Gaussian distance measurement noise and an arbitrary noise factor (NF) in measured distance or a known path loss exponent with independent lognormal shadowing terms to evaluate their algorithms [139, 147, 148, 151, 158]. In other words, even though our collected data is not adequate to test the algorithm with real data, we achieve outcomes which are more reliable for realistic deployments in the field.

The remainder of this chapter is organized as follows: In Section 4.2, we start with concept behind Bayesian and non-Bayesian estimators and proceed to formulate the localization problem, define the notations, include a summary of our measurement campaigns and describe the path loss model along with path loss likelihood function conditioned on node locations. In Section 4.3, we devise a recursive solution to the problem stated in Section 4.2 and propose a specific implementation of this solution based on nodes multicasting in TDMA manner. We proceed with simulations and evaluation of our algorithm along with analytical and numerical comparison with state-of-the-art techniques in Section 4.4.2 and wrap up the chapter with conclusion in Section 4.5.

4.2 The Localization Problem and Path Loss Likelihood Function

As stated in Introduction, pinpoint localization accuracy is not needed for precision agriculture applications such as pest control since knowing approximate location of originating sensors suffices to trigger the relevant actuators. Accordingly, we define the localization problem in a discrete manner which means that the agricultural field is divided into smaller square cells and location of each unknown node is determined as centroid of one of the cells the field is divided into. The precision of the algorithm is adjustable via number of grid cells inside the field, however precision flattens once grid resolution exceeds a threshold. In the following, first we describe the concept behind Bayesian estimators for localization problem, approximate inference methods and message passing algorithms in Section 4.2.1. Formulation of the localization problem based on aggregated path loss samples from neighbour nodes is discussed in Section 4.2.2 and path loss model for orchard environments is explained briefly in Section 4.2.3. The purpose from deriving path loss model is to evaluate the proposed localization algorithm based on realistic assumptions in terms of connectivity between nodes in addition to a realistic path loss likelihood function which expresses probability of a measured path loss value conditioned on a given distance. In Section 4.3, we will see that this likelihood function is an essential part of the proposed distributed algorithm. Besides, our studies with regard to shadowing independence will help us simplify the relationships which will lead to our simple scalable localization algorithm in Section 4.3.

4.2.1 Concept

In this section, we briefly describe the non-Bayesian and Bayesian localization problem in Sections 4.2.1, and 4.2.1. Thereafter, we proceed with a brief introduction to message passing algorithms which are approximate inference methods for Bayesian estimators and include the line of reasoning behind the Bayesian model for information aggregation in Section 4.2.1. Note that in both Bayesian and non-Bayesian methods we are interested to estimate a parameter vector $\mathbf{x}$ from an observation vector $\mathbf{z}$. The observation vector could contain distance or location related measurements such as RSSI, noisy distance measurement, TOA or AOA.

Non-Bayesian Estimators and Distributed Methods

In non-Bayesian estimators, $\mathbf{x}$, the parameter to be estimated, would be treated like an unknown deterministic parameter. Non-Bayesian estimators are divided in to least square (LS) and maximum likelihood (ML) methods. Let $z = g(x) + \mu$ where $g(\cdot)$ is a known function and μ is the measurement error, one can define LS and ML estimators as,

$$\begin{aligned} \widehat{X}_{LS} &= \underset{\mathbf{x}}{\operatorname{argmin}} \|\mathbf{z} - g(\mathbf{x})\|^2, \\ \widehat{X}_{ML} &= \underset{\mathbf{x}}{\operatorname{argmax}} P_{\mathbf{Z}|\mathbf{X}}(\mathbf{z}|\mathbf{x}), \end{aligned} \tag{4.1}$$

where $\|\cdot\|$ represents norm function. As can be seen, the main difference between LS and ML estimators is that the former does not take noise statistics into account. In case observations are RSSI samples, $\widehat{X}_{LS}$ turns into summation of quadratic terms relating distance extracted from $g(\cdot)$ [158, 159] whereas $\widehat{X}_{ML}$ would be equivalent to summation of logarithmic terms [147, 160]. Both of these formulations are strongly non-convex optimization problems and are NP-hard. Therefore SDP [147, 151, 161, 162] or SOCP [152, 153, 163] relaxation techniques are used to create convex optimization problems. Methods such as ADMM [147], descent gradient [148, 149], and SGO [151] among others are used to distribute the convex SDP, i.e., full SDP or edge-based SDP [164] among the sensors. Some of these techniques such as descent gradient are well suited to be directly applied to non-convex problems. In Section 4.4.2, we will compare state-of-the-art distributed techniques which are used to solve these problems with our proposed Bayesian scheme in terms of communication and computation complexity.

Bayesian Estimators and Approximate Inference Methods

Bayesian formulation of the localization problem consists of inference of location of unknown nodes represented by vector $\mathbf{x}$ based on observation vector $\mathbf{x}$. As opposed to non-Bayesian estimators, $\mathbf{x}$ is treated as random variable. The two well known Bayesian estimators are MAP and MMSE which estimate the location of sensors as

$$\begin{aligned} \widehat{X}_{MMSE} &= \int \mathbf{x} P_{\mathbf{X}|\mathbf{Z}}(\mathbf{x}|\mathbf{z}) d\mathbf{x}, \\ \widehat{X}_{MAP} &= \underset{\mathbf{x}}{\operatorname{argmax}} [P_{\mathbf{X}|\mathbf{Z}}(\mathbf{x}|\mathbf{z})]. \end{aligned} \tag{4.2}$$

Note that integration is replaced by summation for discrete problems. It is well-known that Bayesian location estimation (4.2), i.e., joint solution, for large number of sensors is an intractable problem with exponential complexity. Therefore one may resort to solve these estimators with respect to individual location components X_k, i.e., $P_{X_k|\mathbf{Z}}(x_k|\mathbf{z})$. Message passing algorithms have emerged to provide an approximate solution to this problem, which is generally NP-hard. In the next section, a brief review on these algorithms and the rationale behind our proposed algorithm is provided.

Message Passing Algorithms and Bayesian Model for information Aggregation

Consequently message passing algorithms like sum product algorithm (SPA), and its variants such as BP, NBP and other message passing schemes are proposed to approximate marginalization over a MRF, so called factor graph which represents location of nodes and dependencies between them by vertices and edges respectively.

While SPA is a message passing algorithm which gives the exact solution for acyclic graphs, it is extended to provide iterative message passing over cyclic factor graphs in order to provide approximate solution which is no longer equal to the exact marginal a posteriori distribution. In loopy factor graphs there are many ways these messages also known as *message passing schedule* are calculated and with each of them resulting in a different marginal distribution [82]. Most existing message passing schedules entail one or both of the following features;

1. outgoing message from a vertex to each of the neighbouring vertices is different therefore communication overhead scales linearly as a result of increased sensor density,

2. spanning tree of the statistical graph is constructed before message passing runs.

These features increase communication overhead and render the algorithms not suitable for large scale WSNs. Besides, they make the algorithm unsuitable for deployment along with route discovery phase of AODV-based routing protocols running on IEEE802.15.4 COTS. In order to address the issues claimed in Section 4.2.1, we aim to propose a message passing schedule with following properties;

1. outgoing messages from each node is independent from the neighbouring node it arrives at, since this renders the protocol scalable in terms of communication overhead,

2. message passing schedule runs in parallel, i.e., nodes update their location once each observation is made which is highly compatible with multicasting nature of route

discovery phase in AODV routing protocols.

3. there is no setup phase communication overhead since there is no need for spanning tree construction.

4.2.2 Problem Formulation

Let $\mathbb{S} = \{S_1, \ldots, S_N\}$ be a set of sensors randomly scattered in a square field which is divided into $m \times m$ square cells with equal areas, and $\Omega = \{1, 2, \ldots, m^2\}$ be the sample space of all possible cell coordinates. Our objective is to make use of inter-node communications and find the grid cell each node is located in. In the following, we introduce the notations and formalize the localization problem. It is noteworthy that we opt to use thin face letters representing scalar variables whereas bold letters represent variables in vector format.

Without loss of generality, let the first n_a nodes be landmarks $\mathbb{S}_l = \{S_1, \ldots, S_{n_a}\}$, and unknown nodes be represented by $\mathbb{S}_u = \{S_{n_a+1}, \ldots, S_N\}$ while $y_{ij}^{[l]}$ is a path loss sample or average of multiple path loss samples that S_j collects from S_i at l-th time step. Note that in general, multiple samples are collected, in case each calculation time step is composed of multiple communication time slots. Let $\mathbf{Y_k}$ denote the vector of path loss samples which have been communicated between pairs of connected nodes during the first k time steps and let $\mathbf{y_j^{[k]}}$ represent vector of all path loss samples that S_j has collected from its neighbour nodes with index set N_j at k-th time step,

$$\begin{cases} \mathbf{Y_k} = (y_{ij}^{[l]})_{\substack{l=0:k \\ 1 \leq j \leq N, i \in N_j}} \\ \mathbf{y_j^{[k]}} = (y_{ij}^{[k]})_{i \in N_j} \end{cases}. \tag{4.3}$$

Note that $y_{mj}^{[k]}$ is not available in case, S_j has not collected any sample from S_m at k-th time step. Let $X_j^{[k]}$ be a random variable defined over Ω representing location estimation of S_j at k-th time step. Considering that we are looking to estimate location of S_j at M-th time step based on previously aggregated data $\mathbf{Y_M}$,

$$x_j = \underset{x_j}{\operatorname{argmax}}[P(X_j^{(M)} = x_j | \mathbf{Y_M})], \tag{4.4}$$

where $P(\cdot)$ is the probability function and $\underset{x}{\operatorname{argmax}}[f(x)]$ is the set of points x for which $f(x)$ attains its largest value. In the remainder of this section, path loss model for agricultural environment which is the key to generate $y_{ij}^{[l]}$ samples, $\mathbf{Y_k}$ and $\mathbf{y_j^{[k]}}$ is explained. Consequently we derive the path loss likelihood function that underpins the recursive algorithm described in Section 4.3. Moreover, we derive likelihood of $y_{ij}^{[l]}$ given that S_i and S_j are estimated to be located at x_i and x_j respectively, i.e., $P(y_{ij}^{[k]} | X_j^{[k]} = x_j, X_i^{[k]} = x_i)$.

4.2.3 A Representative Path Loss Model for Orchard Environments

In this section, we describe the path loss model resulted from our measurement campaigns in apple orchards located at Keremeos, BC, Canada. This underlies the work in Section 4.2.4 which explains derivation of path loss likelihood function expressing path loss distribution conditioned on the transmitter (Tx) and the receiver (Rx) locations. In the following, first we briefly explain path loss models in vegetated environments with more focus on log-distance path loss model which proves to be the most suitable fit to our collected data. Afterwards, we proceed with our measurement campaign.

Path Loss Models for Vegetated Environments: Several models are proposed for path loss behaviour in vegetated environments. These models are mostly classified into modified exponential decay (MED) [91], modified gradient models, and Nonzero Gradient [165]. A drawback of these models is that they only account for the vegetation path loss. Further, there are more factors such as ground and canopy reflection that contribute to path loss. This makes the aforementioned models unable to make a good prediction of path loss in realistic environments [166]. In [166], modified models that take ground and canopy reflection into account have been proposed. However, these models are more complex because they include summation of multiple terms in order to account for ground and canopy reflection. In order to address this issue, log-distance model is proposed since it encompasses effects of all contributing factors and propagation mechanisms [75, 167–169]. Furthermore, there is an extensive literature on path loss models in forests and agricultural environments, while each model best fits to a different scenario and environment. In several works [75, 168, 169], log-distance path loss model is claimed to provide a good fit to the path loss collected in vegetated environments,

$$PL[dB] = PL_0 + 10n \log(\frac{d}{d_0}) + X_\sigma, \tag{4.5}$$

where X_σ is a zero-mean normal random variable with standard deviation σ, $X_\sigma \sim N(0, \sigma)$, while PL_0 represents path loss at reference distance d_0 and n denotes path loss exponent for the specific case of study.

Measurement Campaign: We carried out the measurements in the Dawson orchards at Keremeos, British Columbia (BC). Measurements were conducted in a 6 hectare (ha) high density apple orchard consisting of apple tree rows with approximately 3 m height. We use the path loss data collected from four directions of along, cross, 30°, 45° and 60° with respect to tree rows, using different transmitter (Tx) and receiver (Rx) antenna heights. Further, we conducted measurements with Tx at 2.5 m (below canopy level) and 4 m (above canopy level) heights and Rx at 2.5 m. This setup is compatible with realistic WSN deployment scenarios where gateways, responsible for aggregating data of their neighbouring sensors, are mounted above canopy while sensors and actuators are placed inside the canopy. As localization is concerned, gateways which have better line-of-sight (LOS) are equipped with GPS to play the landmark role. The measurements were conducted throughout three different measurement campaigns, seven days combined and spread across two summer seasons. Measurements were done in approximate range of 0-100 m at points which are approximately 10 m apart from each other at 9 different parts of the orchard along five directions illustrated in Figure 4.1. Our equipment on the transmitter side, are an Agilent E8267D vector signal generator (VSG) that feeds a 2.45 GHz omnidirectional dipole antenna with 5 multi-tones (5 MHz apart from each other) through a ZVA-213 power amplifier, in order to provide +23 dBm as the antenna input. While, on the receiver side, a Toshiba laptop which runs MATLAB and Agilent connection expert, i.e., specialized proprietary software for connecting computer to Agilent spectrum analyzer, is connected to a N9342C handheld spectrum analyzer (HSA) via a LAN cable. Extra losses and gains resulted from cables, connectors and antennas at both Tx and Rx sides have been taken into account for calibration. We applied Kolmogorov-Smirnov (K-S) test at 5% significance level on our collected path loss data and verified Gaussian distribution of path loss data around mean log-distance path loss data $\overline{PL[dB]}$ in (4.5) both for above and below canopy level communication. Besides, in Table 5.5 fitness of popular path loss models for vegetated environments, e.g., MED, modified MED models and log-distance is tested against the collected data. The statistical measure R^2 indicates how well data fits a specific model, while root-mean-square error (RMSE) is an indication of difference between predicted and observed samples. Since log-distance path loss model is a good fit to the data collected, 95% confidence interval (CI) for PL_0 and n are expressed in Table 4.2, while path loss samples for two modes are illustrated in Figure 4.3. Note that gateway-to-node and node-to-node communications comply with above and below canopy level Tx modes respectively. As illustrated in Figure 4.3 and consistent with [170, 171] path loss improves under raised Tx height conditions. According to our experimental data, path

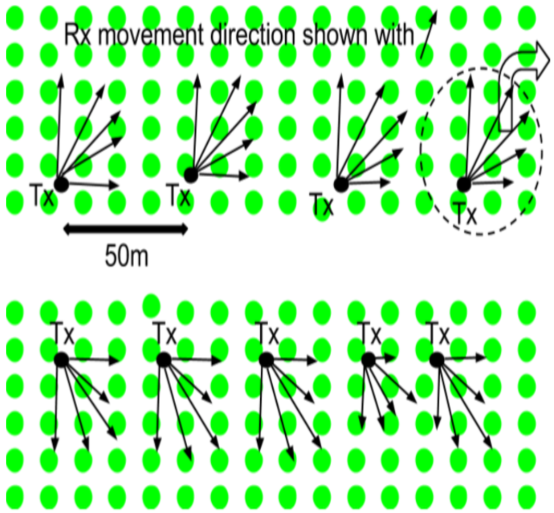

(a) Measurement scenarios are illustrated; Light green dots represent tree rows and black dots show Tx antenna position whereas Rx cart moves along indicated directions

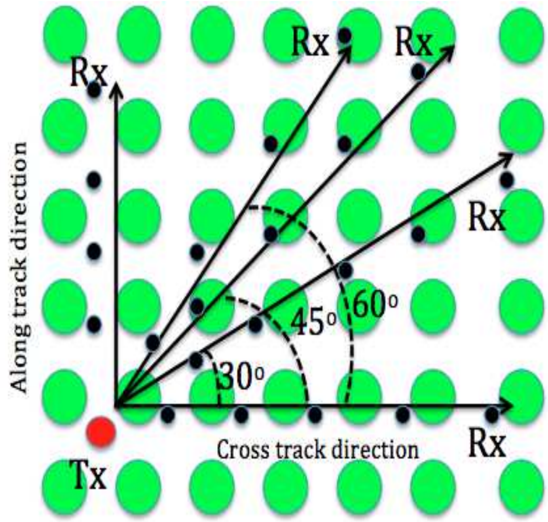

(b) Magnified version of a measurement scenario on the left is illustrated; in each scenario Tx antenna (red dot) is fixed whereas Rx cart (black dots) moves along the designated directions to collect data

Figure 4.1: 9 measurement scenarios inside the orchard is illustrated; Transmitter antenna was moved 50 m across the rows to form a new scenario whereas Rx was moved along five different directions of along, cross, 30°, 45° and 60° for each scenario and path loss samples were collected through 0-100 m range and at $\approx 10\ m$ apart points. Rx antenna was placed at 2.5 m elevation (0.5 m below tree height) while Tx antenna height was at 2.5 m and 4 m elevation (1 m above canopy level).

loss improvement at short distances ($\approx$ 50 m) complies with antenna gain $G_A = 20\log(h_t h_r)$ suggested in literature where h_t and h_r are TX and Rx antenna height respectively. However at longer distances, improvement observed in above canopy communication outperforms the gain predicted by [170, 171]. We believe the additional gain in path loss, particularly at long distances, is associated with extra LOS that we achieve by raising Tx antenna over canopy level.

Shadowing Correlation: In the measurement campaign procedure, we observed that path loss samples are normally distributed around the mean path loss. Studying the correlation between pairs of links, i.e., samples arriving from different directions, is important since the independence between these samples will be exploited in Section 4.3.1. In order to conduct such a study, links are classified pairwise. The classification is based on length of the links and their relative orientation, so-called an arrangement inspired by the approach suggested in [172]. Further, we choose pairs of links which are similar in terms of geometry, i.e., rotated versions of a specific pair in different measurement scenarios. For example in Figure 4.1, an arrangement with specific lengths, e.g., 10 m and 20 m links which are 60° apart from each other contains 4 pairs without replacement in each scenario, therefore 36 pairs in total. We calculate shadowing correlation for all the arrangements that are α° apart from each other and let ρ_α denote average of these correlation values.

In Table 4.3, average correlation values corresponding to arrangements of a specific angle in addition to standard deviation of these values are tabulated. It is noteworthy that in order to calculate the average shadowing, these arrangements are not separated in terms of length. This is because, there is no significant variation observed particularly among the links that matter in this work, i.e., longer than 40 m associated with inter-node distances.

Table 4.1: (R^2,RMSE) for different variants of MED models, modified MED models based on [166] to take the canopy and ground reflection into account as well.

Communication Mode / Model	Above canopy	Below canopy
Weissberger	(0.67,6.85)	(0.3,14.01)
ITU-R	(0.43,9.04)	(0.03,12.08)
FITU-R	(0.71,5.16)	(0.3,10.29)
Log-distance model	(0.78,3.65)	(0.74,5.67)

Table 4.2: Path Loss Model characteristics for above and below canopy level modes

Mode	n	PL_0 $[dB]$	σ $[dB]$	R^2	95% CI for n	95% CI for PL_0
2.45 GHz-Tx below canopy level	3.61	75	5.27	0.74	3.36-3.86	71-79
2.45 GHz-Tx above canopy level	2.91	72	4.14	0.78	2.60-3.22	67-77

Table 4.3: Average shadowing correlation for pairs of links that are extended with specific angles with respect to each other. Each average value is derived from correlation values of arrangements with a specific angle

Mode	below canopy			above canopy	
Shadowing correlation	Number of pairs per arrangement	Average	Standard deviation	Average	Standard deviation
ρ_{0°	45	0.07	0.05	0.05	0.08
ρ_{30°	36	0.04	0.07	-0.03	0.07
ρ_{45°	36	0.06	0.07	-0.06	0.07
ρ_{60°	36	-0.06	0.06	0.08	0.09
ρ_{90°	18	-0.03	0.11	-0.04	0.08

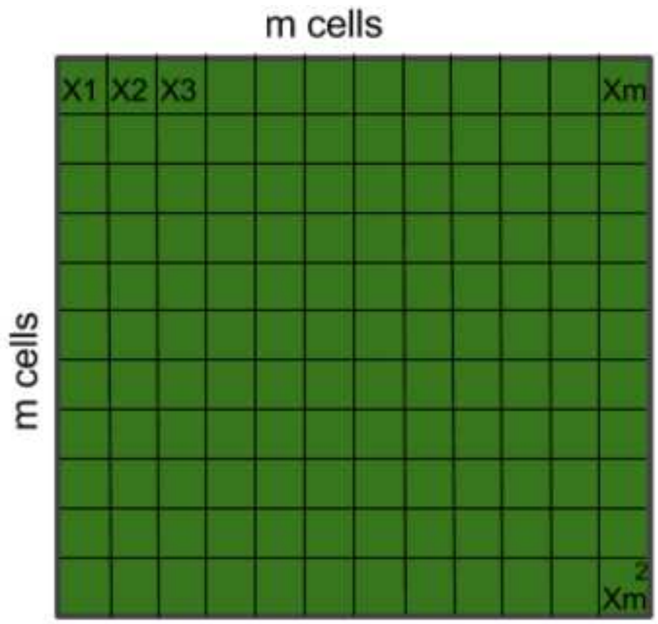

Figure 4.2: Location pmf of unknown nodes is updated recursively. Agricultural field is divided into $m \times m$ cells with equal area and probability of an unknown node being located inside each cell is calculated based on recently aggregated path loss samples and prior location pmf of connected nodes.

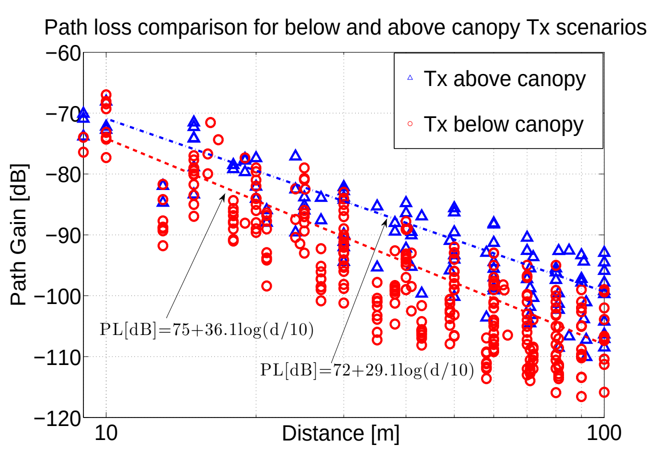

Figure 4.3: Path loss samples for below and above canopy Tx level at 2.45 GHz collected from three measurement campaigns along with linear log-distance fits are illustrated. Values in distance axis appear in logarithmic scale; The difference between the two above and below canopy modes, which is due to more line of sight (LOS) between Tx and Rx in the above canopy case, could be seen.

4.2.4 Path Loss Likelihood Function

In this part, we derive likelihood function $P(y_{ij}^{[k]} \big| X_j^{[k]} = x_j, X_i^{[k]} = x_i)$ which is a key component of the algorithm we propose in the next section since it relates path loss values to inter-node distances. A discretization process on likelihood function is required in order to extract likelihood probability mass function (pmf), because RSSI samples that the proposed algorithm is going to use are discrete in nature. Therefore, we need to calculate the probability that the discretized path loss sample $y_{ij}^{[k]}$ would equal arbitrary value α over the distance d_{ij}, $P(y_{ij}^{[k]} = \alpha \big| D = d_{ij})$. Assuming log-distance path loss model as discussed in Section 4.2.3 and taking a random point on the field into account, the probability of continuous path loss sample pl_{ij} falling in the range $[\alpha - \frac{\Delta}{2}, \alpha + \frac{\Delta}{2}]$, $\Delta << \alpha$ and when S_j is located at distance d_{ij} from S_i is calculated by

$$
\begin{aligned}
P\big(y_{ij}^{[k]} = \alpha \big| D = d_{ij}\big) \approx P\bigg(\alpha - \frac{\Delta}{2} < pl_{ij} < \alpha + \frac{\Delta}{2} \bigg| D = d_{ij}\bigg) = \\
\frac{C\Delta}{\sqrt{2\pi\sigma^2}} e^{-\frac{(\alpha - \overline{PL(d_{ij})})}{2\sigma^2}},
\end{aligned}
\tag{4.6}
$$

where $\overline{PL(d)} = PL_0 + 10n\log(\frac{d}{d_0})$ is mean path loss at distance d while C is the normalization constant. Moreover in practice, in order to approximate the above conditional probability, we collect amplitude of the normal distribution with mean $\overline{PL(d_{ij})}$ and standard deviation σ in the range $\Big[\overline{PL(d_{ij})} - 3\sigma, \overline{PL(d_{ij})} + 3\sigma\Big]$ at 1 dB steps and normalize the values so that they sum up to one. In Figure 4.4, we illustrate how path loss likelihood function is created based on discretization step Δ and observed path loss value α. On the course for discretization, discretization step Δ and the PDF function which is Gaussian due to lognormal path loss model affect normalization value C. This process enables us to label each path loss and distance pair with a likelihood value. Based on (4.6), and the fact that each pair (x_i, x_j) translates into the corresponding distance d_{ij}, sensor S_j calculates $P(y_{ij}^{[k]} = \alpha \big| X_j^{[k]} = x_j, X_i^{[k-1]} = x_i)$, $\forall x_i, x_j \in \Omega$.

4.3 Localization Algorithm for Precision Agriculture Applications

In this section, we derive an algorithm to solve the problem stated in (4.4) which works based on Bayesian model for information aggregation. Further, our objective is to propose a recursive expression for $P(X_j^{[k]} = x_j \big| \mathbf{Y_k})$ that explains how location pmf is updated once

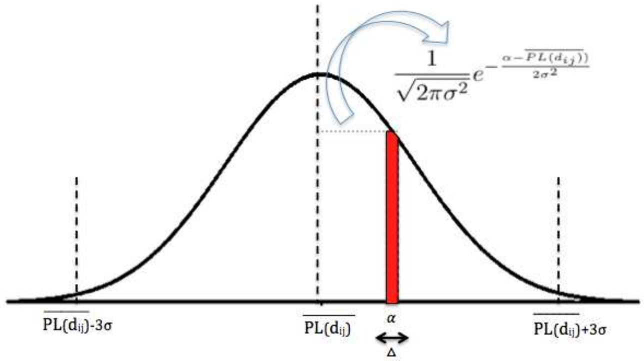

Figure 4.4: Discretization of path loss likelihood function involves sampling the corresponding Gaussian distribution at Δ steps within 3δ distance from mean path loss and normalization afterwards

information is aggregating in the network, i.e., when the most recent evidence, i.e., RSSI sample, is collected. In Section 4.3.1, we first solve the problem for general case where at each calculation time step, arbitrary amount of information or number of packets, between one or multiple pairs of nodes is exchanged. In Section 4.3.2, we proceed with the special case that is more compatible with route discovery phase of AODV-based routing protocols such as ZigBee. This special case, is in fact the algorithm simulated in Section 4.4.2.

4.3.1 General Case

According to the notational definition in Section 4.2 and assuming that at each time step, S_j updates its location pmf only based on the samples it has received from single-hop neighbours, i.e., not samples communicated between other pairs of nodes,

$$\begin{aligned} &P(X_j^{[k]} = x_j \big| \mathbf{Y_k}) = P(X_j^{[k]} = x_j \big| \mathbf{Y_{k-1}}, \mathbf{y_j^{[k]}}) \propto \\ &P(\mathbf{y_j^{[k]}} \big| X_j^{[k]} = x_j, \mathbf{Y_{k-1}}) P(X_j^{[k]} = x_j \big| \mathbf{Y_{k-1}}). \end{aligned} \tag{4.7}$$

The second line in (4.7), results from the fact that $\mathbf{Y_{k-1}} \perp\!\!\!\perp \mathbf{y_j^{[k]}}$ where $\perp\!\!\!\perp$ denotes statistical independence. Note that the mentioned independence is a frequent assumption in Bayesian and non-Bayesian problems which implies that distance observations are independent from each other due to independent measurement noise samples [139, 147, 148, 151, 158]. The difference with RSSI samples in our realistic case is that in addition to random receiver noise, i.e., always independent, random shadowing also adds to mean path loss. Further, it is straightforward to show that in addition to receiver noise samples, shadowing samples also

need to be independent from each other in order for $\mathbf{Y_{k-1}} \perp\!\!\!\perp \mathbf{y_j^{[k]}}$ to hold. In Section 4.2.3, and Table 4.3 we showed that shadowing samples are gaussian and for different scenarios very close to be uncorrelated, therefore independent. Let us recall that in general each calculation time step may be composed of several communication time slots, therefore we have used $\mathbf{y_j^{[k]}}$ which are the path loss samples, S_j collects from one neighbour or a set of neighbours during the k-th time step.
Afterwards, we simplify $P(\mathbf{y_j^{[k]}} \big| X_j^{[k]} = x_j, \mathbf{Y_{k-1}})$ in the second line of (4.7), based on the following conditional independence assumption,

$$\big(y_{ij}^{[k]} \perp\!\!\!\perp y_{mj}^{[k]}\big) \big| \big(X_j^{[k]}, \mathbf{Y_{k-1}}\big) \qquad \forall i, m \in N_j \,, \tag{4.8}$$

where as defined in Section 4.2.2, N and N_j represent total number of nodes and index set of neighbouring nodes of the j-th node, S_j, respectively. Earlier, we explained the logic behind independence of RSSI or measured path loss samples from each other and how it implies $(y_{ij}^{[k]} \perp\!\!\!\perp y_{mj}^{[k]}) \big| (d_{ij}, d_{mj})$. From this, (4.8) looks straightforward, because $\mathbf{Y_{k-1}}$ and $X_j^{[k]}$ at best, only provide noisy distance measurements between other links in addition to d_{ij} and d_{mj}, therefore do not change conditional independence of $y_{ij}^{[k]}$, $y_{mj}^{[k]}$. Consequently, first term on the right-hand side of (4.7) is written as

$$P(\mathbf{y_j^{[k]}} \big| X_j^{[k]} = x_j, \mathbf{Y_{k-1}}) = \prod_{i \in N_j} P(y_{ij}^{[k]} \big| X_j^{[k]} = x_j, \mathbf{Y_{k-1}}). \tag{4.9}$$

Based on conditional expectation rule, we simplify the right-hand side of (4.9),

$$\begin{aligned} &P(y_{ij}^{[k]} \big| X_j^{[k]} = x_j, \mathbf{Y_{k-1}}) = \sum_{x_i} P(y_{ij}^{[k]} \big| X_j^{[k]} = x_j, X_i^{[k]} = x_i, \mathbf{Y_{k-1}}) P(X_i^{(k)} = x_i \big| X_j^{[k]} = x_j, \mathbf{Y_{k-1}}) \\ &= \sum_{x_i} P(y_{ij}^{[k]} \big| X_j^{[k]} = x_j, X_i^{[k]} = x_i) P(X_i^{[k]} = x_i \big| \mathbf{Y_{k-1}}). \end{aligned} \tag{4.10}$$

In (4.10), we use the assumptions $(X_i^{[k]} \perp\!\!\!\perp X_j^{[k]}) \big| \mathbf{Y_{k-1}}$ and $\big(y_{ij}^{[k]} \perp\!\!\!\perp \mathbf{Y_{k-1}}\big) \big| (X_i^{[k]}, X_j^{[k]}\big)$. In order to clarify the first assumption, note that location posterior update of the j-th node, $X_j^{[k]}$, results from previous location update of its neighbours, i.e., $S_i, i \in N_j$ and the most recent path loss observations between S_j and these neighbouring nodes $\mathbf{y_j^{[k]}}$. Traversing up the updating graph, path loss observations along with prior of the nodes suffice for $X_j^{[k]}$ to update. Further, given all the aggregated path loss observations in the network,

$X_i^{[k]}$ does not provide any information about $X_j^{[k]}$. The second assumption results from shadowing correlation study in our measurement campaign following the same discussion we had after (4.8). Combining (4.9) and (4.10) yields

$$P(\mathbf{y_j^{[k]}} \big| X_j^{[k]} = x_j, \mathbf{Y_{k-1}}) = \prod_{i \in N_j} \sum_{x_i} \big[P(y_{ij}^{[k]} \big| X_j^{(k)} = x_j, X_i^{(k)} = x_i) P(X_i^{(k)} = x_i \big| \mathbf{Y_{k-1}})\big]. \tag{4.11}$$

Finally combining (4.7) and (4.11) completes the recursive update,

$$\begin{aligned} &P(X_j = x_j \big| \mathbf{Y_k}) \propto P(X_j = x_j \big| \mathbf{Y_{k-1}}) \times \\ &\prod_{i \in N_j} \sum_{x_i} \big[P(y_{ij}^{[k]} \big| X_j^{[k]} = x_j, X_i^{[k]} = x_i) P(X_i^{[k]} = x_i \big| \mathbf{Y_{k-1}})\big]. \end{aligned} \tag{4.12}$$

This means, in order to update posterior of S_j after observation of new samples collected from S_i, only priors of S_i and S_j in addition to channel information $P(y_{ij}^{[k]} \big| X_j^{[k]} = x_j, X_i^{[k]} = x_i)$ are required. With respect to total number of nodes N, the algorithm has computational and communication complexity of $O(N)$ and $O(1)$ per node, that causes the algorithm to be scalable. The computational complexity is the same as BP-based techniques, while communication overhead which makes up most of power consumption in WSNs is significantly lower since each node only communicates with its single-hop neighbours. As will be explained in the next section, in case the algorithm is deployed in a realistic WSN where only one node multicasts at each time step, communication and computational complexity would both reduce to $O(1)$.

4.3.2 Localization Algorithm Compatible with Wireless Sensor Networks

In this section, we proceed with a realization of the general case algorithm which is a more specific case of the proposed recursive solution in (4.12). Moreover we assume that at k-th time step, only S_k does the multicasting and all connected nodes update their location posterior based on the observed path loss or mean of the path loss samples, i.e., $\mathbf{y_j^{[k]}} = y_{kj}^{[k]}$. This means each node is recipient of at most one sample at a single time step which guarantees compatibility with real world deployment of WSNs such as TDMA or CSMA/CA, where at each time slot, a node can listen to at most one neighbour node without interference. To be more specific, AODV which is the underlying routing protocol in ZigBee works based on flooding and multicasting RREQ packets and receiving RREP messages, therefore our proposed localization algorithm can be integrated in a convenient and inexpensive manner. Transceiver modules such as Synapse which is equipped with light and fast network operating system, SNAP, a more powerful microcontroller and is well-suited for more complex programming (with Python) can be used for mesh networking. In Section 4.4.2, we use numerical examples to evaluate the performance of our algorithm based on radio characteristics of Synapse RF modules.

Path Loss Model Auto-Tuning: In this chapter, as in [139, 147, 148, 151, 158], we assume that path loss is fixed and there is a global awareness of path loss model among sensors. However, this may not be a realistic assumption due to remarkable changes during seasonal environmental variations and also possibility of spatial variations in path loss characteristics in different environments. Complex path loss exponent estimation techniques such as Cayley–Menger determinant and pattern matching [173] could work in complementary with our proposed algorithm. Based on the claimed results in [173], the technique is well-positioned to work for the scenarios of our interest. Even though this technique works well for arbitrary node placements with unknown topology, more simple techniques such as method of moments or quantile-quantile (q-q) plot are adoptable in case knowledge about distribution of distance between neighbouring nodes is available [173]. For example, in [174], closed form internode distance distribution for complex node placement distributions such as uniform and Gaussian has been derived. Accordingly, it is straightforward to derive distance distribution for deterministic deployment, e.g., square grid which is the most frequent node placement method in precision agriculture [173]. Note that realistically, there might be spatial variations over path loss statistics since they may vary between every different pairs of nodes and along different directions. In such situations, iterative techniques mostly inspired by Gauss-Seidel method are used to recursively update nodes locations and path loss exponent afterwards [175]. Convergence is achieved once variations between successive updates fall below a determined threshold.

Even though we have not incorporated these approaches into our scheme, we measured sensitivity of our localization problem with respect to path loss exponent confidence interval tabulated in Table 4.2. Moreover, we assume that the path loss exponent between each node to a neighbouring node is uniformly distributed around the centre value (which is globally known and used to make estimations) with ± 0.25 as margins around this centre value. Simulations show that for uniformly distributed offset, algorithm does not show much sensitivity in terms of accuracy and convergence rate. The reason may be associated with

Algorithm 2 Localization Algorithm For Agricultural Environments

Step 1: Initialization (path loss model auto-tuning if required)

- Initializing landmarks locations

For $i = n_a + 1, \ldots, n_t$ *initializing unknown nodes locations*

- $P(X_i^{[0]}) \sim U[1, m^2]$

Step 2: Landmarks advertise themselves to unknown nodes
For $i = 1, \ldots, n_a$
$\forall j \in N_i$

- $P(X_j^{[i]} \big| \mathbf{Y_i}) = P(X_j^{[i-1]} \big| \mathbf{Y_{i-1}}) \times P(y_{ij}^i \big| X_j^{[i-1]} = x_j, X_i^{[i-1]} = x_i)$
- Normalize $P(X_j^{[i]} \big| \mathbf{Y_i})$
- Multicast and update with (4.12) continue till all unknown nodes are covered for each landmark advertisement.

Step 3: A random node S_i becomes source and multicasts RREQ packet
Step 4:
For $j = n_a + 1, \ldots, N$

- If $d_{ij} < d_{connectivity}, \quad j \neq i$
  - Update rule (4.12) and normalization
  - S_j forwards and multicasts the RREQ packet if hop count, i.e., AODV allows
- else
  - $P(X_j^{[i]} = x_j \big| \mathbf{Y_i}) = P(X_j^{[i-1]} = x_j \big| \mathbf{Y_{i-1}})$
  - no change in location estimation

While RREQ packet has not reached the landmark
$i \leftarrow \forall j \in N_i$
Redo step 4
Step 5: Landmarks return the RREP packet towards the source over the minimum hop route
For $\forall$ consecutive
pairs of (i, j) on landmark-source route

- $P(X_j^{[i]} \big| \mathbf{Y_i}) = P(X_j^{[i-1]} \big| \mathbf{Y_{i-1}}) \times P(y_{ij}^i \big| X_j^{[i-1]} = x_j, X_i^{[i-1]} = x_i)$
- Normalize $P(X_j^{[i]} \big| \mathbf{Y_i})$
- else
  - $P(X_j^{[i]} \big| \mathbf{Y_i}) = P(X_j^{[i-1]} \big| \mathbf{Y_{i-1}})$

Go back to **Step 3**
Step 5: Decision making after M time steps
For $j = n_a + 1, \ldots, N$

- $\widetilde{x}_j = \underset{x_j}{\operatorname{argmax}}[P(X_j^{[M]} = x_j \big| \mathbf{Y_N})]$.

internode distances as well, e.g., given ± 0.25 path loss estimation offset, 40 m internode distance results in ± 1.5 dB path loss offset which in many cases is negligible compared to shadowing statistics and might be compensated in some cases.

Precision Agriculture Accuracy Requirements: Coverage area of the sensors, spatial correlation of the measured features and distance required between actuators determine inter-node distance for deterministic grid WSN deployments. Further, inter-node distance varies from 10 m for soil moisture [176] and electrical conductivity [177], to coarser resolutions, 60 m for pH sensing [178] or mating disruption applications [179]. As will be seen in Section 4.4.2, our algorithm is well-suited to pest management and mating disruption applications, where tolerance for error, caused by the algorithm simplifying assumptions or mistuned path loss model, is higher.

4.4 Performance Evaluation of The Localization Algorithm

In this section, first we describe the essential aspects of our simulation setup in Section 4.4.1. Afterwards, in Section 4.4.2, we present the simulation results regarding performance of our localization scheme, including analytical and numerical comparison with state-of-the-art techniques such as ADMM [147], SGO [151] and decent gradient methods. In order to evaluate performance of our proposed algorithm, we do the simulations for both random and deterministic (grid) deployment of WSN on a square field. Note that as stated in Section 4.1, our measurements allow us to derive the proposed message passing schedule. However, in order to test the algorithm with real data, a lot more measurement is needed. Further, as explained in our measurement campaign in Section 4.2.3, Tx antenna was fixed in each scenario and Rx antenna only moved along certain directions with data being collected at certain distances. However in our cooperative algorithm, communication may occur between any pair of connected nodes at any location in the field, with any relative distance and angle.

We particularly use simulations to show that the average number of unknown nodes and landmarks each node connects to, affect the accuracy of the localization algorithm for a specific landmark arrangement. Therefore, we define two parameters, so called *average landmark degree* and *average unknown node degree*. Let landmark and unknown node degree of an arbitrary node S_i be the number of landmark and unknown nodes S_i is connected to. Note that node degree in graph theory is strongly related to connectivity in the communications context. Further, average unknown node degree depends on the deployment density and transmit power level of unknown nodes, while the transmit power of landmarks, location of the landmarks and number of them affect the landmark average degree. Different metrics have been used to evaluate performance of the localization algorithms [180].

We use Twice the Distance Root Mean Square (2DRMS) as the accuracy metric for our localization technique where 2DRMS=r means there is 95% confidence that the location estimation would fall within a circle with radius r around the actual node's location. Note that location estimation itself is a random variable due to random nature of path loss samples, and the generating source node. This is due to the event-driven data delivery model which is normally used for precision agriculture applications which implies that a sensor transmits data only when a feature exceeds a predetermined threshold, therefore message passing schedule is different after landmarks advertise themselves. The random nature of the problem makes 2DRMS an acceptable accuracy metric. In this work, we do not focus on optimizing landmarks location, however in the next section we describe the logic behind our adopted landmark arrangement. In the remainder of this section, first we explain the simulation setup and assumptions. We will then proceed with numerical examples to evaluate the performance of our algorithm.

4.4.1 Methodology

In this section, it is first explained why we opt for placing landmarks in the corner or middle of border lines, and proceed with justifying assumptions regarding adopted transmit power, orchard size and node density. For precision agriculture applications inside farms, gateways are placed on the corners and borders of the field, however in the following, we present the reason on why this would help to ensure the improvement of localization algorithm.

Landmark Arrangement: Even though, placing landmarks close to each other and at the centre of the field yields a higher average landmark degree, the localization accuracy drops dramatically since their path loss behaviour has a very high correlation at a given direction and the path loss samples collected from them, are fairly close to each other at almost any point inside the field. Moreover, we place landmarks in the middle of borderlines or in the corners, because this arrangement provides more information about unknown node's location. In Figure 4.5, for a random unknown node location, it can be seen that having a more landmark degree does not necessarily result in a better location estimation. This is because distances in Figure 4.5a are fairly close to each other, and given that a noisy estimation of them are made based on path loss samples, the location estimation will be far less accurate compared to the arrangement in Figure 4.5b. It can be easily shown that this scenario holds for most points on the field. Studying other landmark arrangements could be done accordingly, however we avoid to elaborate on it, since it does not add valuable information to evaluation of the algorithm, and is therefore beyond the scope of this work.

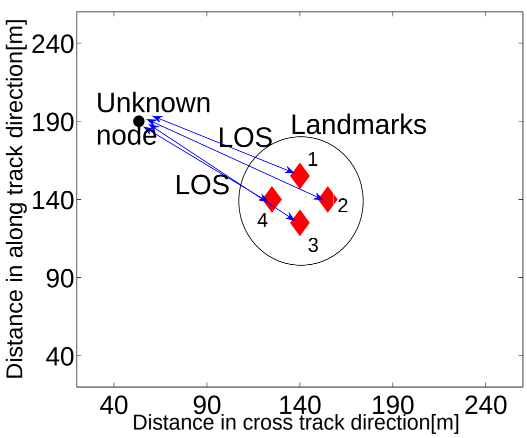

(a) Landmarks placed in the middle with every one of them having line of sight to the unknown node

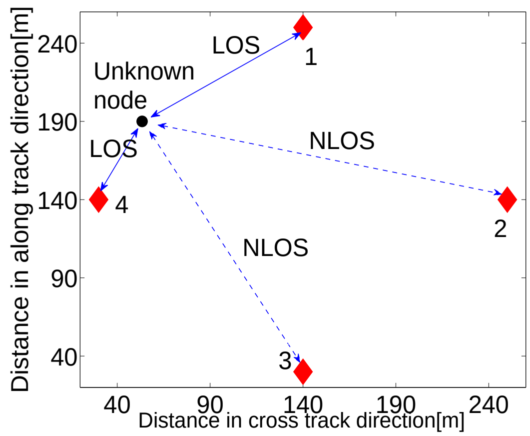

(b) Landmarks placed on the borders with only two of them having line of sight to the unknown node

Figure 4.5: Two different landmark arrangements; The landmark arrangement in (b) provides more information about location of the unknown node despite having fewer nodes having line of sight to the unknown node

Table 4.4: Deployment Scenarios

Orchard size	6 ha, 20 ha
Node density (nodes per hectare)	3, 7
Node arrangement	Grid
Transmit power level of unknown nodes	0-15 dBm
Transmit power level of landmarks	15 dBm
Transmit power increment step	1 dB
Receiver sensitivity for PER=1%	-103 dBm
Grid cell dimension	30 m
Number of landmarks	2,3,4,6 and 8
Location of landmarks	borders and corners
Landmark degree (6 ha orchard)	varying from 1.78 to 6.3
Landmark degree (20 ha orchard)	varying from 0.8 to 2.18
Maximum transmission distance for below canopy mode	120 m
Maximum transmission distance for above canopy mode	220 m

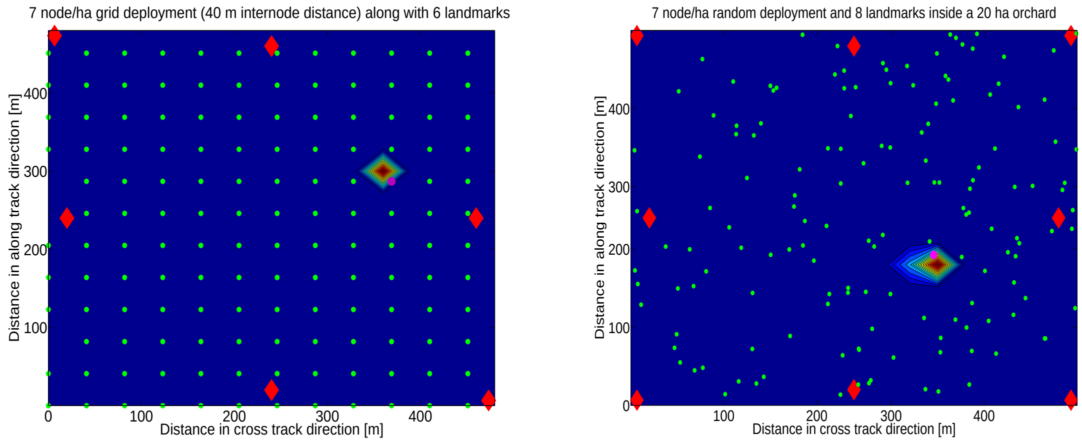

(a) 6 landmarks

(b) 8 landmarks

Figure 4.6: Two different landmark arrangements; unknown nodes and landmarks are demonstrated with green small dots and red large diamonds respectively. Location pmf for the designated unknown node (purple) is illustrated by heat map.

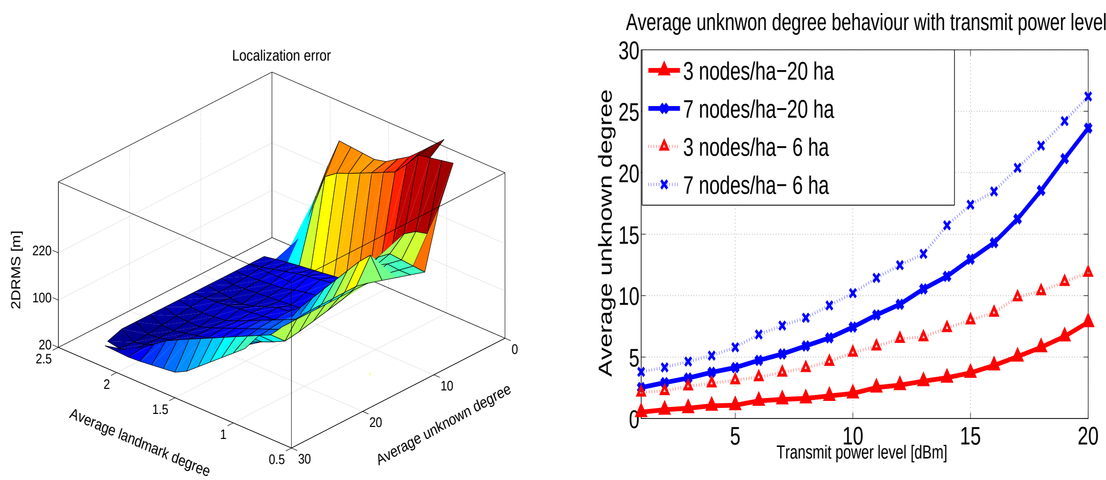

(a) 2DRMS with respect to average landmark and unknown node degree is depicted. Surface points are collected from all deployment scenarios

(b) average unknown node degree of nodes with respect to transmit power level of the unknown nodes. Dotted and solid graphs represent deployment scenarios for 6 ha and 20 ha orchards respectively.

Figure 4.7: Effect of landmark and unknown node degree is illustrated in (a); Effect of transmit power level on average unknown node degree is shown in (b).

Deployment Scenarios and Assumptions: In our simulation setup which is summarized in Table 4.4, we adopt two different orchard sizes including 6 and 20 ha with nodes

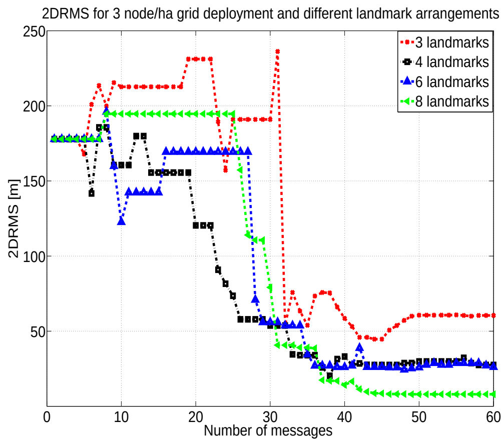

(a) Low density grid deployment

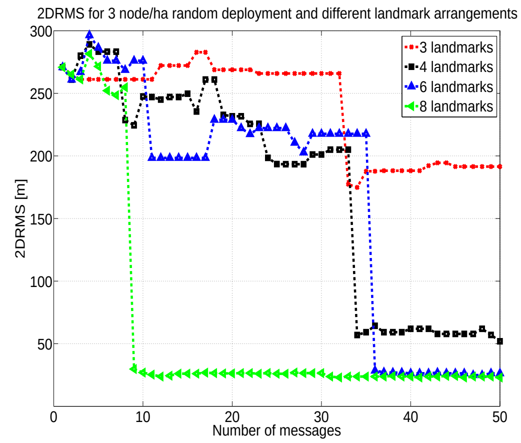

(b) Low density random deployment

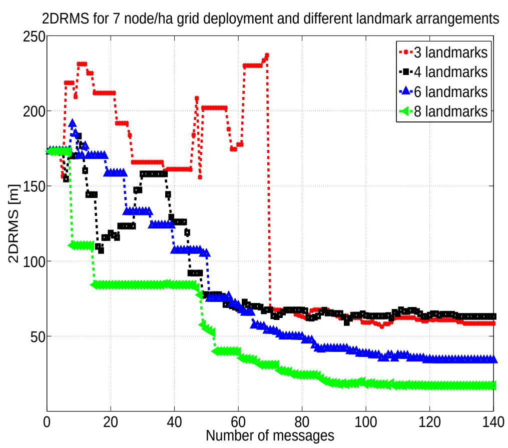

(c) High density grid deployment

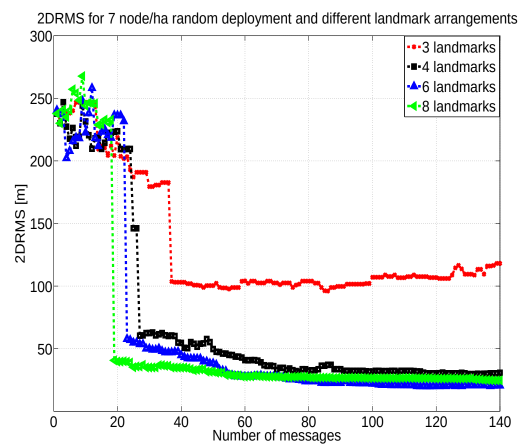

(d) High density random deployment

Figure 4.8: 2DRMS for different node densities and landmark arrangements inside a 20 ha apple orchard; Low and high density grid deployments translate to 60 m and 40 m internode distance respectively and is well-suited to mating disruption.

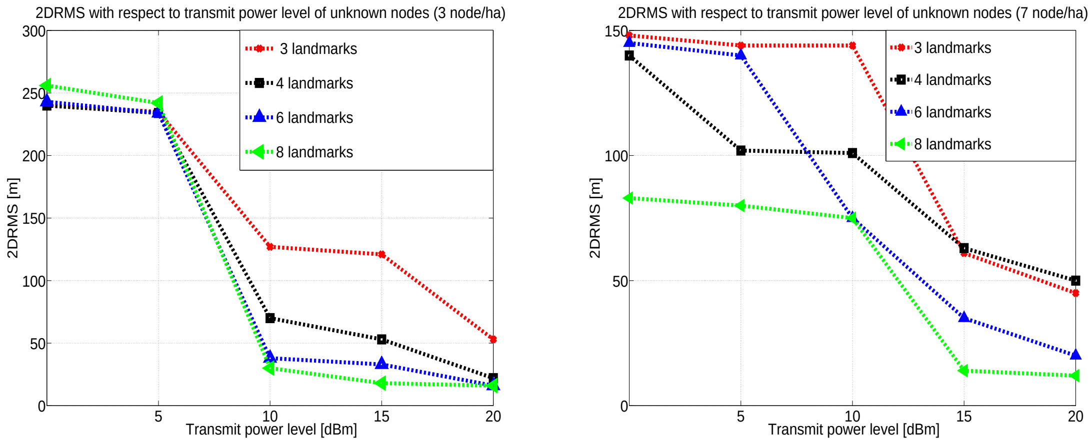

(a) High density grid deployment

(b) High density random deployment

Figure 4.9: 2DRMS variations with transmit power level P_{tx}; different scenarios in terms of node density and number of landmarks inside a 20 ha apple orchard are illustrated. The 2 landmark scenario is excluded for the sake of clarity and lack of space since it achieves a fairly low accuracy. Increasing node density allows us to achieve low 2DRMS with lower number of landmarks and transmit power

randomly scattered inside the field at two different densities, 3 nodes/ha, and 7 nodes/ha. As discussed in Section 4.3, these are the densities used for pest management applications and translate to 60 m and 40 m inter-node distance for grid deployment respectively. Grid cell dimension is chosen to be 30 m so that both these densities could be covered. The average size of an apple orchard varies from 1 to 20 ha in different world regions, while the average size in Canada and the United States is approximately 6 ha and 20 ha respectively according to the United States Department of Agriculture [181]. Node density and type of deployed RF modules varies based on the precision agriculture application and required sampling range [182]. We simulate the algorithm with four landmark arrangements, while transmit power level of unknown nodes is between 0 and +15 dBm. Receiver sensitivity for PER=1%, is -103 dBm, and the communication between landmark and nodes occurs at maximum transmit power (+15 dBm). Variation of landmark degree for different number of landmarks and orchard sizes is also expressed in Table 4.4, which is based on the assumption that Synapse RF200 modules are used [183].

As mentioned earlier in this chapter, we assume that landmarks (gateways) and unknown nodes (sensors) are mounted above and below canopy level respectively. We call S_i and S_j connected, $d_{ij} < d_{connectivity}$, in case the probability of RSSI falling below receiver sensitivity is below 1% or connectivity probability is above 99%. This maximum transmission distance is calculated based on our measurement-based path loss model summarized in Table 4.2. In Table 4.4, we have tabulated the transmission distance of Synapse RF200 module at its maximum transmit power so that connectivity requirement is met [183]. In the next section, we evaluate the performance of our algorithm.

4.4.2 Results

In this section, we study the localization error of our algorithm for different simulation scenarios. In Figure 4.6, two landmark arrangements, 6 and 8, along with 150 deterministically and randomly scattered sensors transmitting at maximum transmit power, are illustrated. Location distribution of one designated node (purple node) after the algorithm converges is illustrated. In Figure 4.7a, we show the behaviour of 2DRMS with respect to average landmark and unknown node degree. As seen in the surface plot, error drops dramatically with average unknown node degree increasing. Further, even for a low average landmark degrees, ≈ 1.5, an approximate average unknown node degree of 8 yields the desired 2DRMS (≈ 20 m).

In Figure 4.7b, we demonstrate how average unknown node degree increases with transmit power level of unknown nodes in different simulation setups. These two figures provide an insight on how algorithm works with different transmit power levels. In Figure 4.8, 2DRMS behaviour for different simulation setups during course of the algorithm is demonstrated which shows that the algorithm converges after a few messages are multicast in the network. As explained in Algorithm 2, the procedure starts with landmarks advertising themselves to the entire network. This accelerates convergence of the algorithm significantly, because one-hop neighbours of landmarks achieve a narrower pmf estimation during the first round. As can be seen in Figure 4.8, generally 6 and 8 landmark/gateway scenarios meet the accuracy requirement for pest management, however in order to make the algorithm work for soil moisture application, number of landmarks or their maximum transmit power needs to increase.

In other words, our simulations showed that a finer grid resolution does not affect the accuracy in case cell dimension already supports the application in terms of internode distance. We also observed that the total number of messages needed for algorithm to converge grows slower than $O(N)$ which is a promising aspect from the scalability stand of view. Moreover, in spanning tree variants of BP-based techniques, at least $O(N)$ messages are required to make the spanning tree and after that every sensor needs to do a multicast at each iteration with algorithm taking anywhere between 1 and 3 iterations to converge. This means our algorithm is faster and consumes less communication energy to converge at the expense of accuracy.

In Figure 4.9, localization error for a 20 ha orchard, 40 m and 60 m inter-node distances, with respect to transmit power level is depicted. Node density has higher influence at low transmit power levels which is compatible with our observations from Figure 4.7a. Once transmit power increases, at a fixed landmark degree, average unknown node degree exceeds the required threshold and error drops to minimum. Based on [173] and our simulations, the algorithm meets pest management (mating disruption) requirements with acceptable probability inside a 20 ha orchard with 8 landmarks. However a different transceiver module demands for different landmark setups since the maximum transmit power level is different, whereas more landmarks are needed in larger orchards in order to meet the average landmark degree.

Comparison with State-of-the-art Distributed Techniques: In this section, we compare our proposed algorithm with state-of-the-art distributed techniques which were briefly explained in Section 4.1 and 4.2.1 and have been applied to similar localization problems, i.e., large static anchor-based WSNs. As seen in Table 4.5, which has been partially extracted or derived from [147, 148], the main advantage of our algorithm is its scalability reflecting in communication and computational cost which does not scale with size of the WSN. Note that in [148] which is a gradient decent algorithm a dynamic step size update along with position update is being used in order to accelerate the normally slow convergence of gradient descent algorithms, i.e., proportional to inverse square root of iterations number [184]. Gradient descent algorithms are more close to our work from the communication cost point of view since each node only transmits its location which is identical for every destination node however they suffer from very slow convergence. Step-size adjustment discussed in [148] introduces communication complexity because of coupled variables however increases convergence rate. Further, in each node two inner and outer sets of iterations corresponding to step size and position updates are running. Both sets of updates require inter-node messages to be exchanged between a node and all its neighbouring sensors which imposes an immense communication overhead.

In [147], ADMM method is used to solve convex edge-based relaxation of localization problem, with coupled variables, in a distributed manner. Moreover each node needs information from neighbouring nodes in order to solve a convex SDP optimization at each iteration, i.e., Algorithm 2 in [147]. On the other hand in [151], an extension of Gauss-Seidel algorithm is used to solve the edge-based relaxation problem in a distributed manner. The main differences compared to [147] is that the optimization problem at each node is SOCP, i.e., less complex and problem is solved sequentially, thus converges significantly slower than [147]. The proposed Bayesian model for information aggregation in this chapter has a communication and computational cost that only grow with field dimensions as opposed to size of the WSN in terms of number of nodes. Since iterations in our work and discussed techniques are different both in terms of duration and communication context, we use the metrics in Table 4.6 for numerical comparison.

In the numerical comparison, we only compare the Bayesian proposed model with the algorithms which can run in parallel [147, 148] since sequential algorithms such as SGO [151] are not well-suited to run in conjunction with route discovery phase of AODV-based protocols. We use the scenario with high density grid deployment and 8 anchors for numerical comparison against [147, 148]. This is one of the scenarios used in Section 4.4.2 and very similar to the scenario used in [148]. We used MATLAB CVX along with SDPT3 package to solve the SDP optimization problems at each node in [147] whereas MATLAB was used to solve Algorithm 2 in [148]. In order for the comparison to be fair, we assume that data containing coupled variables in the discussed non-bayesian techniques is encompassed in one packet and is multicast once since this is compatible with the proposed bayesian model for information aggregation. Note that in gradient descent, number of messages is relatively too high even though amount of exchanged data is lower. This translates to slow convergence rate compared to ADMM [147] and the proposed technique. Aggregate energy consumption of these techniques have been calculated based on transceiver characteristics of Synapse modules. It is noteworthy mentioning that our scheme can be in fact used as an initialization scheme for gradient descent methods in the applications where high accuracy is required while number of anchors is limited.

Table 4.5: Analytical comparison of the proposed technique with state-of-the-art distributed non-Bayesian techniques

Per node per iteration	ADMM [147]	SGO [151]	Gradient descent [148]	Proposed Bayesian Technique
Size of the problem	convex optimization with $7\|N_i\| + 2\|N_{i,a}\| + 3$ variables	convex optimization with $4\|N_i\| + 3$ variables	Local gradient and translation with neighbouring nodes information	m^4 multiplications and summations
Computational complexity	$O(\|N_i\| + \|N_{i,a}\|^3)$	$O(\|N_i\|^3)$	$O(1)$	$O(1)$
Communication cost	$9\|N_i\|$	$2\|N_i\|$	$O(\|N_i\|)$	$O(1)$

Table 4.6: Numerical comparison of the proposed technique with state-of-the-art distributed non-Bayesian techniques for 7 nodes/ha and 8 anchors to achieve the desired accuracy (2DRMS=20 m)

Comparison metric	ADMM [147]	Gradient descent [148]	Proposed Bayesian Technique
Exchanged information [kB]	183	135	24
Number of communication rounds	1700	65000	90
Energy consumption for Synapse [mJ]	10	7.6	1.3

4.5 Discussion

Large size of the WSNs deployed in agricultural fields in addition to nature of higher layer communication algorithms in terms of TDMA-based MAC and multicasting make most existing distributed localization algorithms ill-suited for use in such environments. Moreover Bayesian distributed techniques suffer from communication overhead required for setup phase in order to form loop-free graphs. Whereas non-Bayesian techniques are burdened with excessive communication overhead resulted from coupled variables, remarkable computational complexity needed to solve optimization problems at each iteration and generally suffer from slow convergence.

Our scalable RSSI-based localization algorithm overcomes these limitations by: 1) using only local distance estimates with respect to neighbouring nodes, and 2) using a message passing schedule which benefits from a fixed size outgoing message that does not grow with number of neighbouring nodes, and 3) low computational complexity per node at each iteration which only grows with grid size and only involves summations and multiplications. The algorithm uses a Bayesian model for information aggregation to achieve scalable communication and computational complexity with respect to the number of nodes at the expense of accuracy.

The main strength of our localization algorithm is its compatibility with realistic deployment scenarios of WSNs and the low communication overhead it adds to the already deployed routing protocols. Further, the route discovery phase of AODV routing protocols, e.g., ZigBee and similar schemes, work based on flooding and multicasting RREQ packets; therefore our proposed localization algorithm can be integrated in a convenient and inexpensive manner. Shadowing independence over the links in the apple orchard is an important feature that leads towards the proposed iterative update to the localization problem. However, there are real world scenarios such as urban area where there might be a large correlation among shadowing observed over links.

The main limitation of the proposed algorithm in this chapter is its incapability in terms of achieving high precision localization. Further, as a remedy the proposed algorithm can be used as the initialization step for algorithms such as gradient descent which suffer from high sensitivity to initialization. Moreover the proposed Bayesian model for information aggregation can be used to accelerate convergence of slowly converging gradient descent algorithms in addition to providing them with the initialized location for the scenarios with few number of landmarks and high number of nodes. As a future work, a WSN compatible localization algorithm that overcomes such impairments and eliminate the message dependence and error propagation with low communication and computation complexity would increase applicability domain of this algorithm to a huge extent.

4.6 Acknowledgement

We would like to greatly thank SemiosBio, Vancouver-based startup company specializing in precision agriculture, for generously supporting and funding our measurement campaigns in addition to granting us access to the Dawson orchard at Keremeos, BC. SemiosBio's need for a localization algorithm which could run on Synapse transceiver modules to address mating disruption application was a significant inspiration for the work proposed in this chapter. We would also like to thank UBC Radio Science Lab (RSL) 2012 and 2013 student volunteers for their hard work in preparing for conducting the measurement campaign.

Chapter 5

Directional Path Loss and Its Implications for Node Placement and Network Performance

5.1 Introduction

Existence of radio irregularity and its effects on the performance metrics of routing protocols has been long recognized and studied in the literature [25, 26, 185]. The most dominant features of radio irregularity which have been studied are attributed to shadow and flat fading [25]. Moreover, effect of different radio wave propagation models such as shadowing, two-ray-ground and free space model on the performance of classic routing protocols such as AODV, DSR, OLSR and DSDV routing for fixed and mobile WSNs has been investigated with simulations [86–89, 186, 187]. Zhou et al. introduce different causes of radio irregularity [25] and show that link asymmetry caused by fading does not have a remarkable impact on performance of the AODV routing protocol. This is associated with multi-round discovery phase nature of the protocol, i.e., a new route is found during the next round of route discovery phase. Effect of shadowing on end-to-end connectivity has also been studied [188, 189]. Further, in link level studies, Rajagopalan et al. [188] concluded that higher shadowing variance increases link connectivity, however this is attributed to shadowing independence assumption between links. Whereas Bestseller and Hartmann [189] have taken shadowing correlation into account and studied impact of shadowing on connectivity of multi-hop randomly deployed WSNs showing that higher shadowing variance still increases the link connectivity. There is also a large number of works analytically evaluating the effect of fading, shadowing and different communication coverage models on network throughput, or end-to-end connectivity [188–191].

Our work is similar to [189, 191] in the sense that it is based on connectivity for WSNs in lognormal shadowing environment however directional path loss component is the dominant feature in our study. Further, in previous works, connectivity of sensor nodes is derived based on assumptions which may not be valid for particular environments, e.g., orchards, warehouse or libraries. Moreover in these works, either power-law (disk-shape coverage model) or isotropic log-distance attenuation models have been deployed to study connectivity in WSNs. However in artificial man-made row-like environments, path loss may have directional components. Directional component of path loss in these environments has not been characterized and its impact on routing protocols has not been studied.

In this work, first we show directional path loss is a real phenomenon by measuring it in a realistic environment. Further, we show existence of directional path loss in the farm environments and particularly apple orchards. We proceed to show that its impact on performance metrics of AODV routing protocol such as network lifetime, and average number of hops packets travel is remarkable. Note that average number of hops is an indication of latency and energy consumption in the network. This is a different approach from works in precision agriculture context that have studied node placement and its effect on connectivity [75, 76]. In [75], Liu et al. have compared connectivity of deterministic deployment patterns inside a wheat field during different growing seasons. Even though path loss exponent is characterized for seeding, booting, and jointing stages, both shadowing effect and path loss directionality have been dismissed. Ndzi et al. [76] have characterized path loss inside a mixed crop farmland based on measurements conducted along the rows in different sections of the farm and have derived components of power-law attenuation model for each crop type. Dependence of connectivity on crop type is mentioned however more measurements for each specific crop type and land geometry is required prior to crop-based evaluation of higher communication layers.

We use simulations to show that directional path loss limits the number of nodes each node connects to, so-called mean node connectivity in the network. Afterwards we show that decreased mean connectivity results in increased hop count and shorter network lifetime. As a mitigation strategy, we suggest alternative node placements by narrowing down and widening the inter-node distances along the directions which experience higher and lower impairment respectively as a result of directional path loss. Contribution of this work is twofold:

- Firstly, we choose an apple orchard as an example of realistic environments which are made up of rows of similar aligned objects to show existence of directional path loss by our measurement campaigns. Further we show that its impact on the performance of AODV routing protocols, e.g., network lifetime and latency under conventional node placements is real and measurable.

- Secondly, we generalize the path loss model derived from our measurements in agricultural fields to directional path loss associated with the environments which are similar to apple orchards in terms of geometry and study its effect on AODV routing protocols. Further, we show that directional path loss decreases network lifetime in addition to increasing mean hop count by decreasing mean connectivity in the network.

The remainder of this chapter is organized as follows: In Section 5.2, we explain network performance metrics, conventional deterministic node placements, AODV routing protocols and how their performance is affected by directional path loss. In Section 5.3, we explain our measurement campaign in the Dawson apple orchard, general directional path loss models corresponding to similar environments followed by results and conclusion in Sections 5.4 and 5.5 respectively.

5.2 Concepts

As mentioned in Section 5.1 and as we will show in Sections 5.3 and 5.4 directional path loss is likely to be encountered in many practical scenarios including precision agriculture. In this section, we first explain basic definitions regarding performance of routing protocols then will proceed to explain basics of AODV protocols and how directional path loss affects the established routes. Finally we will explain how this translates to energy efficiency, network lifetime and latency in the network.

5.2.1 Review of Conventional Node Placement Strategies for WSNs

Regular deterministic node placement is the most common technique used for precision agriculture applications [75, 76] and similar man-made environments. Further, even though random deployment strategies are well-suited for applications such as reconnaissance mission during combat or forest fire detection, deterministic node placements are well-poised to address man-made symmetric environments. The most popular deterministic node arrangements are square, triangular and hexagonal tessellations depicted in Figure 5.1. The internode distance d_0 and number of nodes for a specific internode distance and field area A are tabulated in Table 5.1. Precision agriculture applications are diverse in terms of node density requirements since different sampling distances are demanded by each application. For instance, as stated in Chapter 4, applications such as soil moisture monitoring for irrigation or electrical conductivity require high density deployment ($\approx$ 50-100 nodes/ha) [176, 177], whereas pest management or pH monitoring require much sparser deployments ($\approx$ 3-8 nodes/ha) [178, 179].

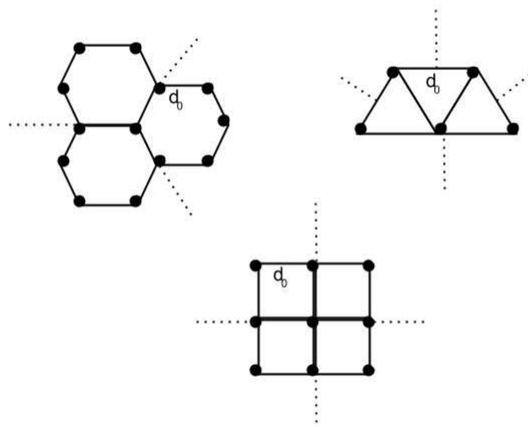

Figure 5.1: Different regular topologies; square, triangular and hexagonal networks

Table 5.1: Parameters for different tessellations corresponding to a WSN with N nodes and inter-node distance d_0 deployed in a field with Area A

Tiling	Triangle	Square	Hexagon
d_0	$\approx 1.07\sqrt{\frac{A}{N}}$	$\approx \sqrt{\frac{A}{N}}$	$\approx 0.88\sqrt{\frac{A}{N}}$
N_e	$\approx 1.15\frac{A}{d_0^2}$	$\approx \frac{A}{d_0^2}$	$\approx 0.77\frac{A}{d_0^2}$

5.2.2 Basic Definitions

In this section, we define network lifetime and mean hop count as two important performance metrics of routing protocol. As stated in Section 5.1, mean hop count is a measure for energy consumption and latency in the network due to the linear relationship between them. We also define link connectivity and end-to-end route connectivity since they form the basis for route discovery phase and communication phase of AODV routing protocols.

Network Lifetime: As mentioned in Chapter 2, various network lifetime definitions are proposed in the WSN context [102] with each network lifetime fitting best for a different application. In this work since we do not make any specific assumption regarding the application and due to structure of the network which consists of a gateway in the corner of the field, percentage of nodes that have a path to BS is defined as the network lifetime measure. To be more specific, we define network lifetime as the duration after which there is no path between any node and the gateway.

Mean Hopcount: We define this metric as the average number of hops a packet takes in order to reach the destination given that transmission is successful [192]. This is an important metric since it provides a measure to identify length of the reliable routes in the network. Besides, it is linearly related to end-to-end delay and aggregate energy consumption in the network.

Link Connectivity: Link connectivity is the probability of signal power remaining above a detectable threshold γ over the link between a transmitting and receiving node. For log-distance ettenuation model, path loss $\beta_{LD}(dB)$ is expressed by

$$\beta_{LD}(dB) = \beta_0 + 10\alpha \log_{10}(\frac{d}{d_0}) + X_\sigma, \tag{5.1}$$

where α denotes path loss exponent, β_0 represents path loss at reference distance d_0 and X_σ accounts for shadowing which is a zero-mean Gaussian random variable with standard deviation σ, $N(0,\sigma)$. Let L_i represent the event that i-th link exists with d_i denoting length of the link. Let us assume β_1 and β_2 are deterministic and stochastic parts of the path loss respectively, i.e., β_1 is the path loss mean and β_2 accounts for shadowing and is a zero-mean Gaussian random variable with standard deviation σ. Link connectivity for i-th link L_i is denoted by

$$\begin{aligned} P\big(L_i \big| d_i\big) &= P(\beta(i) \leq \beta_{th} \big| d_i) \\ &= \int_{-\infty}^{\beta_{th}-\beta_1} f_{\beta_2}(\beta_2) d\beta_2, \end{aligned} \tag{5.2}$$

where $f(\cdot)$ denotes probability distribution function (PDF). Consequently (5.2) yields

$$P\big(L_i \big| d_i\big) = \frac{1}{2} - \frac{1}{2} erf\big(\frac{10\alpha}{\sqrt{2}\sigma} \log_{10} \frac{d_i}{d_{ref}}\big), \tag{5.3}$$

where

$$r_0 = 10^{\frac{\beta_{th}}{\alpha 10dB}}\ m, \tag{5.4}$$

is the maximum distance which guarantees availability of i-th link when $\sigma = 0$ or for a channel with power-law attenuation function $P_r(j) = P_t(i)d^{-\alpha}$ and $\mathrm{erf}(\cdot)$ represents the error function.

End-to-end Route Connectivity: End-to-end route connectivity is the probability that a specific route between source and gateway nodes is up [188]. This definition is useful in the sense that there is usually one gateway in the corner of the farm which collects packets sent by sensing source nodes scattered inside the field. Let us assume there are n hops between a source node and the sink. In case link connectivity over the link arriving at j-th hop is denoted by $P_h^{(j)}$, *end-to-end route connectivity* for i-th route, C_{R_i}, is calculated by

$$C_{R_i} = \prod_{j=1}^{n} P_h^{(j)}. \tag{5.5}$$

Note that link connectivity $P_h^{(j)}$ is a function of path loss model.

Mean Node Connectivity: Mean node connectivity, $\overline{C_i}$ is average number of nodes each node can connect to. Let $P_j^{(i)}$ denote link connectivity between j-th and i-th nodes. Node connectivity for i-th node is then calculated by $\overline{C_i} = \sum_{j \in \mathbb{S}} P_j^{(i)}$, where $\mathbb{S}$ represents set of all sensors in the network.

5.2.3 AODV Routing and Its Performance Under Directional Path Loss

In this part, first we briefly explain how AODV routing protocol performs and then based on the metrics defined in previous section we will use an example to clarify how directional path loss may affect the resulted routes in addition to energy efficiency and network lifetime thereof.

AODV Routing Protocol: AODV-based protocols are important since they form basis for multi-hop networking deployed on IEEE802.15.4 COTS modules in WSNs. In the following we explain the three main phases in AODV [193]:

Route Discovery Phase: Source node originates a RREQ packet which floods through the entire network via multi-hop routing to reach the gateway. Each node adds its own ID to the path list in RREQ and forwards it to its neighbours, while RREQ is discarded in case its travelled path is longer than that of the previous received RREQ packet. Gateway will subsequently send a RREP packet over the shortest hop route and makes each node aware of its next hop node.

Communication Phase: Nodes start to send data based on the assigned routes.

Route Maintenance Phase: *Hello* message is broadcast by node A so that a neighbouring node B would update its entries for which, node B is the next hop to node A. In case, *Hello* message or regular messages from node A are not received for a specific period of time, route discovery phase will start again so that new reliable routes are established.

Effect of Path Loss Model on Performance Metrics of WSNs

As explained in Section 5.2.2, link and route connectivity are functions of path loss model. As stated in Section 5.2.3, for a certain route between a source and the gateway to be chosen, a RREQ packets is required to travel the route up to the gateway and RREP packet is required to return back to the source.

In the following, through a simple example we explain how end-to-end route connectivities and consequently performance metrics of AODV protocols change under directional path loss assumptions,

Example: We clarify the problem with a very simple example. Consider the simple network illustrated in Figure 5.2 with two routes R_1 and R_2 being available between source node (S) and gateway (G). Assume that end-to-end route connectivities C_1 and C_2 are derived based on two different path loss models in terms of directivity degrees so called scenarios 1 and 2. For instance, scenario 1 may represent a situation where directivity is more severe than in scenario 2. This is because even though end-to-end route is longer both in terms of physical length and hop count, end-to-end connectivity is the same on routes R_1 and R_2 whereas in scenario 2, R_1 benefits from a much better connectivity.

As explained in the beginning of this section, these metrics are important since in order for a specific route to be assigned during the route discovery phase, RREQ and RREP packets need to traverse the route successfully. Furthermore, as explained in Section 5.2.2, in fact C_1 and C_2 represent the end-to-end connectivity of routes R_1 and R_2 respectively and represent the probability of signal remaining above a threshold once transmitted from one end of the route and received at the other end.

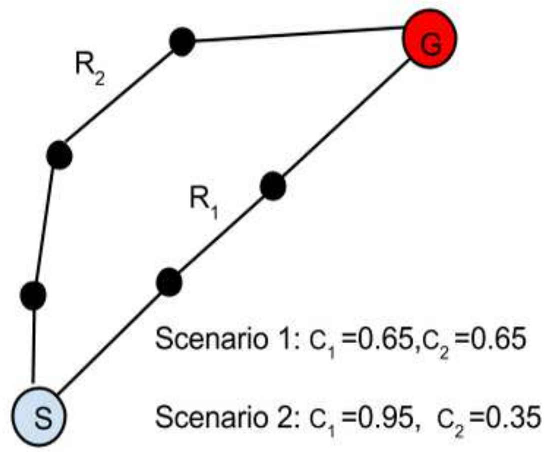

Figure 5.2: Connectivity graph of a simple network with two paths between source and the gateway

For Synapse transceiver modules with amplifier efficiency η=0.2, electrical circuitry power consumption P_{elec}=100 mW, reception power P_{Rx}=80 mW, packet length of 44 bytes, l_1=3, l_2=5 and assumption of nodes transmitting at full transmit power 15 dBm, network performance metrics are tabulated in Table 5.2. As seen in this table and as it is easily calculable, around 30% saving in terms of energy consumption is achieved.

Table 5.2: Performance of the AODV protocol under two different scenarios for the simple network connectivity graph illustrated in Figure 5.2

Scenarios \ Performance	Average energy ($\frac{\mu J}{bit}$)	PDR (%)	Average number of hops
Scenario 1	5.37	65	3.37
Scenario 2	3.83	94	3

5.2.4 Alternative Node Placement Strategies

As explained in Section 5.2.1, deterministic regular patterns are the most common node placements used for WSNs in man-made environments such as precision agriculture. However depending on different design objectives such as coverage, connectivity, network lifetime and data fidelity and constraints such as number of nodes, transmit power among others, alternative node placement techniques have been proposed [8, 194]. In this work, in order to increase node connectivity along directions of interest under directional path loss circumstances, we introduce elongated grid placement technique which includes increasing and decreasing internode distance along least and most impaired directions while keeping node density fixed. Further, we introduce a measure called *elongation index*, ω_{d_0}, as a multiplicative factor for changing internode distance d_0. Introduction of elongation index ω_{d_0} to the regular square pattern demonstrated in Figure 5.1, multiplies internode distance along one direction by ω_{d_0} and the perpendicular direction by $\frac{1}{\omega_{d_0}}$ so that node density, i.e., number of nodes is kept intact. Similarly for triangular and hexagonal patterns, this translates to scaling the internode distances so that the area of the newly formed triangle and hexagon is kept fixed. In this work we only study grid square deployment however its extension to other regular patterns is straightforward. Our purpose from this technique is to make node connectivity along different directions more uniform, therefore increase node connectivity along directions that result in lower hop count towards gateway. The effect of such a scheme on realistic directional path loss scenarios will be simulated in Section 5.4.3.

5.3 Methodology

In this part, first in Section 5.3.1 we explain our measurement campaign in the Dawson orchard, Keremeos, BC which helps us observe directional path loss in agricultural environments, particularly apple orchards. In Section 5.3.2, we explain how node connectivity is affected by path loss model observed in agricultural environments since this model serves as a representative case study for similar man-made environments. Afterwards, inspired by the directional path loss observed in this specific environment, in Section 5.3.1 we generalize this model to encompass similar environments which are made up of similar objects aligned on side-by-side rows. We also introduce a metric so called directivity degree to represent the general model introduced in this section. Finally in Section 5.3.3, we explain the deployment scenarios and simulation assumptions which underlie the results explained in Section 5.4.

5.3.1 Observations of Directional Path Loss in Precision Agriculture

In this section, we first explain management of high density apple orchards in terms of rootstock type, tree density and between-row-spacing. We proceed with path loss models for vegetated environments and measurement campaign.

Management of High Density Apple Orchards: Any orchard with more than 150 trees/acre is considered high density. There are various ways high density apple orchards are managed in terms of rootstocks and training system [195–197]. Rootstock type determines tree height, while training system is decisive in terms of number of trees per acre defined by in-row and between-row-spacing. The majority of rootstocks used in Similkameen valley, BC are M9 and B9 which are medium in terms of height, 2.5-3 m. Training systems, on the other hand, are categorized into vertical axis (550-900 trees/acre), slender spindle (700-1500 trees/acre), and super spindle (2000-5000 trees/acre). Vertical axis, and slender spindle with between-row-spacing of 13 ft-15 ft and 10 ft-12 ft respectively, are very popular in the region. In-row spacing for vertical axis is 4-6 ft, whereas 3-5 ft is required for slender spindle management.

Path Loss Models for Vegetated Environments: As explained in Chapter 4, drawback of existing models for vegetated environments is that they only account for the vegetation path loss. Further, there are more factors such as ground and canopy reflection contributing to path loss which make the aforementioned models unable to make a good prediction of path loss in realistic environments. Besides, modified models that take ground and canopy reflection into account have been proposed however are more complex since they include summation of multiple terms to take ground and canopy reflection into account [166]. In order to address this issue, log-distance model is proposed since it encompasses effects of all contributing factors and propagation mechanisms [75, 167–169].

Measurement Campaign: We carried out our measurements in Dawson orchards at Keremeos, Similkameen valley, BC, the majority of which is under vertical axis training system. Measurements were done in two 15 acre (ac) orchards consisting of apple tree rows which are considered high density in terms of vegetation with tree rows being approximately 4.5 m/15 ft apart from each other. We did our measurements along five directions of along, across, 30°, 45°, and 60° with respect to tree rows, using different transmitter and receiver antenna heights. The measurements were conducted throughout three different measurement campaigns, seven days combined and spread across two summer seasons.

We did the measurements in approximate range of 0-100 m at points which are approximately 10 m apart from each other in 9 different parts of the orchard with scenarios having been illustrated in Figure 5.3. Our equipment on the transmitter side, are an Agilent E8267D VSG feeding a 2.45 GHz omnidirectional dipole antenna with 5 multi-tones (5 MHz apart from each other) through a ZVA-213 power amplifier which provides +23 dBm as the antenna input. On the receiver side, a Toshiba laptop which runs MATLAB and Agilent connection expert, specialized proprietary software for connecting computer to Agilent spectrum analyzer, is connected to a N9342C HSA via a LAN cable. Extra losses and gains resulted from cables, connectors and antennas at both Tx and Rx sides are taken into account for calibration. Using the explained setup, we were able to capture path loss up to

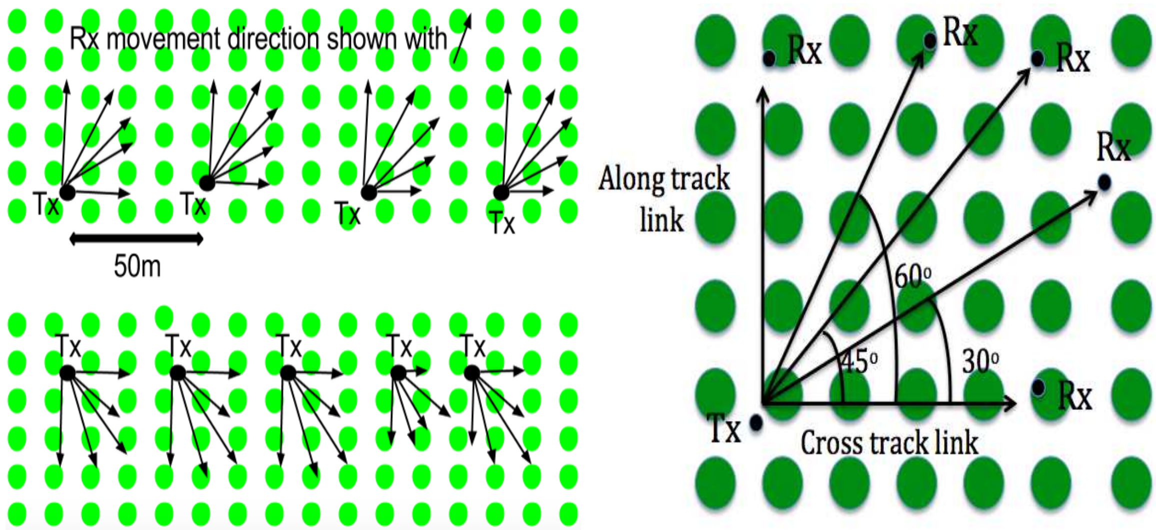

(a) (b)

Figure 5.3: 9 measurement scenarios inside the orchard is illustrated; Transmitter antenna was moved 50 m across the rows to form a new scenario whereas Rx was moved along five different directions of along, cross, 30°, 45° and 60° for each scenario, with path loss samples being collected from 0-100 m range and at ≈10 m apart points

≈ 115 dB which is suitable for our study case since attenuation is fairly high for *through vegetation* propagation and the amount of path loss IEEE802.15.4 compliant modules such as synapse transceivers tolerate is limited to at most 115 dB [183] based on their maximum transmit power level and sensitivity. Path loss samples collected during our measurement campaigns are illustrated in Figure 5.6. Path loss along the crass track link, appears to be higher than other directions, whereas rotation of links towards the along track lowers path loss. Path loss behaviour characteristics along different directions is tabulated in Table 5.4. Note that path loss exponent α is maximum for cross track links where signal propagates through the most number of tree rows, while along track link shows the minimum path loss exponent which could intuitively be associated with waveguide characteristics of along track rows. In Section 5.4, we will show log-distance path loss mode provides a good fit to data compared to popular existing path loss models. Coefficient of determination, R^2, indicates how well observed outcomes are replicated by the model. The closer R^2 gets to one, the better the variability in data is captured by the model.

5.3.2 Representative Path Loss Model and Directivity Degree

Based on our measurement campaign results, path loss exponent increases as number of tree rows through which the signal propagates rises. Further our extensive measurements show that path loss inside apple orchards is directional, i.e., signal attenuation is higher over the paths which are oriented diagonally or cross-wise with respect to tree rows compared to links that are extended along these rows. Moreover, path loss exponent in the log-normal shadowing model increases as angle between the tree rows and wireless link gets closer to 90°. As a generalization to the path loss model observed in the farm and in order to represent similar environments, we define a parameter so-called *directivity degree*, D_α as the ratio of transmission range along the least to the most impaired direction when there is no shadowing present. This is a suitable measure since shadowing is not a dominant feature in agricultural fields and large static WSNs with similar structure. A new path loss model is created by multiplying path loss exponents α corresponding to different directions derived from our measurement campaign with a fixed number, ω_α, which is greater than one while only along track path loss exponent is kept fixed. Obviously D_α would increase as this multiplicative constant increases. Note that in order to be focused on the impact of directional path loss, i.e., not shadowing, we calibrate shadowing effect so that it is the same along all directions and in all scenarios.

As discussed in management of high density apple orchards in Section 5.3.1, between-tree-row spacing varies from 10 ft to 15 ft depending on the adopted type of training system. As mentioned in Section 5.3.1, our measurement campaign was conducted in a high density apple orchard where the spacing was relatively high, i.e., 15 ft. Therefore, we refer to directivity associated with Dawson orchard as low directivity degree (LDD), $D_\alpha \approx 2$, while the directivity corresponding to smaller between-row-spacing as in slender spindle training system is referred to as high directivity degree (HDD) with $D_\alpha \approx 3$. In Figure 5.4, we have illustrated a schematic view of no shadowing transmission range, r_0, along different directions in the orchard. In Section 5.4, we will study effects of the representative path loss models with $1 < D_\alpha < 5$.

Effect of Directional Path Loss on Node Connectivity: As discussed in Section 5.2.2, node connectivity results from adding up connectivity of links that emanate the node. There-

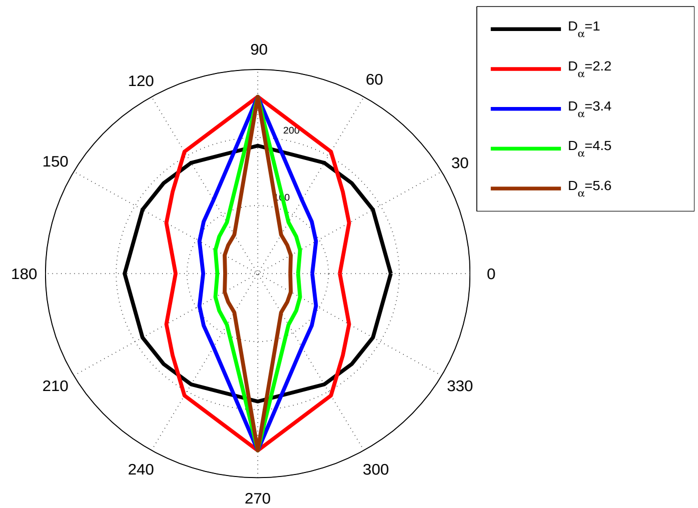

Figure 5.4: No shadowing transmission range, r_0, for different scenarios is illustrated; Along track transmission range is the same for all directional path loss scenarios scenarios since in-row path loss is assumed to be kept intact for different scenarios. $D_\alpha = 1$ represents directional path loss and other scenarios correspond to $\omega_\alpha = 1$, $\omega_\alpha = 1.2$, $\omega_\alpha = 1.4$ and $\omega_\alpha = 1.6$.

fore, directional path loss that is resulted from degradation of links in different directions, i.e., increasing path loss exponent in log-distance path loss model, would decrease connectivity of nodes. In Figure 5.5, a schematic view of directional path loss impact on node connectivity is illustrated, however we are going to simulate this in Section 5.4. Consequently the effect of node connectivity on hop count and WSN lifetime for AODV-based routing protocol will also be studied.

5.3.3 Deployment Scenarios and Performance Metrics

As discussed in Section 5.2.4, deterministic grid deployment is the most common node placement strategy used in precision agriculture. Therefore, we choose square grid pattern as our chosen deployment scheme. Mean hop count is a measure for average energy consumption and latency in the network, while network lifetime as defined in Section 5.2.2, i.e., the duration after which all nodes get disconnected from gateway, serve as the performance metrics.

MAC Layer: As frequent for precision agriculture applications, TDMA MAC underlies the deployed networking protocol. Further, we assume no retransmission occurs due to

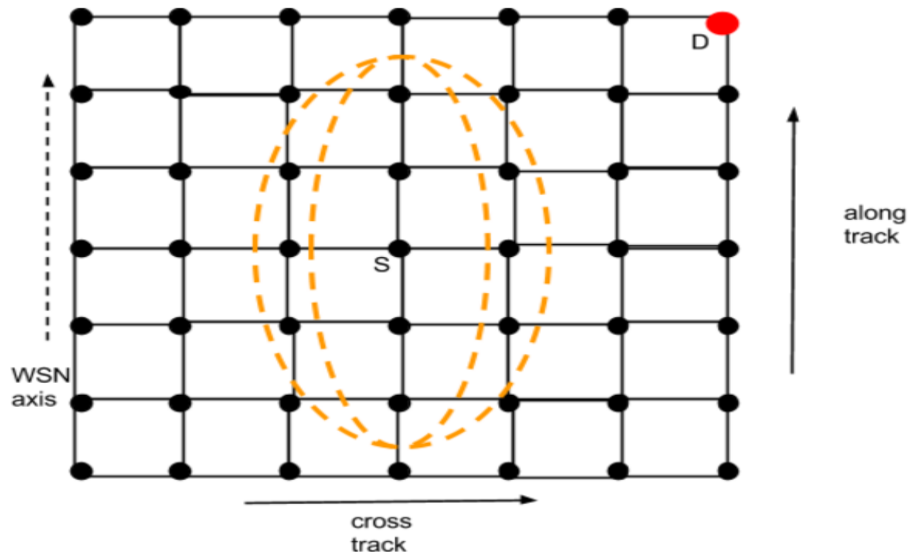

Figure 5.5: Effect of path loss directivity degree on node connectivity is illustrated; Coverage along all directions except for along track has got limited as a result of increased path loss exponent and decreased r_0 in (5.4) which results in decreased node connectivity for S

collision or congestion in the network. Therefore, retransmissions happen because of link failures as a result of shadowing or signal falling below a specific threshold level. In this work, we neglect MAC layer energy consumption since our study is focused on the routing protocol performance. Simulation setup parameters are included in Table 5.3.

Simulation Setup: We tabulated the simulation parameters in Table 5.3. We use MATLAB to simulate the effects of directional path loss on square grid deployment and elongated grid with elongation indices applied. At each time instance a new connectivity graph is made based on path loss models discussed in Section 5.3.2, tabulated in Table 5.3 and the packet is assumed to go through a single link in case the received power is above the reception threshold. For the route discovery phase, as soon as a source node is decided, all the alternative routes from the node to gateway are simulated accordingly in order to select those along which RREQ and RREP packets have traversed successfully. Consequently the route with the shortest hop count is selected from these routes which is the AODV routing protocol characteristics.

Communication then starts between the designated node and the gateway along this selected route which is held unless a packet drops. In the event of packet drops, source node

Table 5.3: Simulation Parameters

Parameter	Value
Topology	square with different elongation indices ω_{d_0}
Topological area	$700 \times 700\ m^2$
Node density (node/ha)	4
Wireless channel	log-normal shadowing with $1 < D_{alpha} < 6$ and $\sigma = 2\ dB$
Transmit power	+15 dBm
Radio model	Synapse RF 200
Center frequency	2.45 GHz
Data rate	250 kbit/s
Data delivery model	query-based
Initial sensors energy	40 μJ
Gateway location	Far right end of the field

would be notified and route maintenance phase will start as discussed in Section 5.2.3.

5.4 Results

In this section we first show the outcome of our measurement campaigns in the apple orchards at Keremeos, BC which shows directional path loss is a real phenomenon. Afterwards we go on with studying the effect of such directivity on node connectivity and network lifetime thereof.

5.4.1 Observation of Directional Path Loss in Precision Agriculture

In Section 5.3.1, we elaborated our measurement campaign in the Dawson orchards as an example for row-like environments, i.e., man-made environments made up of similar objects aligned in side by side rows. We also explained representative path loss models for vegetated environments in Section 5.3.1. In Table 5.5, we show that log-distance path loss model provides a good fit to collected data in the Dawson orchard, while Table 5.4 shows path loss characteristics along different directions. In Figure 5.7, link connectivity for different types of links in terms of direction is illustrated. Link connectivity decreases as the wireless link passes through more number of tree rows.

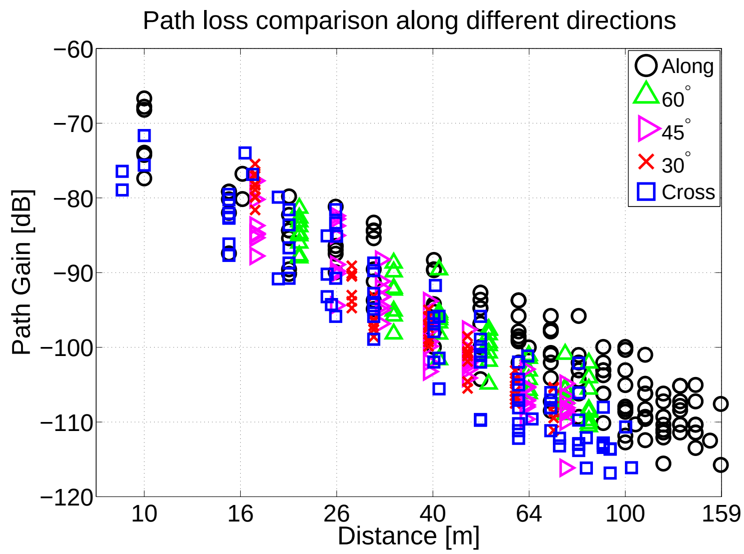

Figure 5.6: Path loss comparison between along, cross, 30°, 45°, and 60° directions; Cross track shows a higher slope followed by 30°, 45°, 60° and along track directions.

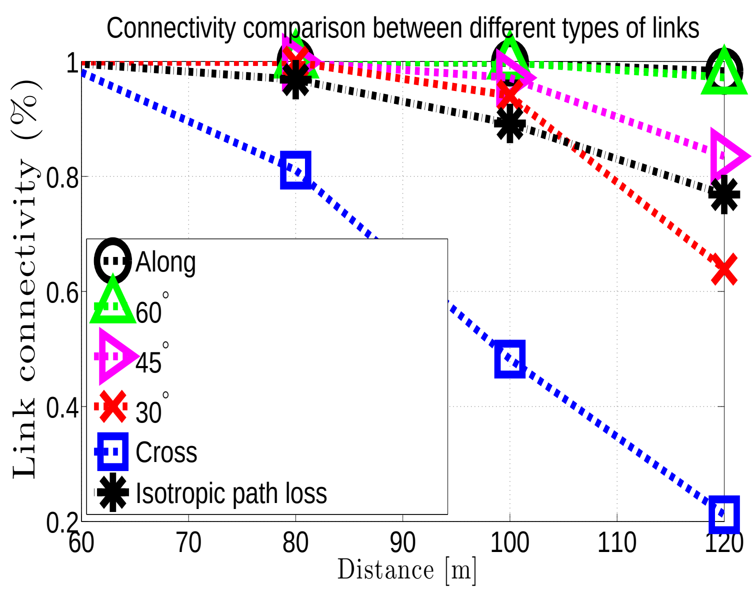

Figure 5.7: Connectivity for different types of links is illustrated; Synapse transceiver module assumptions for transmit power and sensitivity level have been taken into account. It could be seen that most diagonal track links perform worse than the link which corresponds to isotropic path loss model

Table 5.4: Path loss characteristics along different directions in the Dawson apple orchards

Direction	β_0	α	σ	95% CI for β_0	95% CI for α
Along	74	3.12	3.65	70-76	2.94-3.3
Cross	73	4.25	4.45	67-77	3.91-4.59
30°	76	3.92	2.58	73-81	3.62-4.21
45°	76	3.70	3.15	72-82	3.34-4.06
60°	75	3.49	2.79	71-81	3.17-3.81
Isotropic path loss model	75	3.61	5.67	71-79	3.36-3.86

Table 5.5: (R^2,RMSE) for different variants of MED models, modified MED models based on [166] to take the canopy and ground reflection into account as well.

Model \ Track direction	Along	Cross	30°	45°	60°	*Isotropic path loss model*
Weissberger	(0.67,6.85)	(0.41,9.74)	(-4.17,21.95)	(-2.32,16.47)	(-1.23,12.2)	(-0.3,14.01)
ITU-R	(0.43,9.04)	(0.72,6.76)	(-2.65,18.43)	(-1.02,12.83)	(-0.02,8.25)	(0.03,12.08)
FITU-R	(0.81,5.16)	(0.73,6.57)	(-1.8,16.14)	(-0.5,11.06)	(0.12,7.67)	(0.3,10.29)
COST235	(-2.15,21.25)	(-0.38,14.93)	(0.92,2.71)	(0.4,7)	(-0.91,11.27)	(-0.58,15.43)
Log-distance model	(0.9,3.65)	(0.87,4.45)	(0.92,3.92)	(0.4,3.7)	(0.9,3.49)	(0.75,5.67)

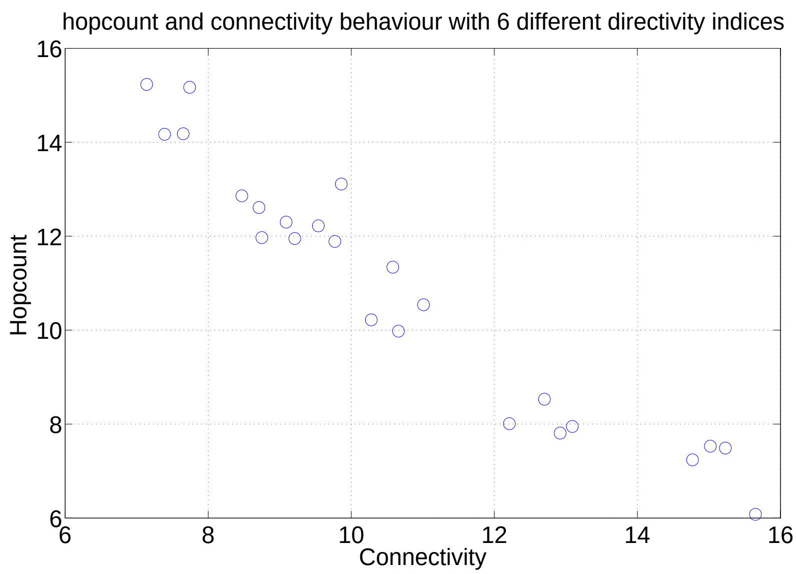

Figure 5.8: Behaviour of mean hop count with respect to mean node connectivity is illustrated; 4 simulations have been run for each directivity degree scenario

5.4.2 Effect of Directional Path Loss on Node Connectivity

In Section 5.3.2, we used a schematic figure to discuss how directional path loss affects node connectivity in the network. In this section, we use simulations to show effect of directional

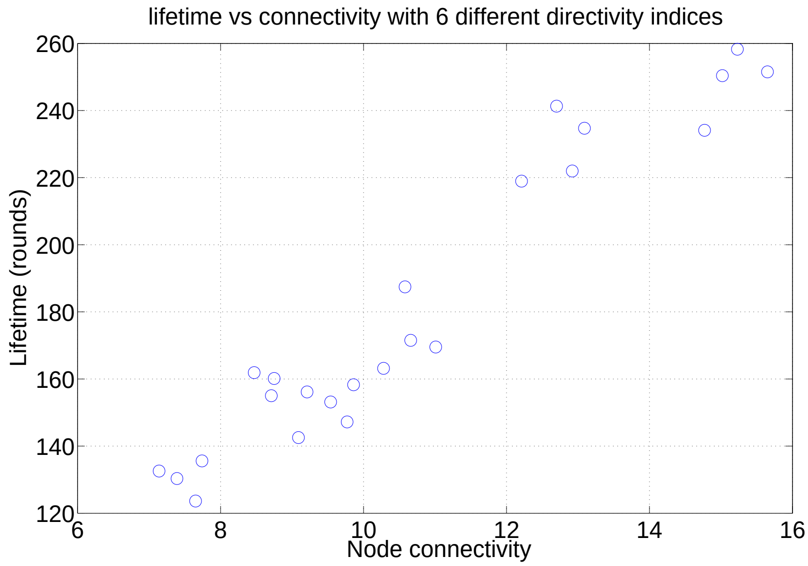

Figure 5.9: Behaviour of network lifetime with respect to mean node connectivity resulted from various path loss directivity degrees is shown.

path loss on mean node connectivity and the manner in which network lifetime and mean hop count are affected by directional path loss for the simulation scenario shown in Table 5.3. In Figure 5.10, effect of directivity degree D_α, i.e., measure of directional path loss, on mean node connectivity. Figures 5.8 and 5.9 show effect of node connectivity on mean hop count and lifetime respectively. As illustrated in Figure 5.8, mean hop count for a packet travelling between a source and gateway drops linearly as mean node connectivity grows. In Figure 5.9, lifetime in terms of rounds with respect to mean node connectivity is depicted. As can be seen, the relationship between these two performance metrics is close to linear.

5.4.3 Mitigation Strategies

As explained in Section 5.2.4, different alternative node placement schemes have been proposed to meet various design objectives for WSNs. In this work we opt for a simple alternative node placement identified by elongation index ω_{d_0} to combat impairments caused by directional path loss in row like man-made environments. Our purpose is to mimic the behaviour of non-directional path loss in the sense that neighbouring nodes surround each node in a more uniform manner along different directions. In Figure 5.11, behaviour of mean hop count and network lifetime for different elongation indices and for three different directivity degrees, D_α, is illustrated. These D_α values correspond to three realistic scenarios explained

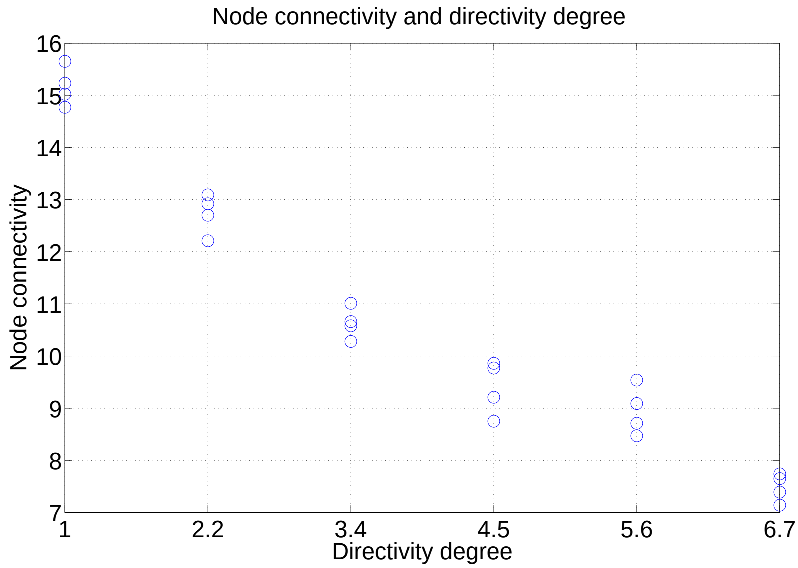

Figure 5.10: Behaviour of mean node connectivity with respect to directivity degree is illustrated; 4 simulations have been run for each directivity degree.

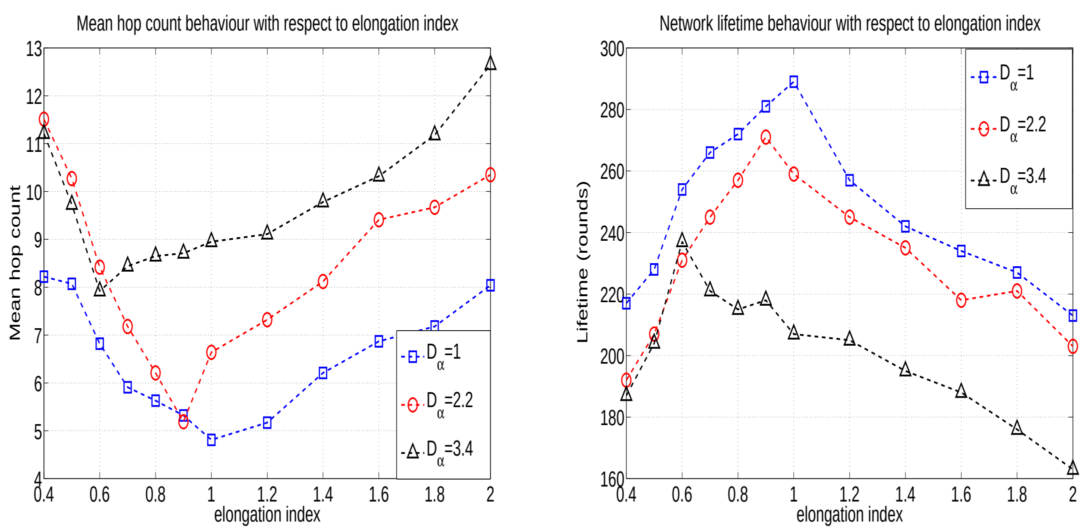

(a) Mean hop count and elongation index

(b) Network lifetime and elongation index

Figure 5.11: Behaviour of network performance metrics with respect to elongation index, ω_{d_0}, for isotropic and two directional path loss scenarios which are common in high density apple orchards is illustrated

in Section 5.3.2, where $D_\alpha = 1$ corresponds to isotropic path loss, while $D_\alpha \approx 2$ and $D_\alpha \approx 3$ correspond to high density apple orchards with larger and smaller between-tree-row spacing as explained in Section 5.3.1. As could be seen effect of elongated grid on higher directivity degree scenarios is higher since node connectivity along cross track and diagonal directions is very limited. The proposed alternative node placement technique, increases number of neighbouring nodes along other directions apart from along track which results in lower hop count and also network lifetime since it takes longer for network graph node groups to become disconnected. As seen in Figure 5.11b, elongated grid with $\omega_{d_0} = 0.8$ results in $\approx 5\%$

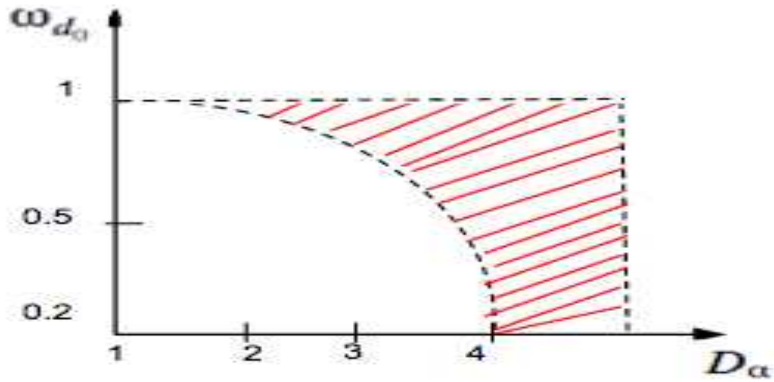

Figure 5.12: Approximate applicability range of the proposed mitigation strategy; Shaded region shows the range where elongated grid outperforms square grid for different directivity degrees in the studied scenario

lifetime improvement for $D_\alpha \approx 2$, while $\omega_{d_0} = 0.6$ yields $\approx 15\%$ lifetime improvement for $D_\alpha \approx 3$. In Figure 5.12, applicability range of the proposed mitigation strategy is illustrated with the shaded region. The shaded region shows the approximate area where elongated grid outperforms square grid in terms of network lifetime. Figures 5.11b, and 5.12 show that higher range of elongation indices are applicable to higher directivity degrees, whereas more lifetime improvement compared to square grid is possible given that elongation index is appropriately chosen.

5.5 Discussion

In this work, we first showed that directional path loss is a real phenomenon which happens in realistic man-made environments such as warehouses, libraries or agricultural environments. Further, we characterized directional path loss with a measure called directivity degree and showed that effect of this phenomenon on performance metrics of WSNs such as network lifetime and mean hop count which translates to latency and energy efficiency is measurable. Our simulations showed that directional path loss decreases network lifetime and increases mean packet hop count by decreasing node connectivity. As a mitigation strategy we suggested elongated grid deployment, i.e., decreasing internode distances along impaired directions, to increase node connectivity along various directions, therefore improving network lifetime. This technique in fact mimics behaviour of isotropic path loss by distributing neighbouring nodes in a more uniform way along different directions which helps network achieve higher lifetime as a result of higher time it takes network graph to become disconnected.

The limitation of this node placement technique is its sub-optimality since pattern of the grid, i.e., square in addition to its density is kept intact. Further, more complex node placement techniques with irregular patterns, increasing node density surrounding the gateway or adding gateways to other corners of the field may result in better enhancements in network performance. In addition to node placement strategies, geographical routing, i.e., forwarding packets along certain directions, and transmit power control would help achieve more energy efficiency.

It is noteworthy that the mitigation strategy proposed in this chapter, is suitable for low shadowing environments with organized geometrical structure. As a practice for future research, characterizing directional path loss in the environments that experience heavy shadow fading and proposing mitigation strategies to combat such impairments in order to increase network lifetime is fundamental.

Chapter 6

Conclusions and Recommendations

In this chapter, we conclude the thesis with: 1) Conclusions regarding the effectiveness of our proposed schemes, the limitations of our algorithm and the implications for current research practice, and 2) recommendations for future research that could overcome the limitations of our work.

6.1 Conclusions

Few previous studies have sought to assess the impact of propagation impairments on higher layer protocols and algorithms and have devised schemes for mitigating such impacts. Here, we have presented four case studies that demonstrate how higher layer protocols and algorithms can be devised to achieve greater energy efficiency by accounting for the nature of the propagation impairments experienced in two radically different environments; WBANs and PAWSNs. In this chapter, first we review the effectiveness of our proposed schemes, the relationships between the design and performance parameters that we investigated, and the implications for current practice or future research. In Section 6.2, we discuss limitations of the work reported in our work and possible methods for overcoming them.

In Chapter 2, we proposed a routing protocol that uses linear programming techniques to ensure that all nodes in a WBAN expend energy at a similar rate and thereby maximize network lifetime. Moreover, in the existing protocols, communication overhead caused by frequent link assessments and computation burden imposed by routing table calculation make existing link-state routing protocols unsuitable for dynamic WBANs. We overcome these by: 1) monitoring RSSI in a dynamic and distributed manner on data packets communicated over links, therefore changing the transmit power levels only when large RSSI variations is observed 2) only having limb-torso links participate in link assessment process since RSSI variations over limb-limb or torso-torso links is not remarkable in terms of the required transmit power level, 3) using linear programming to derive link likelihoods.

The algorithm is well-suited to maximize WBAN lifetime, and address connectivity for monitoring applications and mobility model which involves stationary postures and actions in the context of routine daily activities. Even though the algorithm is proposed for WBANs, the LP-based link likelihood assignment proposed in this chapter can be used in conjunction with other transmit power adjustment techniques to maximize IEEE802.15.4 network lifetime for other types of WSNs. The algorithm is particularly useful in future implementations of WBANs, as low listening power COTS are emerging, therefore multi-hop networking in WBANs will become more beneficial in terms of energy conservation. As far as lifetime maximization is concerned, the work in Chapter 2 applies to WBANs which are built upon IEEE802.15.4 MAC layer. As a future practice, deriving lifetime maximization LP for other standards, e.g., IEEE802.15.6, would be very useful because as opposed to IEEE802.15.4, IEEE802.15.6 only supports one and two hop star networks.

In Chapter 3, we proposed a scheduling algorithm that accounts for the periodic shadowing observed over many WBAN links and thereby reduce the transmit power required to transfer information and thereby increase energy efficiency. This technique helps us achieve single hop communication by adopting low transmit power levels over some limb-torso links that experience severe shadowing, however show periodic connectivity as opposed to stationary actions studied in Chapter 2. Further, periodic prolonged actions such as fitness activities cause on-body links to undergo periodic predictable connectivity sessions that can be exploited for low power single hop communications at the expense of latency. The energy efficiency is achieved by avoiding multi hop nature of store and forward scheduling techniques and excessive energy expenditure caused by idle listening and channel sensing in opportunistic scheduling algorithms. Furthermore, the periodicity and predictability observed in on-body links can be exploited in opportunistic scheduling techniques to reduce beacon transfers required for channel sensing. The proposed technique is particularly suited to increase energy efficiency for delay tolerant applications such as ambient assisted living that can tolerate latency because data can be logged and analyzed in an offline manner. Beside periodicity which can be used for energy efficient communication, diversity of RSSI samples over such links provides us with mean and standard deviation features which makes simple real-time action recognition based on naive Bayes classification possible.

One of the most important implications of this work in terms of node placement is that sensors with looser placement and latency requirements can be mounted on extremities, e.g., ankles and wrists, so that energy efficiency is achieved by single hop communication and low transmit power levels. The most fundamental future research subjects is to devise node placement and scheduling techniques in order to maximize throughput with low transmit power levels for scenarios, where several periodic links are available. Moreover in this work as a case study, we studied energy efficiency and achievable bandwidth for a single link. However, in real world scenarios many nodes with looser placement requirements may be available.

In Chapter 4, we proposed an efficient localization algorithm based on the Bayesian model for information aggregation. Moreover, existing Bayesian distributed techniques suffer from communication overhead required for setup phase in order to form loop-free graphs. While, non-Bayesian techniques are burdened with excessive communication overhead resulted from coupled variables, remarkable computational complexity needed to solve optimization problems at each iteration and generally suffer from slow convergence. Our scalable RSSI-based localization algorithm overcomes these limitations by: 1) using only local distance estimates with respect to neighbouring nodes, and 2) using a message passing schedule which benefits from a fixed size outgoing message that does not grow with number of neighbouring nodes, and 3) low computational complexity per node at each iteration which only grows with grid size and only involves summations and multiplications.

The algorithm uses a Bayesian model for information aggregation to achieve scalable communication and computational complexity with respect to the number of nodes at the expense of accuracy. The proposed technique plays an important role in reducing energy expenditure of PAWSNs, because the amount of data required to be exchanged for localization is comparable to the actual data exchanged in the network since in these types of networks, sensors may only transmit very small amount of data, e.g., one byte per day.

The main strength of our localization algorithm is its compatibility with realistic deployment scenarios of WSNs and the low communication overhead it adds to the already deployed routing protocols. Further, the route discovery phase of AODV routing protocols, e.g., ZigBee and similar schemes, work based on flooding and multicasting RREQ packets. Therefore, our proposed localization algorithm can be integrated in a convenient and inexpensive manner, while remarkable amount of communication overhead is needed in case state-of-the-art localization techniques are to be deployed. In this work, we exploited shadowing independence over the links in the agricultural field to propose an algorithm with low communication and computation complexity. However, there are real world scenarios such as urban area where there might be a large correlation among shadowing observed over links. As a future work, a WSN compatible localization algorithm that could overcome such impairments and eliminate the message dependence and error propagation with low communication and computation complexity would be very beneficial.

In Chapter 5, we demonstrated that directional path loss is a real phenomenon which happens in realistic man-made and row-like environments such as warehouses, libraries or agricultural environments. Further, we showed that increase of directional path loss decreases network lifetime and increases mean packet hop count by decreasing node connectivity along specific directions. As a mitigation strategy, we suggested elongated grid deployment, i.e., decreasing internode distances along impaired directions, to increase node connectivity along various directions, therefore improving network lifetime.

This technique in fact simulates the behaviour of non-directional path loss by distributing neighbouring nodes in a more uniform way along different directions which helps network achieve higher lifetime as a result of higher time it takes network graph to become disconnected. The mitigation strategy proposed in Chapter 5, is well-suited to low shadowing environments with organized geometrical structure. As a future research, characterizing directional path loss in the environments that experience heavy shadow fading and proposing mitigation strategies to combat such impairments in order to increase network lifetime is of huge interest.

6.2 Recommendations

In this section, we discuss the limitations of our work in the four research chapters in addition to suggesting methods to overcome them. As a general recommendation, even though different techniques in PHY, MAC, and network layers have been proposed to make WSNs more energy efficient, cross layer integration and design techniques help towards more energy consumption when dealing with application-based deployment of WSNs. A great deal of attention has been paid to integration of higher layers such as transport and application layers into routing, scheduling and node placement techniques, however the impact of channel propagation on these techniques is not much explored.

In the routing technique proposed in Chapter 2, due to the limitations of TDMA-based IEEE802.15.4 MAC which mandates all time slots to have equal duration, the proposed algorithm may not be efficient in terms of bandwidth utilization. Therefore design of MAC protocols with dynamic time slot duration and variable time slots throughout a transfer round helps towards more efficient utilization of bandwidth with higher number of sensors having been deployed. Data compression techniques can be used to reduce the time slot duration that is a fixed parameter of our algorithm, therefore cut down the idle listening and electric circuit power consumption. It is beneficial to design a routing protocol that can work based on contention-based IEEE802.15.4 MAC layer. Another limitation of this work is limited number of actions that have been used to evaluate the algorithm. Further, the action variation recognition technique proposed in this work needs to be tested on more various activities.

In the scheduling technique proposed in Chapter 3, fixed pace and limited number of actions is the main limitation of the work. Moreover, the work only serves as a proof of concept to achieved energy efficiency by using periodic limb-torso links. Action recognition may not work when actions pool gets bigger. As a remedy to this, periodic links and their period should be recognized with link assessment techniques in the beginning of the action rather than assuming that these links and their period is known once action is recognized.

In the localization technique proposed in Chapter 4, the main limitation of the proposed algorithm is its incapability in terms of achieving high precision localization. Further, as a remedy the proposed algorithm can be used as the initialization step for algorithms such as gradient descent which suffer from high sensitivity to initialization. Moreover the proposed Bayesian model for information aggregation can be used to accelerate convergence of slowly converging gradient descent algorithms in addition to providing them with the initialized location for the scenarios with few number of landmarks and high number of nodes.

In the directional path loss study and mitigation strategies conducted in Chapter 5, the limitation of this node placement technique is its sub-optimality since pattern of the grid, i.e., square in addition to its density is kept intact. Further, more complex node placement techniques with irregular patterns, increasing node density surrounding the gateway or adding gateways to other corners of the field result in better enhancements in network performance. In addition to node placement strategies, geographical routing, i.e., forwarding packets along certain directions, and transmit power control would help achieve more energy efficiency.

References

[1] I. Akyildiz, W. Su, Y. Sankarasubramaniam, and E. Cayirci, "A survey on sensor networks," *IEEE Commun. Mag.*, vol. 40, pp. 102–114, Aug. 2002.

[2] K. Sohrabi, J. Gao, V. Ailawadhi, and G. Pottie, "Protocols for self-organization of a wireless sensor network," *IEEE J. Pers. Commun.*, vol. 7, pp. 16–27, Oct. 2000.

[3] V. Rajaravivarma, Y. Yang, and T. Yang, "An overview of Wireless Sensor Network and applications," in *Proc. SSST*, pp. 432–436, Mar. 2003.

[4] C. Buratti, A. Conti, D. Dardari, and R. Verdone, "An overview on wireless sensor networks technology and evolution," *Sensors*, vol. 9, pp. 6869–6896, Aug. 2009.

[5] K. Akkaya and M. Younis, "A survey on routing protocols for wireless sensor networks," *Ad Hoc Networks*, vol. 3, no. 3, pp. 325–349, 2005.

[6] J. Al-Karaki and A. Kamal, "Routing techniques in wireless sensor networks: a survey," *IEEE Wireless Commun.*, vol. 11, pp. 6–28, Dec. 2004.

[7] I. Demirkol, C. Ersoy, and F. Alagoz, "MAC protocols for wireless sensor networks: a survey," *IEEE Commun. Mag.*, vol. 44, pp. 115–121, Apr. 2006.

[8] M. Younis and K. Akkaya, "Strategies and techniques for node placement in wireless sensor networks: a survey," *Ad Hoc Netw.*, vol. 6, pp. 621–655, Jun. 2008.

[9] N. Patwari, J. Ash, S. Kyperountas, A. Hero, R. Moses, and N. Correal, "Locating the nodes: cooperative localization in wireless sensor networks," *IEEE Signal Processing Mag.*, vol. 22, pp. 54–69, Jul. 2005.

[10] Y. Sankarasubramaniam, I. Akyildiz, and S. McLaughlin, "Energy efficiency based packet size optimization in wireless sensor networks," in *Proc. IEEE IWSNPA*, pp. 1–8, 2003.

[11] "IEEE standard for telecommunications and information exchange between systems - LAN/MAN - specific requirements - part 15: Wireless medium access control (MAC) and physical layer (PHY) specifications for wireless personal area networks (WPANs)," *IEEE Std 802.15.1-2002*, pp. 1–473, Jun. 2002.

[12] "Part 15.4:wireless medium access control (MAC) and physical layer (PHY) specifications for low-rate wireless personal area networks (LR-WPANs)," *IEEE approved Draft Std P802.15.4*, 2003.

[13] I. Akyildiz, W. Su, Y. Sankarasubramaniam, and E. Cayirci, "Wireless sensor networks: a survey," *Computer Networks*, vol. 38, no. 4, pp. 393–422, 2002.

[14] D. Puccinelli and M. Haenggi, "Wireless sensor networks: applications and challenges of ubiquitous sensing," *IEEE Circuits Syst. Mag.*, vol. 5, no. 3, pp. 19–31, 2005.

[15] B. Latré, B. Braem, I. Moerman, C. Blondia, and P. Demeester, "A survey on wireless body area networks," *Wireless Netw.*, vol. 17, pp. 1–18, Jan. 2011.

[16] H. Cao, V. Leung, C. Chow, and H. Chan, "Enabling technologies for wireless body area networks: A survey and outlook," *IEEE Commun. Mag.*, vol. 47, pp. 84–93, Dec. 2009.

[17] N. Wang, N. Zhang, and M. Wang, "Wireless sensors in agriculture and food industry-recent development and future perspective," *Comput. Electron. Agric.*, vol. 50, pp. 1–14, Jan. 2006.

[18] P. Harrop and R. Das, "Wireless sensor networks (WSN) 2014-2024: Forecasts, technologies, players," 2014.

[19] Frost and Sullivan, "Global wireless sensor networks market." `http://www.frost.com/sublib/display-report.do?id=N92B-01-00-00-00`, 2014. Retrieved Aug. 2015.

[20] M. Hatler, D. Guraganious, and C. Chi, "Wireless sensor networks (WSN) 2012-2022: Forecasts, technologies, players," 2013.

[21] U. Nations, "World population prospects, the 2010 revision." `http://www.un.org/en/development/desa/population/publications/pdf/trends/WPP2010/WPP2010_Volume-I_Comprehensive-Tables.pdf`.

[22] H. Charles, J. Godfray, J. R. Beddington, and I. R. Crute, "Food security: The challenge of feeding 9 billion people," *Sci. Mag.*, 2010.

[23] "Precision farming market worth 4.80 billion USD by 2020." `http://www.marketsandmarkets.com/PressReleases/precision-farming.asp`. Retrieved Jun. 2016.

[24] G. Anastasi, M. Conti, and M. Di Francesco, "A comprehensive analysis of the MAC unreliability problem in IEEE 802.15.4 wireless sensor networks," *IEEE Trans. Ind. Inform.*, vol. 7, pp. 52–65, Feb. 2011.

[25] G. Zhou, T. He, S. Krishnamurthy, and J. Stankovic, "Impact of radio irregularity on wireless sensor networks," in *Proc. MobiSys*, pp. 125–138, 2004.

[26] D. Kotz, C. Newport, and C. Elliott, "The mistaken axioms of wireless-network research," Tech. Rep. TR2003-467, Jul. 2003.

[27] S. Ullah, H. Higgins, B. Braem, B. Latre, C. Blondia, I. Moerman, S. Saleem, Z. Rahman, and K. Kwak, "A comprehensive survey of wireless body area networks," *J. Med. Syst.*, vol. 36, pp. 1065–1094, Jun. 2012.

[28] S. Movassaghi, M. Abolhasan, J. Lipman, D. Smith, and A. Jamalipour, "Wireless body area networks: A Survey," *IEEE Commun. Surveys Tuts.*, vol. 16, pp. 1658–1686, Mar. 2014.

[29] M. Oliver, "An Overview of Geostatistics and Precision Agriculture," in *Geostatistical Applications for Precision Agriculture*, pp. 1–34, Springer Netherlands, 2010.

[30] A. McBratney, B. Whelan, T. Ancev, and J. Bouma, "Future directions of precision agriculture," *Precision Agriculture*, vol. 6, pp. 7–23, Feb. 2005.

[31] M. Anisi, "A survey of wireless sensor network approaches and their energy consumption for monitoring farm fields in precision agriculture," *Precision Agriculture*, vol. 16, pp. 216–238, Apr. 2015.

[32] "Wireless sensor networks see uptake in global industries due to technological breakthroughs." Frost & Sullivan, 2015.

[33] z wavealliance, "About Z-Wave Technology." `http://z-wavealliance.org/about_z-wave_technology/`. Retrieved Aug. 2015.

[34] E. Electric, "System engineering guidelines IEC 62591 WirelessHART." http://www2.emersonprocess.com/siteadmincenter/PM%20Central%20Web%20Documents/EMR_WirelessHART_SysEngGuide.pdf, 2014. Retrieved Aug. 2015.

[35] Z. Shelby and C. Bormann, "6LoWPAN: The wireless embedded Internet - Part 1: Why 6LoWPAN?." http://www.eetimes.com/document.asp?doc_id=1278794, 2011. Retrieved Aug. 2015.

[36] O. Puzanov, "Short-range wireless: Comparison of the key technologies," Nov. 2013.

[37] "ZigBee setting standards for energy-efficient control networks," Tech. Rep. WP40110601EN-US, Schneider electric, Jun. 2011.

[38] "Wireless - ISA 100." http://www.smar.com/en/technical-article/wireless-isa-100, 2012. Retrieved Aug. 2015.

[39] G. Fang and E. Dutkiewicz, "BodyMAC: Energy efficient TDMA-based MAC protocol for wireless body area networks," in *Proc. ISCIT*, pp. 1455–1459, 2009.

[40] N. Timmons and W. Scanlon, "An adaptive energy efficient MAC protocol for the medical body area network," in *Proc. VITAE*, pp. 587 –593, 2009.

[41] A. El-Hoiydi and J. Decotignie, "WiseMAC: an ultra low power MAC protocol for the downlink of infrastructure wireless sensor networks," in *Proc. ISCC*, pp. 244–251, 2004.

[42] T. Watteyne, I. Augé-Blum, M. Dohler, and D. Barthel, "Anybody: a self-organization protocol for body area networks," in *Proc. ICST*, pp. 1–7, 2007.

[43] B. Culpepper, L. Dung, and M. Moh, "Design and analysis of Hybrid Indirect Transmissions (HIT) for data gathering in wireless micro sensor networks," in *Proc. SIGMOBILE Mob. Comput. Commun.*, pp. 61–83, 2004.

[44] N. Javaid, Z. Abbas, M. Fareed, Z. Khan, and N. Alrajeh, "M-attempt: A new energy-efficient routing protocol for wireless body area sensor networks," *Procedia Computer Science*, vol. 19, pp. 224 – 231, 2013.

[45] C. Oey and S. Moh, "A survey on temperature-aware routing protocols in wireless body sensor networks," *Sensors*, vol. 13, pp. 9860–9877, Aug. 2013.

[46] A. G. Ruzzelli, R. Jurdak, G. M. O'Hare, and P. Van Der Stok, "Energy-efficient multi-hop medical sensor networking," in *Proc. ACM SIGMOBILE*, pp. 37–42, 2007.

[47] B. Braem, B. Latre, I. Moerman, C. Blondia, and P. Demeester, "The wireless autonomous spanning tree protocol for multihop wireless body area networks," in *Proc. MobiQuitous- Workshops*, pp. 1–8, 2006.

[48] B. Latre, B. Braem, I. Moerman, C. Blondia, E. Reusens, W. Joseph, and P. Demeester, "A low-delay protocol for multihop wireless body area networks," in *Proc. MobiQuitous*, pp. 1–8, Aug. 2007.

[49] M. Quwaider and S. Biswas, "Probabilistic routing in on-body sensor networks with postural disconnections," in *Proc. ACM Int. Symp. on MobiWAC*, pp. 149–158, 2009.

[50] S. Yang, J. Lu, F. Yang, L. Kong, W. Shu, and M. Wu, "Behavior-aware probabilistic routing for wireless body area sensor networks," in *Proc. IEEE GLOBECOM*, pp. 444–449, Dec. 2013.

[51] A. Maskooki, C. Soh, E. Gunawan, and K. Low, "Opportunistic routing for body area network," in *Proc. IEEE CCNC*, pp. 237–241, Jan. 2011.

[52] M. Nabi, T. Basten, M. Geilen, M. Blagojevic, and T. Hendriks, "A robust protocol stack for multi-hop wireless body area networks with transmit power adaptation," in *Proc. BodyNets*, pp. 77–83, 2010.

[53] G. Tsouri, A. Prieto, and N. Argade, "On increasing network lifetime in body area networks using global routing with energy consumption balancing," *Sensors*, vol. 12, pp. 13088–13108, Sep. 2012.

[54] W. Heinzelman, A. Chandrakasan, and H. Balakrishnan, "Energy-efficient communication protocol for wireless microsensor networks," in *Proc. HICSS*, pp. 1–10, 2000.

[55] S. Lindsey and C. Raghavendra, "PEGASIS: Power-efficient gathering in sensor information systems," in *Proc. IEEE AeroConf*, vol. 3, pp. 1125–1130, 2002.

[56] M. Quwaider, J. Rao, and S. Biswas, "Body-posture-based dynamic link power control in wearable sensor networks," *IEEE Commun. Mag.*, vol. 48, pp. 134 –142, Jul. 2010.

[57] A. Ehyaie, M. Hashemi, and P. Khadivi, "Using relay network to increase life time in wireless body area sensor networks," in *Proc. IEEE WoWMoM*, pp. 1–6.

[58] Y. Tselishchev, L. Libman, and A. Boulis, "Reducing transmission losses in body area networks using variable TDMA scheduling," in *Proc. IEEE WoWMoM*, pp. 1–10, Jun. 2011.

[59] X. Liu, E. Chong, and N. Shroff, "Opportunistic transmission scheduling with resource-sharing constraints in wireless networks," *IEEE J. Sel. Areas Commun.*, vol. 19, pp. 2053 –2064, Oct. 2001.

[60] X. Liu, E. Chong, and N. Shroff, "A framework for opportunistic scheduling in wireless networks," *Comput. Netw.*, vol. 41, pp. 451–474, Mar. 2003.

[61] B. Shrestha, E. Hossain, S. Camorlinga, R. Krishnamoorthy, and D. Niyato, "An optimization-based GTS allocation scheme for IEEE 802.15.4 MAC with application to wireless body-area sensor networks," in *Proc. IEEE ICC*, pp. 1–6, 2010.

[62] Y. Huang, A. Pang, and H. Hung, "An adaptive GTS allocation scheme for IEEE 802.15.4," *IEEE Trans. Parallel Distrib. Syst.*, vol. 19, pp. 641–651, May 2008.

[63] N. Karthickraja, V. Sumathy, and J. Ahamed, "A novel hybrid routing protocol for data aggregation in agricultural applications," in *Proc. IEEE ICCCCT*, pp. 227–231, 2010.

[64] S. Sutar, K. Swapnita-Jayesh, and M. Pune, "Irrigation and fertilizer control for precision agriculture using WSN: energy efficient approach," *Int. J. Advances in Comput. and Info. Researches*, vol. 1, no. 1, 2012.

[65] A. Mittal, K. Chetan, S. Jayaraman, B. Jagyasi, A. Pande, and P. Balamuralidhar, "mKRISHI wireless sensor network platform for precision agriculture," in *Proc. ICST*, pp. 623–629, Dec. 2012.

[66] K. P. Ferentinos, T. A. Tsiligiridis, and K. G. Arvanitis, "Energy optimization of wireless sensor networks for environmental measurements," in *Proc. IEEE CIMSA*, pp. 250 – 255, 2005.

[67] H. Sahota, R. Kumar, A. Kamal, and J. Huang, "An energy-efficient wireless sensor network for precision agriculture.," in *Proc. IEEE Symp. Comput. Commun.*, Jun. 2010.

[68] H. Sahota, R. Kumar, and A. Kamal, "A wireless sensor network for precision agriculture and its performance," in *Proc. WCMC*, pp. 1628–1645, 2011.

[69] W. Ye, J. Headmen, and D. Estrin, "An energy-efficient MAC protocol for wireless sensor networks," in *Proc. IEEE INFOCOM*, pp. 1567–1576, 2002.

[70] T. van Dam and K. Langendoen, "An adaptive energy-efficient MAC protocol for wireless sensor networks," in *Proc. ACM SenSys.*, pp. 171–180, 2003.

[71] S. Yoo, J. Kim, T. Kim, S. Ahn, J. Sung, and D. Kim, "A2S: Automated agriculture system based on WSN," in *Proc. IEEE ISCE*, pp. 1–5, Jun. 2007.

[72] A. Baggio, "Wireless sensor networks in precision agriculture," in *Proc. ACM REAL-WSN*, 2005.

[73] M. Keshtgari and A. Deljoo, "A wireless sensor network solution for precision agriculture based on ZigBee technology," *Wireless Sensor Network*, pp. 25–30, 2012.

[74] K. Fleming, D. Westfall, D. Wiens, and M. Brodahl, "Evaluating farmer defined management zone maps for variable rate fertilizer application," *Precision Agriculture*, vol. 2, no. 2, pp. 201–215, 2000.

[75] H. Liu, Z. Meng, and Y. Shang, "Sensor nodes placement for farmland environmental monitoring applications," in *Proc. WiCom*, pp. 1–4, Sep. 2009.

[76] A. Awasthi and S. Reddy, "Monitoring for precision agriculture using wireless sensor network- a review," *Computers and Electronics in Agriculture*, vol. 105, pp. 83–94, Jul. 2014.

[77] K. Seada, M. Zuniga, A. Helmy, and B. Krishnamachari, "Energy efficient forwarding strategies for geographic routing in lossy wireless sensor networks," in *Proc. ACM SenSys.*, 2004.

[78] R. C. Shah and J. M. Rabaey, "Energy aware routing for low energy ad hoc sensor networks," in *Proc. IEEE WCNC*, vol. 1, pp. 350–355, 2002.

[79] P. Baronti, P. Pillai, W. Chook, S. Chessa, A. Gotta, and Y. Hu, "Wireless sensor networks: A survey on the state of the art and the 802.15.4 and ZigBee standards," *Comput. Commun.*, vol. 30, no. 7, pp. 1655 – 1695, 2007.

[80] N. Salodkar, A. Karandikar, and V. Borkar, "A stable online algorithm for energy-efficient multiuser scheduling," *IEEE Trans. Mobile Comput.*, vol. 9, pp. 1391 –1406, Oct. 2010.

[81] X. Liu, "Opportunistic scheduling in wireless communication networks," *Ph.D. Thesis, Purdue University, 2002.*

[82] H. Wymeersch, J. Lien, and M. Win, "Cooperative localization in wireless networks," *UWB Technol. and Emerg. Appl.*, vol. 97, pp. 427–450, Feb. 2009.

[83] G. Mao, B. Fidan, and B. Anderson, "Wireless sensor network localization techniques," *Comput. Netw.*, vol. 51, pp. 2529 – 2553, Jul. 2007.

[84] K. Kim, I. Lee, M. Yoon, J. Kim, H. Lee, and K. Han, "An efficient routing protocol based on position information in mobile wireless body area sensor networks," in *Proc. NETCOM*, pp. 396–399, 2009.

[85] L. Sang, A. Arora, and H. Zhang, "On link asymmetry and one-way estimation in wireless sensor networks," *ACM Trans. Sen. Netw.*, vol. 6, pp. 1–25, Feb. 2010.

[86] T. Yang, T. Oda, L. Barolli, J. Iwashige, A. Durresi, and F. Xhafa, "Investigation of packet loss in mobile WSNs for AODV protocol and different radio models," in *Proc. IEEE AINA*, pp. 709–715, 2012.

[87] G. Sharma, V. Sahu, P. Maurya, and R. Paulus, "Analyzing the effect of constant and lognormal shadowing model on ad-hoc routing protocols," *Int. J. Comp. Appl.*, vol. 66, no. 8, pp. 16 –19, 2013.

[88] S. Itoua, "Effect of propagation models on ad hoc networks routing protocols," in *Proc. SENSORCOMM*, pp. 752–757, 2008.

[89] I. Eltahir, "The impact of different radio propagation models for mobile ad hoc networks (MANET) in urban area environment," in *Proc. AusWireless*, p. 30, 2007.

[90] Y. S. Meng, Y. H. Lee, and B. C. Ng, "Path-loss modeling for near-ground VHF radio-wave propagation through forests with tree-canopy reflection effect," *Progress In Electromagnetics Research M*, pp. 131–141, 2010.

[91] M. Weissberger, "An initial critical summary of models for predicting the attenuation of radio waves by trees," Tech. Rep. ESD-TR-81-101, 1982.

[92] M. O. Al-Nuaimi and R. B. L. Stephens, "Measurements and prediction model optimization for signal attenuation in vegetation media at centimetre wave frequencies," *IEE Microwaves, Antennas and Propagation*, vol. 145, pp. 201–206, Jun. 1998.

[93] A. Natarajan, B. De Silva, K.-K. Y., and M. Motani, "To hop or not to hop: Network architecture for body sensor networks," in *Proc. IEEE SECON*, pp. 1–9, Jun. 2009.

[94] M. Cardei and D. Du, "Improving wireless sensor network lifetime through power aware organization," *IEEE/ACM Trans. Netw., 2005*, vol. 11, pp. 333–340, Mar.

[95] A. Lindgren, A. Doria, and O. Schelen, "Probabilistic routing in intermittently connected networks," *SIGMOBILE Mob. Comput. Commun. Rev.*, vol. 7, pp. 19–20, Jul. 2003.

[96] S. Ahmed, N. Javaid, S. Yousaf, A. Ahmad, M. Sandhu, M. Imran, Z. Khan, and N. Alrajeh, "Co-LAEEBA: cooperative link aware and energy efficient protocol for wireless body area networks," *Computers in Human Behavior*, vol. 51, pp. 1205–1215, 2015.

[97] N. Javaid, A. Ahmad, Q. Nadeem, M. Imran, and N. Haider, "iM-SIMPLE: iMproved stable increased-throughput multi-hop link efficient routing protocol for wireless body area networks," *Computers in Human Behavior*, vol. 51, pp. 1003–1011, 2015.

[98] F. Di Franco, C. Tachtatzis, R. Atkinson, I. Tinnirello, and I. Glover, "Channel estimation and transmit power control in wireless body area networks," *IET Wireless Sensor Systems*, vol. 5, no. 1, pp. 11–19, 2015.

[99] L. Liang, Y. Ge, G. Feng, W. Ni, and A. Wai, "A low overhead tree-based energy-efficient routing scheme for multi-hop wireless body area networks," *Computer Networks*, vol. 70, pp. 45–58, 2014.

[100] Q. Wang, M. Hempstead, and W. Yang, "A realistic power consumption model for wireless sensor network devices," in *Proc. IEEE SECON*, pp. 286–295, 2006.

[101] C. Cordeiro and M. Patel, "Body area networking standardization: present and future directions," in *Proc. ICST*, p. 10, 2007.

[102] I. Dietrich and F. Dressler, "On the lifetime of wireless sensor networks," *ACM Trans. Sen. Netw.*, vol. 5, pp. 1–39, Feb. 2009.

[103] K. Srinivasan and P. Levis, "RSSI is under appreciated," in *Proc. EmNets*, 2006.

[104] C. Antonopoulos, A. Prayati, T. Stoyanova, C. Koulamas, and G. Papadopoulos, "Experimental evaluation of a WSN platform power consumption," in *Proc. IEEE IPDPS*, pp. 1–8, 2009.

[105] C. Guo, R. Prasad, and M. Jacobsson, "Packet forwarding with minimum energy consumption in body area sensor networks," in *Proc. IEEE CCNC*, pp. 1–6, 2010.

[106] Y. Yu, B. Krishnamachari, and V. Prasanna, "Energy-latency tradeoffs for data gathering in wireless sensor networks," in *Proc. INFOCOM*, pp. 244–255, 2004.

[107] F. Xiangning and S. Yulin, "Improvement on LEACH protocol of wireless sensor network," in *Proc. SensorComm*, pp. 260–264, 2007.

[108] A. Dhamdhere, V. Sivaraman, V. Mathur, and S. Xiao, "Algorithms for transmission power control in biomedical wireless sensor networks," in *Proc. IEEE APSCC*, pp. 1114 –1119, 2008.

[109] S. Misra and S. Sarkar, "Priority-based time-slot allocation in wireless body area networks during medical emergency situations: An evolutionary game-theoretic perspective," *IEEE J. Biomed. Health Inform.*, vol. 19, no. 2, pp. 541–548, 2015.

[110] S. Xiao, V. Sivaraman, and A. Burdett, "Adapting radio transmit power in wireless body area sensor networks," in *Proc. ACM BodyNets'08*, pp. 141–148, 2008.

[111] Q. He and C. Debrunner, "Individual recognition from periodic activity using hidden markov models," in *Workshop Human Motion*, pp. 47–52, 2000.

[112] E. Ijjina and C. Mohan, "One-shot periodic activity recognition using convolutional neural networks," in *Proc. ICMLA*, pp. 388–391, 2014.

[113] A. Yang, R. Jafari, S. Shankar, and R. Bajcsy, "Distributed Recognition of Human Actions Using Wearable Motion Sensor Networks," *J. Ambient Intell. Smart Environ.*, vol. 1, pp. 103 –115, Feb. 2009.

[114] E. Guenterberg, H. Ghasemzadeh, V. Loseu, and R. Jafari, "Distributed continuous action recognition using a hidden markov model in body sensor networks," in *Proc. IEEE ICDCS*, pp. 145–158, 2009.

[115] H. Ghasemzadeh, V. Loseu, and R. Jafari, "Structural action recognition in body sensor networks: distributed classification based on string matching," *IEEE Trans. Inf. Technol. Biomed.*, vol. 14, pp. 425 –435, Mar. 2010.

[116] I. Rish, "An empirical study of naive Bayes classifier," *int. joint on AI*, pp. 41–46, 2001.

[117] G. F. Cooper, "The computational complexity of probabilistic inference using bayesian belief networks," *J. AI*, vol. 42, no. 2-3, pp. 393 – 405, 1990.

[118] "Chipcon data sheet for CC2420, 2.4 GHz IEEE 802.15.4/ZigBee RF transceiver." `http://focus.ti.com/lit/ds/symlink/cc2420.pdf`, 2004.

[119] H. Liu, H. Darabi, P. Banerjee, and J. Liu, "Survey of wireless indoor positioning techniques and systems," *IEEE Trans. Syst. Man Cybern.*, vol. 37, no. 6, pp. 1067–1080, 2007.

[120] Y. Gu, A. Lo, and I. Niemegeers, "A survey of indoor positioning systems for wireless personal networks," *IEEE Commun. Surveys Tuts.*, vol. 11, no. 1, pp. 13–32, 2009.

[121] Z. Farid, R. Nordin, and M. Ismail, "Recent advances in wireless indoor localization techniques and system," *J. Comput. Netw. and Commun.*, vol. 2013, 2013.

[122] M. Allen, E. baydere, and G. Gaura, "Evaluation of localization algorithms," in *Localization Algorithms and Strategies for Wireless Sensor Networks*, 2009.

[123] C. Pearson, M. McGuire, and Y. Coady, "The application of Wi-Fi radiolocation research to mobile devices," in *Proc. IEEE Pacific Rim Conf. on Commun., Comput. and Signal Process.*, pp. 768–773, Aug. 2009.

[124] O. Hernandez, V. Jain, S. Chakravarty, and P. Bhargava, "Position location monitoring using IEEE 802.15.4/ZigBee technology." in Freescale Wireless Connectivity Operation in Mexico, 2007.

[125] K. G. Cassman, "Ecological intensification of cereal production systems: Yield potential, soil quality, and precision agriculture," *Proceedings of the National Academy of Sciences*, vol. 96, pp. 5952–5959, May 1999.

[126] S. El-kader and B. El-Basioni, "Precision farming solution in Egypt using the wireless sensor network technology," *Egyptian Informatics Journal*, vol. 14, no. 3, pp. 221–233, 2013.

[127] M. Keshtgari and A. Deljoo, "A wireless sensor network solution for precision agriculture based on ZigBee technology," *Wireless Sensor Networks*, vol. 4, pp. 25–30, 2012.

[128] Y. Zhu, J. Song, and F. Dong, "Applications of wireless sensor network in the agriculture environment monitoring," *Wireless Sensor Networks*, vol. 4, pp. 25–30, 2012.

[129] A. Boukerche, H. Oliveira, E. Nakamura, and A. Loureiro, "Localization systems for wireless sensor networks," *IEEE Wireless Commun.*, vol. 14, pp. 6–12, Dec. 2007.

[130] G. Han, H. Xu, T. Duong, J. Jiang, and T. Hara, "Localization algorithms of wireless sensor networks: a survey," *Telecommunication Systems*, vol. 52, pp. 2419–2436, Aug. 2013.

[131] T. He, C. Huang, B. M. Blum, J. Stankovic, and T. Abdelzaher, "Range-free localization schemes for large scale sensor networks," in *Proc. MobiCom*, pp. 81–95, 2003.

[132] Y. Shang, W. Ruml, Y. Zhang, and M. J. Fromherz, "Localization from mere connectivity," in *Proc. ACM MobiHoc*, pp. 201–212, 2003.

[133] Y. Wang, X. Wang, D. Wang, and D. Agrawal, "Range-free localization using expected hop progress in wireless sensor networks," *IEEE Trans. Parallel Distrib. Syst.*, vol. 20, pp. 1540–1552, Oct. 2009.

[134] D. Niculescu and B. Nath, "DV based positioning in ad hoc networks," *Telecommun. Syst.*, vol. 22, pp. 267–280, Jan. 2003.

[135] H. Shen, Z. Ding, S. Dasgupta, and C. Zhao, "Multiple source localization in wireless sensor networks based on time of arrival measurement," *IEEE Trans. Signal Process.*, vol. 62, pp. 1938–1949, Apr. 2014.

[136] J. Xu, M. Ma, and C. Law, "Cooperative angle-of-arrival position localization," *Measurement*, vol. 59, pp. 302–313, 2015.

[137] F. Yaghoubi, A. Abbasfar, and B. Maham, "Energy-efficient RSSI-based localization for wireless sensor networks," *IEEE Commun. Lett.*, vol. 18, pp. 973–976, Jun. 2014.

[138] F. Bandiera, A. Coluccia, and G. Ricci, "A cognitive algorithm for received signal strength based localization," *IEEE Trans. Signal Process.*, vol. 63, pp. 1726–1736, Apr. 2015.

[139] G. Wang and K. Yang, "A new approach to sensor node localization using RSS measurements in wireless sensor networks," *IEEE Trans. Wireless Commun.*, vol. 10, pp. 1389–1395, May 2011.

[140] A. Coluccia, "Reduced-bias ML-based estimators with low complexity for self-calibrating RSS ranging," *IEEE Trans. Wireless Commun.*, vol. 12, pp. 1220–1230, Mar. 2013.

[141] A. Coluccia and F. Ricciato, "RSS-based localization via bayesian ranging and iterative least squares positioning," *IEEE Commun. Lett.*, vol. 18, pp. 873–876, May 2014.

[142] H. Sahota and R. Kumar, "Network based sensor localization in multi-media application of precision agriculture Part 1: Received signal strength," in *Proc. ICNSC*, pp. 191–196, Apr. 2014.

[143] A. Ihler, J. Fisher, R. Moses, and A. Willsky, "Nonparametric belief propagation for self-localization of sensor networks," *IEEE J. Sel. Areas Commun.*, vol. 23, pp. 809–819, Apr. 2005.

[144] V. Savic and S. Zazo, "Cooperative localization in mobile networks using nonparametric variants of belief propagation," *Ad Hoc Networks*, vol. 11, no. 1, pp. 138 – 150, 2013.

[145] J. Yedidia, W. Freeman, and Y. Weiss, "Exploring artificial intelligence in the new millennium," ch. Understanding belief propagation and its generalizations, pp. 239–269, 2003.

[146] M. Welling and J. Lim, "A distributed message passing algorithm for sensor localization," in *Proc. ICANN*, pp. 767–775, 2007.

[147] A. Simonetto and G. Leus, "Distributed maximum likelihood sensor network localization," *IEEE Trans. Signal Process.*, vol. 62, pp. 1424–1437, Mar. 2014.

[148] G. Calafiore, L. Carlone, and M. Wei, "A distributed technique for localization of agent formations from relative range measurements," *IEEE Trans. Syst., Man, Cybern. A, Syst.,Humans*, vol. 42, pp. 1065–1076, Sep. 2012.

[149] J. A. Costa, N. Patwari, and A. O. Hero, III, "Distributed weighted-multidimensional scaling for node localization in sensor networks," *ACM Trans. Sen. Netw.*, vol. 2, pp. 39–64, Feb. 2006.

[150] R. Garg, A. Varna, and M. Wu, "Gradient descent approach for secure localization in resource constrained wireless sensor networks," in *Proc. IEEE ICASSP*, pp. 1854–1857, Mar. 2010.

[151] Q. Shi, C. He, H. Chen, and L. Jiang, "Distributed wireless sensor network localization via sequential greedy optimization algorithm," *IEEE Trans. Signal Process.*, vol. 58, pp. 3328–3340, Jun. 2010.

[152] S. Tomic, M. Beko, and R. Dinis, "Distributed RSS-based localization in wireless sensor networks based on second-order cone programming," *Sensors*, vol. 14, pp. 18410–18432, Feb. 2014.

[153] S. Srirangarajan, A. Tewfik, and L. Zhi-Quan, "Distributed sensor network localization using SOCP relaxation," *IEEE Trans. Wireless Commun.*, vol. 7, pp. 4886–4895, Dec. 2008.

[154] A. T. Ihler, W. Fischer III, John, and A. S. Willsky, "Loopy Belief Propagation: Convergence and Effects of Message Errors," *J. Mach. Learn. Res.*, vol. 6, pp. 905–936, Dec. 2005.

[155] V. Krishnamurthy, O. Gharehshiran, and M. Hamdi, "Interactive sensing and decision making in social networks," *Found. Trends Signal Process.*, vol. 7, no. 1-2, pp. 1–196, 2014.

[156] V. Krishnamurthy and M. Hamdi, "Mis-information removal in social networks: Constrained estimation on dynamic directed acyclic graphs," *IEEE J. Sel. Topics Signal Process.*, vol. 7, pp. 333–346, Apr. 2013.

[157] R. Peng and M. Sichitiu, "Robust, probabilistic, constraint-based localization for wireless sensor networks," in *Proc. SECON*, 2005.

[158] M. Rabbat and R. Nowak, "Decentralized source localization and tracking," in *Proc. IEEE ICASSP*, vol. 3, pp. 921–924, May 2004.

[159] P. Oguz-Ekim, J. Gomes, J. Xavier, and P. Oliveira, "A convex relaxation for approximate maximum-likelihood 2D source localization from range measurements," in *Proc. IEEE ICASSP*, pp. 2698–2701, Mar. 2010.

[160] K. Lui, W. Ma, H. So, and F. Chan, "Semi-definite programming algorithms for sensor network node localization with uncertainties in anchor positions and/or propagation speed," *IEEE Trans. Signal Process.*, vol. 57, pp. 752–763, Feb. 2009.

[161] P. Biswas, T. Liang, K. Toh, Y. Ye, and T. Wang, "Semidefinite programming approaches for sensor network localization with noisy distance measurements," *IEEE Trans. Autom. Sci. Eng.*, vol. 3, pp. 360–371, Oct. 2006.

[162] Z. Luo, W. Ma, A.-C. So, Y. Ye, and S. Zhang, "Semidefinite relaxation of quadratic optimization problems," *IEEE Signal Processing Mag.*, vol. 27, no. 3, pp. 20–34, 2010.

[163] P. Tseng, "Second-order cone programming relaxation of sensor network localization," *SIAM J. Optim.*, vol. 18, pp. 156–185, Feb. 2007.

[164] Z. Wang, S. Zheng, Y. Ye, and S. Boyd, "Further relaxations of the semidefinite programming approach to sensor network localization," *SIAM J. Optim.*, vol. 19, pp. 655–673, Jul. 2008.

[165] A. Seville and K. Craig, "Semi-empirical model for millimetre-wave vegetation attenuation rates," *Electron. Lett.*, vol. 31, pp. 1507–1508, Aug. 1995.

[166] Y. Meng, Y. Lee, and B. Ng, "Path loss modelling for near-ground VHF radio-wave propagation through forests with tree-canopy reflection effect," *Prog Electromagn Res*, vol. 12, pp. 131–141, 2010.

[167] J. Gay-Fernandez, M. Garcia Sanchez, I. Cuinas, and A. Alejos, "Propagation analysis and deployment of a wireless sensor network in a forest," *Prog Electromagn Res*, vol. 106, pp. 121–145, 2010.

[168] A. Harun, M. Ramli, L. Kamarudin, D. Ndzi, A. Shakaff, A. Zakaria, and M. Jaafar, "Comparative performance analysis of wireless RSSI in wireless sensor networks motes in tropical mixed-crop precision farm," in *Proc. ISMS '12.*, pp. 606–610, Feb. 2012.

[169] S. Phaiboon and S. Somkuarnpanit, "Mobile path loss characteristics for low base station antenna height in different forest densities," in *Proc. ISWPS'06*, pp. 1–6, 2006.

[170] Y. Meng, Y. Lee, and B. Ng, "Empirical near ground path loss modeling in a forest at VHF and UHF bands," *IEEE Trans. Antennas Propag.*, vol. 57, pp. 1461–1468, May 2009.

[171] R. Tewari, S. Swarup, and M. Roy, "An empirical result for the height gain in forest medium," *IEEE Trans. Antennas Propag.*, vol. 32, pp. 1265–1268, Nov. 1984.

[172] P. Agrawal and N. Patwari, "Correlated link shadow fading in multi-hop wireless networks," *IEEE Trans. Wireless Commun.*, vol. 8, pp. 4024–4036, Aug. 2009.

[173] G. Mao, B. D. O. Anderson, and B. Fidan, "Path loss exponent estimation for wireless sensor network localization," *Comput. Netw.*, vol. 51, pp. 2467–2483, Jul. 2007.

[174] L. Miller, "Distribution of link distances in a wireless network," *J. Res. Natl. Inst. Stand. Technol.*, vol. 106, pp. 401–412, Mar. 2001.

[175] A. Bel, J. Vicario, and G. Seco-Granados, "Localization algorithm with on-line path loss estimation and node selection," *Sensors*, vol. 11, pp. 6905–6925, 2011.

[176] B. Majone, A. Bellin, E. Filippi, L. Loriatti, M. Martinelli, A. Massa, and G. Toller, "Wireless sensor network deployment for monitoring soil moisture dynamics at the field scale," *Procedia Environmental Sciences*, pp. 426–435, 2013.

[177] R. Grisso, "Precision farming tools: soil electrical conductivity." Virginia Cooperative Extension, 2009.

[178] T. Mueller, F. Pierce, O. Schabenberger, and D. Warncke, "Map quality for site-specific fertility management," *J. Soil Sci. Soc. of America*, vol. 65, pp. 1547–1558, 2001.

[179] A. Agnello and H. Reissig, "comparison of mechanically applied pheromone dispensing technologies for mating disruption of tree fruit pest lepidoptera." Virginia Cooperative Extension, 2008.

[180] J. Eckert, F. Villanueva, R. German, and F. Dressler, "Considerations on Quality Metrics for Self-localization Algorithms," in *Proc. IEEE SASO'11*, pp. 104–115, 2011.

[181] "Apple facts." `http://urbanext.illinois.edu/apples/facts.cfm`. Retrieved Aug. 2015.

[182] H. Liu, Z. Meng, H. Wang, and M. Xu, "Systematic random deployment for wireless sensor network in agricultural sampling-interpolation applications," in *Proc. CCTA '13*, vol. 393, pp. 53–59, 2013.

[183] "Proven solutions for the internet of everything." `https://www.synapse-wireless.com/snap-components/rf-engine`. Retrieved Aug. 2014.

[184] J. C. Duchi, A. Agrawal, and M. Wainright, "Dual averaging for distributed optimization: Convergence analysis and network scaling," *IEEE Trans. Automat. Control*, vol. 57, no. 3, pp. 592–606, 2012.

[185] A. Cerpa, N. Busek, and D. Estrin, "SCALE: A tool for simple connectivity assessment in lossy environments," Tech. Rep. 0021, UCLA CENS, 2003.

[186] S. Shaik and S. Setty, "Performance comparison of AODV, DSR and ANODR for grid placement model," *Int. J. Comp. Appl.*, vol. 11, no. 12, pp. 6–9, 2010.

[187] K. Raju and S. Setty, "Performance evaluation of AODV and DSR in feasible and random placement models," *Int. J. Computer Sci. Manage. Stud.*, 2014.

[188] R. Rajagopalan and P. Varshney, "Connectivity analysis of wireless sensor networks with regular topologies in the presence of channel fading," *IEEE Trans. Wireless Commun.*, vol. 8, pp. 3475–3483, Jul. 2009.

[189] C. Bettstetter and C. Hartmann, "Connectivity of wireless multihop networks in a shadow fading environment," *Wireless Netw.*, vol. 11, pp. 571–579, Sep. 2005.

[190] X. Liu and M. Haenggi, "The impact of the topology on the throughput of interference-limited sensor networks with rayleigh fading," in *2nd Annu. IEEE Commun. Soc. Conf. on Sensor and Ad Hoc Commun. and Netw.*, pp. 317–327, 2005.

[191] R. Hekmat and P. Van Mieghem, "Connectivity in wireless ad-hoc networks with a log-normal radio model," *Mob. Netw. Appl.*, vol. 11, pp. 351–360, Jun. 2006.

[192] Z. Zhang, G. Mao, and B. Anderson, "On the hop count statistics in wireless multihop networks subject to fading," *IEEE Trans. Parallel Distrib. Syst.*, vol. 23, pp. 1275–1287, Jul. 2012.

[193] C. Perkins and E. Royer, "Ad-hoc on-demand distance vector routing," in *Proc. WMCSA '99*, pp. 90–100, 1999.

[194] J. Li, L. Andrew, C. Foh, M. Zukerman, and H. Chen, "Connectivity, coverage and placement in wireless sensor networks," *Sensors*, vol. 9, pp. 7664–7693, 2009.

[195] "Steps to success in replanting." `http://www.al.gov.bc.ca/treefrt/replant/Steps_to_Success_in_Replanting.pdf`, 1994.

[196] "High density apple production." `http://bayfield.uwex.edu/files/2011/02/High-Density-Apple-Production.pdf`, 2011.

[197] T. Robinson, "Should new york apple growers move up to higher tree densities?," *New York Fruit Quarterly*, vol. 13, no. 1, pp. 27 –31, 2005.